

JCU ePrints

This file is part of the following reference:

Page, Michael C. (2006) *Late Pleistocene-Holocene deposition of mixed siliciclastic-carbonate sediments on slopes east of the Great Barrier Reef, northeast Australian margin.* PhD thesis, James Cook University.

Access to this file is available from:

<http://eprints.jcu.edu.au/17442>



**Late Pleistocene–Holocene deposition of mixed
siliciclastic-carbonate sediments on slopes east of the
Great Barrier Reef, northeast Australian margin**

Thesis submitted by

Michael C. PAGE BSc., BSc.(Hons)

in January 2006

for the degree of Doctor of Philosophy
in the School of Earth Sciences
James Cook University

STATEMENT OF ACCESS

I, the undersigned, author of this work, understand that James Cook University will make this thesis available for use within the University Library and, via the Australian Digital Theses Network, for use elsewhere.

I understand that, as an unpublished work, a thesis has significant protection under the Copyright Act and I do not wish to place any further restrictions on this work.

Signature

9.01.2006

Date

STATEMENT OF SOURCES

DECLARATION

I declare that this thesis is my own work and has not been submitted in any form for any other degree or diploma at any university or other institution of tertiary education. Information derived from the published or unpublished work of others has been acknowledged in the text and a list of references is given.

Signature

9.01.2006
Date

ABSTRACT

Continental margins are dynamic systems where the flux and accumulation of sedimentary components varies over space and time. Along passive continental margins, relative changes in sea level and sediment supply to the shelf are the predominant influences on sediment fluxes to slopes and basins and are incorporated in generic models of continental margin evolution. Generic depositional models differ depending on the composition of sediments deposited within the system, and can be classified as siliciclastic, carbonate, mixed siliciclastic-carbonate, or evaporite models. The principles governing generic models for end-member siliciclastic and carbonate systems have been tested widely in modern environments, resulting in the general acceptance of ‘lowstand shedding’ to the slope and basin for siliciclastic systems, and ‘highstand shedding’ to the slope and basin for carbonate systems. Conversely, relatively little attention has been afforded modern examples of mixed siliciclastic-carbonate systems. Nevertheless, generic models for the evolution of mixed siliciclastic-carbonate margins, developed mostly via the study of ancient examples in the geological record, are accepted widely, and incorporate the combined paradigms for end-member siliciclastic and carbonate margins to model off-shelf sediment accumulations in response to relative sea-level change. Thus, along mixed siliciclastic-carbonate margins, siliciclastic fluxes to slopes and basins should be highest during sea-level lowstands, when rivers can incise across exposed shelves, and carbonate fluxes to slopes and basins should be highest during sea-level highstands, when flooded shelves provide greatest neritic accommodation space. Lowest fluxes of both components should occur during sea-level transgressions when rivers retreat landward and carbonate production is inhibited by proximal fluvial inputs.

The passive continental margin of northeastern Australia, extending from ~7 to 25°S, is the largest extant mixed siliciclastic-carbonate system. Significant quantities of siliciclastic sediment from rivers draining tropical and subtropical watersheds in Australia and Papua New Guinea are discharged onto a highly productive carbonate shelf that includes the Great Barrier Reef (GBR). Sedimentary successions on slopes east of the GBR are characterised by alternating siliciclastic-rich and carbonate-rich intervals, originally interpreted as forming during lowstands and highstands, respectively. However, recent investigations have demonstrated that

the uppermost siliciclastic-rich interval offshore the central GBR province around 17°S formed during the last postglacial transgression. Despite these findings, the late Pleistocene-Holocene deposition of mixed siliciclastic-carbonate sediments east of the GBR remains equivocal, because it is unclear if: (1) siliciclastic fluxes to slopes all along the central GBR province were highest during transgression, (2) off-shelf fluxes of carbonate sediment were highest during highstand, lowstand, or transgression, and (3) the depositional response to relative sea-level change is consistent all along the northeast Australia margin, especially in areas where physiography and climate are different.

This thesis aims to resolve these issues and to thus develop a more complete understanding of the latest Quaternary evolution of the mixed siliciclastic-carbonate margin of northeastern Australia. High-resolution chronostratigraphies were developed for multiple sediment cores from repositories east of the modern GBR via the determination of thirty-one accelerator mass spectrometry radiocarbon ages and stable isotope stratigraphy. Bulk carbonate content, and carbonate mineralogy and geochemistry, were examined in each of these cores and in other cores with previously developed age models. These datasets enabled the determination of mass accumulation rates for siliciclastic and carbonate components of the bulk sediment, and for individual carbonate minerals down each core. Mass accumulation rates unequivocally demonstrate that all along the northeast Australian margin from ~15 to 21°S, fluxes of both siliciclastic and carbonate sediment to repositories in Queensland Trough and on Marion Plateau were lowest during the last glacial lowstand, highest during the postglacial transgression, and moderate to high during the Holocene highstand, regardless of modern differences in physiography, climate and sediment supply. The history of off-shelf sediment fluxes on the northeast Australian margin during the latest Quaternary could be affected by climate change over glacial-interglacial cycles, but is probably heavily influenced by fluvial aggradation on the shelf during lowstand, and basin-ward remobilisation of siliciclastic sediment and subaerially eroded carbonate during transgression. The northeast Australian margin is an outstanding example of the strong influence margin physiography and physical processes, in conjunction with relative sea level and climate change, can have on the development of sedimentary sequences on slopes of mixed siliciclastic-carbonate margins, and may serve as an analogue for other mixed siliciclastic-carbonate systems throughout the geological record, especially tropical platforms rimmed by reefs.

STATEMENT OF THE CONTRIBUTION BY OTHERS

This thesis has benefited greatly from the contribution by others to the formulation of ideas, the development of research approaches, and the interpretation and critical review of data. Acknowledgement of many of these contributors is made at the conclusion of relevant chapters, but is due here to several individuals in particular:

Gerald Dickens and Gavin Dunbar were instrumental in providing the initial impetus to investigate the development of mixed siliciclastic-carbonate sequences east of the Great Barrier Reef. Many of the fundamental questions that have been addressed in this thesis stemmed from previous work undertaken by these individuals and from ideas and hypotheses that were generated from the same. Gerald Dickens acquired the initial funding and support necessary to begin this work based on the recognition of important research avenues. Both of these individuals have also contributed much to the acquisition and interpretation of data generated herein, and in the presentation of results. The importance of their contribution to this research is apparent in their status as co-authors to published papers, or manuscripts submitted for publication, however, both recognise this author's role as chief investigator in these studies, and as having acquired the majority of the data, formulating the bulk of the interpretations, preparing drafts, and refining of the manuscripts.

Paul Hearty, Michael O'Leary, and Darrell Kaufman set the foundations for investigations involving amino-acid racemization in single foraminifera from the northeast Australian margin. Many of the primary hypotheses and groundwork for initiating this research is due to Paul Hearty, while Michael O'Leary provided the first systematic test of the technique (the results of which form the basis of his Honours thesis), and Darrell Kaufman provided analytical and interpretative expertise. The research presented here forms part of a pilot program further evaluating the utility of the method and is inherently collaborative. The contribution of these individuals is recognised by their status as co-authors on the manuscript presented herein, however, all recognise this author's role as chief investigator in this particular avenue of the research.

ACKNOWLEDGEMENTS

I wish to extend my deepest thanks to all the individuals and organisations that have made this research possible and that have supported me throughout the course of my doctoral studies. Firstly, to the staff of the School of Earth Sciences at James Cook University, both academic and administrative, who have had the foresight to foster postgraduate programs and to provide the opportunity to undertake this research in a vibrant, productive atmosphere. Special thanks go to my primary supervisor, Jerry Dickens, who was always extremely encouraging from the day I was lobbed onto his desk with little or no warning, and who has continued to provide irreplaceable feedback since Uncle Sam stole him back. To Bob Henderson who has ensured that after Jerry's departure I somehow always managed to stay enrolled, and to my surrogate supervisor, Raphael Wüst, who continuously went beyond the call of duty to provide me with support even though I was not one of his official students. Thanks also to Peter Crosdale, Paul Hearty, and Graham Shields, who were always ready to listen, offer their opinion, and to give advice, and to Gavin Dunbar who somehow manages to email back within five minutes every time. Many thanks are extended to Rachel Mahon and Melissa Thomson, for providing the best administrative support in completely underrated and often thankless roles, and to Kevin Hooper and Don Battersby for facilitating great research on the *Kirby* and keeping us entertained at the same time. There are also many people outside JCU who deserve thanks for helping me out for no gain on their part. Thanks to you all and especially to Chris Fielding, Darrell Kaufman, Flavio Anselmetti, Alex Isern, Philipp Reza Heck, the ODP Leg 194 scientists and crew of the *JOIDES Resolution*. Special thanks go to all the funding agencies that have sponsored my doctoral research, specifically Australian Institute of Nuclear Science and Engineering for providing radiocarbon analyses, American Association of Petroleum Geologists for providing US dollars under the Grants-In-Aid scheme, CRC Reef (thanks especially to Tim Harvey) for not only funding geologists researching corals, Ocean Drilling Program (Australian Division), and James Cook University. Last but definitely not least, thanks to my family for always supporting me in whatever I choose to do, even if they can't work out why, especially Nadine for never giving up on me no matter how stretched her patience, and friends old and new for providing enjoyable distractions and excuses for procrastinations.

TABLE OF CONTENTS

Statement of access	i
Statement of sources	ii
Abstract	iii
Statement of the contribution by others	v
Acknowledgements	vi
Table of Contents -----	vii
List of Tables.....	xi
List of Figures.....	xiii
Chapter 1 – Introduction -----	1
1.1. Generic continental margin stratigraphy.....	2
1.2. Mixed siliciclastic-carbonate depositional systems.....	3
1.3. Northeast Australian Margin.....	4
1.4. Recent sedimentation east of the Great Barrier Reef.....	8
1.5. Sedimentation east of the Great Barrier Reef through time.....	9
1.6. Thesis overview.....	11
Chapter 2 -----	20
Tropical view of Quaternary sequence stratigraphy: Siliciclastic accumulation on slopes east of the Great Barrier Reef since the Last Glacial Maximum	
Abstract.....	21
2.1. Introduction.....	22
2.2. Location, samples and methods.....	23
2.3. Results.....	25
2.3.1. Carbonate profiles.....	25
2.3.2. Radiocarbon ages.....	25
2.3.3. Timing and accumulation of siliciclastic-rich intervals.....	26
2.4. Discussion.....	27

Acknowledgements.....30

Chapter 3 -----38

Periplatform carbonate accumulation on slopes east of the Great Barrier Reef since the Last Glacial Maximum: Toward a coherent model for sedimentation in a tropical mixed siliciclastic-carbonate system

Abstract.....39

3.1. Introduction.....41

3.2. Background.....43

3.3. Samples and analytical methods.....46

3.4. Compositional variation.....48

 3.4.1. Carbonate mineralogy (XRD).....48

 3.4.2. Strontium concentrations.....50

 3.4.3. Carbonate grains.....52

3.5. Mass accumulation rates.....53

3.6. Discussion.....56

 3.6.1. Origin and problem of carbonate abundance and accumulation patterns.....56

 3.6.2. Changes on the shelf and a solution to slope accumulation.....59

 3.6.3. Lowstand ca. 25–12 ka.....60

 3.6.4. Transgression ca. 12–7 ka.....61

 3.6.5. Highstand ca. 7 ka–present62

 3.6.6. Discrepancies63

3.7. Conclusions.....64

Acknowledgements.....67

Chapter 4 -----85

Sediment fluxes to Marion Plateau (southern Great Barrier Reef Province) over the last 130 ky: New constraints on ‘transgressive-shedding’ off northeastern Australia

Abstract.....86

4.1. Introduction.....88

4.2. Location, samples and methods.....90

 4.2.1. The northeast Australian margin.....90

 4.2.2. Core GC10.....92

 4.2.3. Analytical methods.....92

4.3. Results.....95

 4.3.1. Bulk carbonate content.....95

 4.3.2. Carbonate mineralogy.....96

 4.3.3. Strontium content.....96

 4.3.4. Chronostratigraphy.....97

4.4. Mass accumulation rates.....98

 4.4.1. Calculation.....98

 4.4.2. Last Glacial Maximum (~25 ka) to mid Holocene (~6 ka).....99

 4.4.3. Last Interglacial (~130 ka) to Last Glacial Maximum (~25 ka).....100

4.5. Discussion.....101

4.6. Conclusion.....107

Acknowledgements.....109

Chapter 5 – Conclusion -----124

References Cited -----132

Appendix A -----140

**High-resolution amino-stratigraphy of cores from Queensland Trough and
Marion Plateau: insights into AAR kinetics in the western Coral Sea since the
Last Glacial Maximum**

Abstract.....141

A.1. Introduction.....143

A.2. Approach and methods.....144

 A.2.1. Core selection.....144

 A.2.2. The AAR method.....146

A.2.3. Age models.....	147
A.2.4. Stable isotopes.....	148
A.3. Results.....	149
A.3.1. D/L ratios.....	149
A.3.2. $\delta^{18}\text{O}$	151
A.4. Modelling racemization rates.....	152
A.5. Summary, conclusions and future work.....	153
Acknowledgements.....	155
References.....	168
Appendix B -----	170

***DATA REPORT: Variations in bulk carbonate content in ODP Hole 1198A, 0–
23.69 mbsf***

Abstract.....	171
B.1. Introduction.....	172
B.2. Methods.....	173
B.3. Results.....	174
Acknowledgements.....	175
References.....	182

LIST OF TABLES

Chapter 2

Table 2.1: Measured bulk carbonate content in cores 51GC43, FR4/92 PC11, FR4/92 PC12, FR4/92 PC13, FR4/92 PC14, and FR5/90 PC27a.....**31-33**

Table 2.2: Results of accelerator mass spectrometry radiocarbon analyses and calibration of conventional ages for cores 51GC43, FR4/92 PC11, FR4/92 PC12, FR4/92 PC13, FR4/92 PC14, and FR5/90 PC27a. (N.A.–Beyond the range of calibration).....**34**

Chapter 3

Table 3.1: Location and other information pertaining to sediment cores FR5/90 PC27a, ODP Hole 820A, FR4/92 PC13, FR4/92 PC16, FR4/92 PC11, and 51GC43.....**69**

Table 3.2: Bulk carbonate content and carbonate mineral abundances in sediment cores FR5/90 PC27a, ODP Hole 820A (1H to 2H-1), FR4/92 PC13, FR4/92 PC16, FR4/92 PC11, and 51GC43.....**70-71**

Table 3.3: Measured and corrected (for siliciclastic dilution) strontium concentration down sediment cores FR5/90 PC27a, ODP Hole 820A (1H to 2H-1), FR4/92 PC13, FR4/92 PC11, and 51GC43.....**72-73**

Chapter 4

Table 4.1: Bulk carbonate content of core FR03/99 GC10.....**111**

Table 4.2: Carbonate mineral abundances and Sr concentrations in core FR03/99 GC10.....**112**

Table 4.3: $\delta^{18}\text{O}$ and $\delta^{13}\text{C}$ in planktonic foraminifers from core FR03/99 GC10.....**113**

Table 4.4: Results of AMS radiocarbon analysis of planktonic foraminifers from core FR03/99 GC10.....**114**

Table 4.5: Mass accumulation rates of sedimentary components in core FR03/99 GC10.....**115**

Appendix A

Table A.1: Location and other information for sediment cores FR03/99 GC10, 51GC43, FR4/92 PC16, FR4/92 PC11, FR4/92 PC12, and FR5/90 PC27a. Bottom water temperatures in Queensland Trough were measured on CSIRO cruises 1985/05, 1990/06, 1991/07, 1992/09 and 1997/01 and are available at www.marine.csiro.au/datacentre. *Temperature estimated from same depth in Queensland Trough. SPCW – South Pacific Central Water; AAIW – Antarctic Intermediate Water.....**156**

Table A.2: Sample information, extrapolated ages, and results of RP-HPLC analysis (D/L ratios) for cores FR03/99 GC10, 51GC43, FR4/92 PC16, FR4/92 PC11, FR4/92 PC12, and FR5/90 PC27a. n – number of tests included in average. ex – number of tests excluded from average.....**157-158**

Table A.3: Results of stable isotope analysis of benthic foraminifera from core 51GC43.....**159**

Appendix B

Table B.1: Bulk carbonate content, ODP Hole 1198A, 0 – 23.69 mbsf.....**176-179**

LIST OF FIGURES

Chapter 1

Figure 1.1: Global map showing the location of some modern and ancient examples of mixed siliciclastic-carbonate depositional systems. The location of modern examples is indicated, as is the age of examples in the geological record.....17

Figure 1.2: (A) Eustatic change since 25 ka. (B) Generic depositional model for sediment deposition on slopes of tropical mixed siliciclastic-carbonate systems. (C) Schematic representation of observed sedimentation patterns on slopes of the northeast Australian margin. H/stand – sea-level highstand. Trans – transgression. Lowstand – sea-level lowstand. MAR – mass accumulation rate.....18

Figure 1.3: The northeast continental margin of Australia, including mean annual rainfall, the location of major rivers draining the hinterland, distribution of modern reefs of the Great Barrier Reef, and bathymetric features of the western Coral Sea...19

Chapter 2

Figure 2.1: The northeast Australian margin between ~15 and 20°S, including mean annual rainfall, location of major rivers, distribution of modern reefs on the shelf, bathymetry (m) of the western Coral Sea, and location of cores FR5/90 PC27a, ODP Hole 819, 820, 821, FR4/92 PC14, FR4/92 PC13, FR4/92 PC12, FR4/92 PC16, FR4/92 PC11, and 51GC43.....35

Figure 2.2: Downcore profiles of bulk carbonate content for cores 51GC43, FR4/92 PC11, FR4/92 PC12, FR4/92 PC13, FR4/92 PC14, and FR5/90 PC27a, and radiocarbon ages (calibrated years before present) of planktonic foraminifera.....36

Figure 2.3: Mass-accumulation rates of siliciclastic and carbonate sediment in cores 51GC43, FR4/92 PC11, FR4/92 PC12, FR4/92 PC13, FR4/92 PC14, and FR5/90

PC27a. Dashed line approximates the time when sea level reached the shelf edge (ca. 12 ka). H/stand – sea-level highstand; Trans – sea-level transgression; Lowstand – sea-level lowstand.....37

Chapter 3

Figure 3.1: The central portion of the northeast Australian margin, bathymetry (m) of the Coral Sea, and mean annual rainfall on the continent. Circles indicate cores examined from Queensland Trough. Triangles indicate cores through reefs on the shelf (BRR – Britomart Reef, Johnson et al., 1984; RBR5 – Ribbon Reef 5, BOR – Boulder Reef, International Consortium for Great Barrier Reef Drilling, 2001). Transects A–A’, B–B’ and C–C’ appear as cross-sections on Fig. 3.10.....74

Figure 3.2: Mass accumulation rates of bulk siliciclastic and bulk carbonate components in cores from ODP 820A, 51GC43, FR5/90 PC27a, FR4/92 PC16, FR4/92 PC13, and FR4/92 PC11 (modified after: Peerdeman and Davies, 1993; Dunbar et al., 2000; Page et al., 2003). H/stand – sea-level highstand. Trans – transgression. Lowstand – sea-level lowstand. WD – water depth. Dist – distance offshore of the 120 m isobath. Note the different Y-scale for ODP 820A.....75

Figure 3.3: Downcore profiles of carbonate mineralogy and radiocarbon ages (modified from Peerdeman and Davies, 1993; Dunbar et al., 2000; Page et al., 2003) for ODP Hole 820A, 51GC43, FR5/90 PC27a, FR4/92 PC16, FR4/92 PC13, and FR4/92 PC11. Original age models for ODP 820A and PC16 (based on conventional radiocarbon ages) have been calibrated with the CALIB 4.3 freeware (Stuiver et al., 1998) to maintain consistency with the age models of Page et al. (2003). H/stand – sea-level highstand. Trans – transgression. Lowstand – sea-level lowstand. WD – water depth. Dist – distance offshore of the 120 m isobath.....76

Figure 3.4: The sand-sized fraction of sediment deposited in core 51GC43 during: (A–B) The last glacial lowstand, ~21 ka (209 cmbsf), planktonic (PF) and benthic (BF) foraminifers are the dominant components, pteropods (PT) are also common; (C–E) The postglacial transgression, ~11 ka (120 cmbsf) and (F–H) ~9 ka (90 cmbsf), foraminifera are abundant, shell fragments (SF) and LMC clasts are common, LMC

clasts occur as both cemented aggregates (LMC-A) and recrystallised grains (LMC-R); (I–J) The Holocene highstand, ~2.5 ka (5 cmbsf), foraminifers are abundant and shell fragments are common, LMC clasts are present in minor quantities.....77-78

Figure 3.5: Relative abundances (A) and mass accumulation rates (B) of low-Mg calcite, aragonite, and high-Mg calcite during lowstand, transgression, and highstand, in cores from ODP Hole 820A, 51GC43, FR5/90 PC27a, FR4/92 PC16, FR4/92 PC13, and FR4/92 PC11, plotted against distance from the 120 m isobath. With increasing distance from the shelf, the relative abundance of LMC generally increases, and the relative abundances of aragonite and HMC generally decrease. Note, however, that with increasing distance from the shelf, the mass accumulation rates of all carbonate minerals generally decrease.....79

Figure 3.6: Strontium concentration versus the percentage of aragonite in the bulk carbonate fraction of sediment from cores FR5/90 PC27a, ODP 820A (1H to 2H-1), FR4/92 PC13, FR4/92 PC11, and 51GC43. Circles represent samples deposited prior to 12 ka; squares represent samples deposited after 12 ka. Assuming that Sr-rich aragonite contains 7500 ppm Sr, and that Sr-poor aragonite contains 1500 ppm Sr, samples in which the aragonite present in the bulk carbonate fraction is composed entirely of Sr-rich aragonite should plot along the solid line marked Sr-rich aragonite, and samples in which the aragonite present in the bulk carbonate fraction is composed entirely of Sr-poor aragonite should plot along the solid line marked Sr-poor aragonite. Samples in which the aragonite present in the bulk carbonate fraction is composed of equal parts Sr-rich aragonite and Sr-poor-aragonite should plot along the solid line marked 50/50. The linear trendline ($y = 45.5x + 1391$; $r^2 = 0.74$) indicates that more than 50% of the aragonite present in most samples is composed of Sr-rich aragonite.....80

Figure 3.7: Mass accumulation rates of low-Mg calcite, aragonite and high-Mg calcite in cores from ODP Hole 820A, 51GC43, FR5/90 PC27a, FR4/92 PC16, FR4/92 PC13, and FR4/92 PC11. H/stand – sea-level highstand. Trans – transgression. Lowstand – sea-level lowstand. WD – water depth. Dist – distance offshore of the 120 m isobath.....81

Figure 3.8: General stratigraphy of cores through individual reefs on the Great Barrier Reef (modified from: Johnson et al., 1984; International Consortium for Great Barrier Reef Drilling, 2001; Webster and Davies, 2001) the location of which are shown on **Fig. 3.1**. Holocene reefs are founded upon Pleistocene substrates that have been subaerially exposed and altered from aragonite (and high-Mg calcite) to low-Mg calcite, and are separated by erosional ('solution') unconformities. The lowermost age for BRR2 is estimated based on the distance between the lowermost radiocarbon age and the underlying solution unconformity, and published growth rates for Britomart Reef (Johnson et al., 1984).....82

Figure 3.9: Schematic model of sedimentary processes and off-shelf fluxes on the northeast Australian margin since the Last Glacial Maximum.....83

Figure 3.10: Bathymetric profiles across the shelf-slope break of the northeast Australian margin (location of transects shown on **Figure 3.1**) and the approximate position of cores in Queensland Trough and on the shelf. Note that the areas of seafloor within 120 m of the sea surface during lowstand ('LGM productivity window') increase by up to an order of magnitude almost immediately upon sea level rising above the shelf break during transgression.....84

Chapter 4

Figure 4.1: The central and southern northeast Australian margin showing major physiographic features, the location of core FR03/99 GC10 on Marion Plateau, previous study areas in Queensland Trough (Harris et al., 1990; Peerdeman and Davies, 1993; Dunbar et al., 2000; Dunbar and Dickens, 2003b; Page et al., 2003), and the locations of four previously studied cores mentioned specifically in the text.....116

Figure 4.2: Photograph and physical properties of core FR03/99 GC10, including bulk carbonate content, relative abundance of carbonate minerals, Sr concentration in the carbonate fraction, and $\delta^{18}\text{O}$ stratigraphy. Note the position of AMS radiocarbon ages ($\times 1000$ years) and the last occurrence of pink *Globigerinoides ruber* (*) on the right side of the core photograph. Marine isotope stages (MIS) as interpreted from

correlation of isotope stratigraphy with the SPECMAP record (Martinson et al., 1987) appear on the far right.....117

Figure 4.3: Age model for core FR03/99 GC10, produced by correlation of $\delta^{18}\text{O}$ stratigraphy with the SPECMAP record of Martinson et al. (1987). The positions of four AMS radiocarbon ages and the last occurrence of pink *G. ruber* are also noted relative to the isotope data. The bulk continuous sedimentation rate was formulated based on the isotope correlation and calculated by Analyseries v1.1 (Paillard et al., 1996). The bulk linear sedimentation rate was calculated using the AMS radiocarbon ages only. Note that both bulk continuous and bulk linear sedimentation rates increase abruptly during the last postglacial transgression.....118

Figure 4.4: Mass accumulation rates of (A) bulk sediment, bulk carbonate, and bulk siliciclastic material, and (B) low-Mg calcite, aragonite, and high-Mg calcite, over the last 25 ky in core FR03/99 GC10, calculated using the continuous sedimentation rate (Fig. 4.3). Mass accumulation rates of all components were lowest during lowstand, highest during transgression, and moderate during highstand.....119

Figure 4.5: Mass accumulation rates of (A) bulk sediment, bulk carbonate, and bulk siliciclastic material, and (B) low-Mg calcite, aragonite, and high-Mg calcite, in core FR03/99 GC10, relative to (C) sea-level changes over the last 130 ky (adapted from Lambeck and Chappell, 2001), calculated using the continuous sedimentation rate (Fig. 4.3). Note the in-phase relationship between all components, and that highest accumulation rates coincide with major sea-level transgressions following MIS 6 and 2.....120

Figure 4.6: Mass accumulation rates of bulk siliciclastic and bulk carbonate components of core FR03/99 GC10 (shaded) and selected cores from Queensland Trough (modified from; Peerdeman and Davies, 1993; Dunbar et al., 2000; Page et al., 2003) since the Last Glacial Maximum, calculated using the bulk linear sedimentation rate (Fig. 4.3) to maintain consistency with data from Queensland Trough. Mass accumulation rates of both components were highest in all cores during transgression, however, the magnitude generally decreases with distance from the shelf. Note that in GC10, carbonate mass accumulation rates were comparable to

those in cores at a similar distance from the shelf in Queensland Trough, but mass accumulation rates of siliciclastic material were lower. WD–water depth. Dist–distance from the 120 m isobath. Lat–latitudinal position in degrees south.....121

Figure 4.7: Mass accumulation rates of low-Mg calcite, aragonite, and high-Mg calcite in core FR03/99 GC10 (shaded) compared to cores from Queensland Trough (modified from **Fig. 3.7**) since the Last Glacial Maximum, calculated using the bulk linear sedimentation rate (**Fig. 4.3**) to maintain consistency with data from Queensland Trough. Note that mass accumulation rates of all components are lowest and highest during lowstand and transgression, respectively, and generally decrease with distance from the shelf. WD–water depth. Dist–distance from the 120 m isobath. Lat–latitudinal position in degrees south.....122

Figure 4.8: Conceptual model for the evolution of the southern GBR province over the last 130 ky. Bathymetric information modified from Shipboard Scientific Party (2002). Sea-level reconstructions based on the eustatic curve of Lambeck and Chappell (2001). Course of the paleo-Fitzroy River and cross-sections of the shelf adapted from Maxwell (1968). Dark shaded areas on the shelf indicate areas of possible siliciclastic deposition.....123

Appendix A

Figure A.1: The continental margin of northeastern Australia. Circles indicate the position of cores FR03/99 GC10, 51GC43, FR4/92 PC16, FR4/92 PC11, FR4/92 PC12, and FR5/90 PC27a. Bathymetry of the western Coral Sea is indicated in metres.....160

Figure A.2: Generalised temperature profile and water mass boundaries in the western Coral Sea (modified after: Corregge, 1993a; Hearty et al., submitted). Circles indicate the modern seabed depth at the location of cores FR03/99 GC10, 51GC43, FR4/92 PC16, FR4/92 PC11, FR4/92 PC12, and FR5/90 PC27a. SLW – Subtropical Lower Water; SPCW – South Pacific Central Water; AAIW – Antarctic Intermediate Water; UDWM – Undefined deep water mass.....161

Figure A.3: Age/depth relationships in cores FR03/99 GC10, 51GC43, FR4/92 PC16, FR4/92 PC11, FR4/92 PC12, and FR5/90 PC27a, based on calibrated radiocarbon dates, and derived age models using least squares polynomial functions.....**162**

Figure A.4: Covariance relationships between the D/L ratios of Asp and Glu for all samples from core FR03/99 GC10 (left) and for the mean D/L ratios of all intervals from cores FR03/99 GC10, 51GC43, FR4/92 PC16, FR4/92 PC11, FR4/92 PC12, and FR5/90 PC27a (right). Black circles – GC10 samples. Grey circles – samples from Queensland Trough cores. Grey squares – rejected ratios.....**163**

Figure A.5: The relationship between time and the D/L ratios of Aspartic acid in foraminifera from cores FR03/99 GC10, 51GC43, FR4/92 PC16, FR4/92 PC11, FR4/92 PC12, and FR5/90 PC27a.....**164**

Figure A.6: Variations in $\delta^{18}\text{O}$ and $\delta^{13}\text{C}$ in benthic foraminifera from core 51GC43, relative to sea-level changes on the northeast Australian margin over the last glacial-interglacial cycle. H/Stand – sea-level highstand. Trans – sea-level transgression. Lowstand – sea-level lowstand.....**165**

Figure A.7: The relationship between time and the D/L ratios of Aspartic acid in foraminifera from cores FR03/99 GC10, 51GC43, FR4/92 PC16, FR4/92 PC11, FR4/92 PC12, and FR5/90 PC27a, modelled using power functions. Correlation coefficient and equation shown in brackets indicate modelling results for FR03/99 GC10 with one outlier removed.....**166**

Figure A.8: Comparison of the modelled kinetic pathways for Aspartic acid in cores FR03/99 GC10, 51GC43, FR4/92 PC16, FR4/92 PC11, FR4/92 PC12, and FR5/90 PC27a, over the last 20 to 25 ky. GC10: solid line – all data, dashed line – outlier removed. Grey dashed lines indicate the estimated position of temperature gradients for racemization rates of Aspartic acid in the western Coral Sea.....**167**

Appendix B

Figure B.1: Major physiographic and bathymetric features of Marion Plateau and the location of ODP Site 1198A.....**180**

Figure B.2: Variations in bulk carbonate content from 0 to 23.69 mbsf in ODP Hole 1198A.....**181**

CHAPTER 1

Introduction

1. INTRODUCTION

1.1. Generic continental margin stratigraphy

Patterns of sediment deposition on slopes of passive continental margins are influenced primarily by variations in sea level and sediment supply (e.g., Vail et al., 1977; van Wagoner et al., 1988; Walker, 1992; Miall, 1997). These factors are generally viewed within the context of idealised siliciclastic or carbonate systems, wherein rivers or shallow marine sources, respectively, dominate sediment supply. For both cases, widely accepted paradigms describe the effects of relative sea-level changes on cross-shelf sediment fluxes and accumulation rates on slopes (e.g., Vail et al., 1977; Posamentier and Vail, 1988; Shanmugan and Moiola, 1988; van Wagoner et al., 1988; James and Kendall, 1992; Schlager et al., 1994).

These models predict that along siliciclastic margins sediment fluxes to slopes should be greatest during sea-level lowstands. Rivers are expected to incise across exposed shelves to equilibrate with lower depositional base levels (e.g., Miall, 1991; van Heijst and Postma, 2001) and discharge directly on upper slopes. Siliciclastic fluxes to slopes should be minimal during the latter part of transgressions when rising sea level forces rivers to retreat landward, and fluxes should be low to moderate during sea-level highstands when sediments prograde basinward across the shelf. Thus, generic models for siliciclastic systems (e.g., Shanmugan and Moiola, 1988) are characterised by 'lowstand shedding' of sediments to the slope and basin.

In direct contrast, widely accepted models for carbonate margins (e.g. Sarg, 1988; Handford and Loucks, 1993) predict that sediment fluxes to slopes should be lowest during sea-level lowstands. Exposure of shelves reduces the area of sea floor within the photic zone, and shallow marine accommodation space and carbonate production is restricted to narrow fringes along upper slopes (e.g., James and Bourge, 1992; Jones

and Desrochers, 1992). Off-shelf fluxes of carbonate sediment should increase when sea level rises above shelves during transgressions, thereby expanding the area of seafloor within the photic zone and allowing for increased volumes of shallow marine carbonate production. Carbonate fluxes should be largest during sea-level highstands when shallow marine accommodation space is greatest on flooded shelves, a situation that promotes high volumes of carbonate production. Thus, generic models for carbonate systems (e.g., Schlager et al., 1994) are characterised by 'highstand shedding' of sediments to the slope and basin.

1.2. Mixed siliciclastic-carbonate depositional systems

As opposed to idealised end-member siliciclastic or carbonate systems, some continental margins receive substantial influxes of both terrestrial siliciclastic and biogenic carbonate sediments. These are referred to as mixed siliciclastic-carbonate depositional systems (e.g., Mount, 1984; Dolan, 1989). Modern examples (Fig. 1.1) can be found along the continental margins of northeastern Australia (Davies et al., 1991) and Belize (Jones and Desrochers, 1992). Mixed siliciclastic-carbonate systems are also widely represented throughout the geological record, and include amongst numerous other examples (Fig 1.1), Precambrian sequences in eastern Greenland (e.g., Tirsgaard, 1996), Permian strata in the central-western United States (e.g., Borer and Harris, 1991), and Tertiary sediments offshore of the western continental margin of India (e.g., Whitmarsh et al., 1974).

Most workers discussing the development of mixed siliciclastic-carbonate margins have concluded that variations in relative sea level affect sediment deposition on slopes according to widely accepted paradigms for end-member siliciclastic and carbonate systems (e.g., Wilson, 1967; Sarg, 1988; Dolan, 1989; James and Kendall,

1992). Thus, generic models for mixed siliciclastic-carbonate depositional systems predict lowstand shedding of siliciclastics and highstand shedding of carbonates. The resulting deposition of alternate siliciclastic-rich and carbonate-rich sediments on the slope has been dubbed 'cyclic-reciprocal sedimentation' (Wilson, 1967).

According to the principles of cyclic-reciprocal sedimentation, highest fluxes of siliciclastic and carbonate sediments to slopes of mixed depositional systems should be completely out-of-phase (Fig. 1.2B). Highest fluxes of siliciclastics should occur during lowstands, and highest fluxes of carbonates should occur during highstands. Importantly, however, and equally entrenched in key geological tenets, models of cyclic-reciprocal sedimentation provide that lowest fluxes of both components to the slope should occur contemporaneously during the latter part of transgressions, when sea level first rises above the shelf. During this time, the potential for increased volumes of carbonate production in shallow outer shelf environments should be suppressed by proximal riverine inputs (e.g., Dolan, 1989; James and Bourge, 1992; Jones and Desrochers, 1992), resulting in very low off-shelf fluxes of both components, and the formation of condensed sections (cf. Loutit et al., 1988) on the slope .

1.3. Northeast Australian Margin

The northeast Australian margin (Fig. 1.3) is the largest extant mixed siliciclastic-carbonate depositional system (Maxwell and Swinchatt, 1970; Davies et al., 1991), extending from ~7°S latitude in the Gulf of Papua to ~25°S latitude in the southern Coral Sea. The margin receives substantial input of terrigenous sediment from rivers draining tropical and subtropical watersheds in Australia and Papua New Guinea, and vast quantities of carbonate sediment produced by a shallow marine environment that includes the largest active coral reef system, the Great Barrier Reef (GBR).

Accordingly, the northeast Australian margin is an example of a type of mixed siliciclastic-carbonate depositional system that is commonly referred to as a *tropical mixed siliciclastic-carbonate margin* (cf. Mount, 1984). Tropical mixed siliciclastic-carbonate margins are characterised by the development of large bioherms, such as reefs, on the shelf, and are relatively common throughout the low latitudes, such as offshore of Belize (e.g. Jones and Desrochers, 1992), Puerto Rico (e.g. Bush, 1991), and other locations in Central America.

Below $\sim 10^{\circ}\text{S}$, the northeast Australian margin can be divided rather simplistically into three physiographic regions: (1) a continental hinterland of steep mountains and broad coastal plains dissected by both ephemeral and perennial river systems, (2) a shallow, low-gradient shelf between ~ 50 and 200 km wide that hosts the GBR, and (3) adjacent deeper plateaux and basins of the Coral Sea. These regions can be subdivided further based on other general characteristics such as climate, ecology, geomorphology, and sedimentology.

Northeastern Australia experiences a quasi-monsoonal climate (Suppiah, 1992) that together with topographic differences causes spatially variable rainfall and vegetation (Fig. 1.3). The terrestrial wet tropics, above $\sim 19^{\circ}\text{S}$, receive higher rates of rainfall (mostly 1500 – 5000 mm/yr) and include abundant thick rainforest vegetation. The terrestrial dry tropics, below $\sim 19^{\circ}\text{S}$, receive lower rates of rainfall (mostly <1500 mm/yr) and mainly include open woodland and savannah. Coupled with differences in the size of individual catchments, these characteristics have important consequences for siliciclastic supply to the margin (Belperio, 1983; Neil and Yu, 1995; Neil et al., 2002). Relatively small catchments and dense vegetative cover offset high runoff from rivers draining the wet tropics. Collective pre-colonisation sediment yields from wet tropical rivers are estimated at less than 1.0 Mt/yr (Neil et al., 2002). On the contrary, less dense

vegetation and larger catchments offset low runoff from rivers draining the dry tropics. Collective pre-colonisation sediment yields are estimated at close to 5.0 Mt/yr, over 90% of which is sourced from the combined discharges of Burdekin and Fitzroy rivers alone (Neil et al., 2002).

The continental shelf adjacent to northeastern Australia, sometimes referred to as the GBR platform, can be loosely divided into three shore-parallel zones (Maxwell, 1968; Maxwell and Swinchatt, 1970; Belperio, 1983; Larcombe and Carter, 2004). The *inner shelf* is considered generally to extend from the coastline to around the 20 m isobath and is mostly less than 5 km wide. A few near-shore reefs occur on the inner shelf, but terrigenous sediments composed mainly of sand and mud sized quartz, feldspar, and clay minerals are the dominant sedimentary component. These sediments constitute the bulk (>70%) of a coastal sediment prism (Belperio, 1983; Carter et al., 1993; Larcombe and Carter, 1988; Lambeck and Woolfe, 2000) that accumulates preferentially near river sources, in northward-facing embayments, and in the lee of headlands. The *middle shelf* is considered generally to occur between the 20 and 40 m isobaths. Carbonate contents are higher (30 to 80%) because most terrigenous sediment is trapped on the inner shelf (Belperio, 1983; Belperio and Searle, 1988). Reefs are more prevalent on the middle shelf but commonly occur as isolated patch reefs. Relict pre-Holocene material constitutes a significant proportion of middle shelf sediments (Johnson and Searle, 1984). The *outer shelf* is generally considered to extend from the 40 m isobath to the shelf-slope break, which usually is located between the 70 and 80 m isobaths (Maxwell, 1968; Larcombe et al., 1995; Fielding et al., 2003). The outer shelf hosts a high-density network of reefs that comprise the main GBR complex and commonly form a relatively continuous shelf edge barrier. Carbonate contents are high and commonly approach 100% near reefs, but siliciclastic content can exceed 30%

within deeper inter-reef passages and channels (Maxwell and Swinchatt, 1970; Belperio and Searle, 1988; Flood and Orme, 1988).

Shelf characteristics also vary significantly along the margin, providing the basis for subdivision of the region into the southern, central, and northern GBR provinces of Maxwell (1968). In the southern GBR province, below $\sim 18^{\circ}\text{S}$, shelf widths approach 200 km. Reefs are generally distal to the coast and are separated by an expansive middle shelf, dissected by a shore-parallel, southward deepening depression known as the Capricorn Channel. In the central GBR province, between $\sim 15\text{--}18^{\circ}\text{S}$, shelf widths decrease from approximately 150 km in the south to less than 50 km in the north. Density of the reef network also increases to the north and approaches the coast as the width of the gently dipping middle shelf decreases. In northern parts of the central GBR province, elongated 'ribbon reefs' form an almost continuous barrier along the outermost shelf. In the northern GBR province, above $\sim 15^{\circ}\text{S}$, shelf widths increase from less than 50 km to around 100 km offshore the northernmost tip of Australia. Density of the reef network generally remains high and ribbon reefs along the outer shelf extend north from the central GBR province.

Seaward of the GBR platform, three main bathymetric features in the western Coral Sea act as the main repositories for sediments shed from the adjacent shelf: Marion Plateau and the Townsville and Queensland troughs (Fig. 1.3). Offshore of the southern GBR province, a poorly developed, shallow-dipping continental slope terminates abruptly on Marion Plateau, a block of subsided continental crust (Ewing et al., 1970) that dips gently away from the shelf. Water depths over the plateau are generally between 300 and 500 m, but a few isolated reefs rise to near sea level. Marion Plateau terminates in the east along a steep slope into Cato Trough, and in the north along a steep slope into Townsville Trough, an east-west trending rift basin that

separates the Marion and Queensland plateaux (Ewing et al., 1970; Symonds et al., 1983). Townsville Trough occurs near the boundary between the southern and central GBR provinces. The shelf break is not well defined and relatively gentle gradients characterise the slope. Water depths increase from around 900 m in the west to more than 2500 m in the east. Offshore of the central and northern GBR provinces, the shelf break is well defined and the slope dips steeply into Queensland Trough, a north-south trending rift basin that separates the GBR platform from the Queensland Plateau (Symonds et al., 1983; Scott, 1993). Water depths in Queensland Trough increase from around 900 m in the south, where a sill separates it from Townsville Trough, to greater than 2500 m in the north, where it opens into the Coral Sea Basin. Queensland Trough also widens to the north and the western continental slope steepens markedly. To the east, isolated reef platforms on Queensland Plateau, a shallow block of detached continental crust (Symonds et al., 1983; Scott, 1993), also serve as less significant point sources of carbonate sediment shed to Queensland and Townsville troughs.

1.4. Recent sedimentation east of the Great Barrier Reef

The composition of seafloor sediments east of the GBR reflects the admixing of material from disparate sources, including the overlying water column, the adjacent shelf and continent, and to a lesser extent isolated neritic environments on Queensland and Marion plateaux (Harris et al., 1990; Davies and McKenzie, 1993; Dunbar et al., 2000). Consequently, sediments on Marion Plateau and in Townsville and Queensland Troughs are invariably characterised by hemipelagic drape and drift deposits, although the absolute abundance of terrigenous and neritic components is highly variable.

The surface distribution of individual sedimentary components east of the GBR is relatively well constrained in Queensland Trough offshore of the central GBR

province, (Sutherland, 2000; Dunbar and Dickens, 2003b), but remains poorly constrained over Marion Plateau and in Townsville Trough. However, within Queensland Trough surface distribution patterns partly reflect differences in the transport processes affecting individual sedimentary components, and partly reflect proximity to sediment sources.

The carbonate content of surface sediment in Queensland Trough steadily decreases towards the north (Sutherland, 2000; Dunbar and Dickens, 2003b). This pattern primarily represents increased siliciclastic accumulation rates in the northern Queensland Trough, rather than diminished carbonate accumulation rates, although the source to sink pathway of terrigenous sediments remains unclear (Dunbar and Dickens, 2003b; Francis et al., 2003). Surface distribution patterns of carbonate minerals are better understood and are consistent with partitioning between neritic and pelagic sources of biogenic carbonate (Dunbar and Dickens, 2003b). Towards the axis of Queensland Trough, and hence with increasing distance from neritic point sources such as reefs on the GBR platform and Queensland Plateau, the relative abundances of aragonite and high-Mg calcite, and bulk sediment Sr concentrations, all decrease, while the relative abundance of low-Mg calcite increases.

1.5. Sedimentation east of the Great Barrier Reef through time

Precursors to the modern GBR have existed on the shelf of the northeast Australian margin since at least 500 ka (Davies and McKenzie, 1993; International Consortium for Great Barrier Reef Drilling, 2001), experiencing cycles of growth and decay in concert with glacio-eustatic variations of the late Quaternary. For the duration of this time, and indeed since the Miocene (Davies and McKenzie, 1993; Pigram, 1993), both siliciclastic and carbonate sediments have been accumulating in repositories east of the

GBR platform. All along the margin, sediment cores from slopes and basins record this depositional history as a series of alternating dark-coloured and light-coloured intervals, corresponding to sections of relatively siliciclastic-rich and relatively carbonate-rich sediment, respectively (Harris et al., 1990; Glenn et al., 1993b; Peerdeman and Davies, 1993; Dunbar et al., 2000; Dunbar and Dickens, 2003a).

Patterns of mixed siliciclastic-carbonate sediment deposition on slopes east of the GBR was initially considered to be consistent with conventional principles surrounding continental margin evolution (Harris et al., 1990). On the slope offshore Townsville, darker-coloured, siliciclastic-rich intervals were interpreted to have been deposited during sea-level lowstands, when terrigenous fluxes to the slope presumably increased and carbonate production decreased, lighter-coloured, carbonate-rich intervals were interpreted to have been deposited during sea-level highstands, when terrigenous fluxes were presumably restricted to the inner shelf and carbonate production maximised, and sediment accumulation rates on the slope were considered to be nominal during transgression.

Subsequently, extensive coring associated with Ocean Drilling Program Leg 133 recovered high-resolution successions of late Pleistocene–Holocene mixed siliciclastic-carbonate sediments on the slope offshore Cairns (Davies et al., 1991). Contrary to initial interpretations, and completely opposite to generic models of continental margin evolution, siliciclastic-rich intervals on the upper slope were interpreted as being deposited during transgression. Furthermore, lowest abundances of siliciclastic sediment on the upper slope were interpreted as being deposited during the last sea-level lowstand. Glenn et al. (1993a) and Kronen and Glenn (2000) circumvented the latter issue, but suggested that the transgressive record resulted from either carbonate starvation, or from increased rainfall and amplified fluvial discharge from the continent

during deglaciation. Their former explanation, however, is inconsistent with the findings of Peerdeman and Davies (1993), who demonstrated that both the abundance and flux of siliciclastic sediment was lowest during lowstand and highest during transgression. This record was attributed to sediment bypassing of the upper slope during the last lowstand, but no mechanism was proposed to account for amplified siliciclastic accumulation rates during transgression.

More recently, comprehensive studies involving almost forty cored sites throughout the slope and basin of Queensland Trough have suggested that minimum and maximum fluxes of siliciclastic sediment occurred during the last lowstand and transgression, respectively, regardless of location (Dunbar et al., 2000; Dunbar and Dickens, 2003a). Furthermore, while recognising that widespread climate change over glacial-interglacial cycles may have significantly affected fluvial discharge to the coast over time, these workers proposed an alternative model to explain siliciclastic deposition east of the GBR: Low fluxes of terrigenous sediment during the last lowstand might have resulted from fluvial aggradation and siliciclastic deposition on the subaerially exposed shelf, and high terrigenous fluxes during transgression may have resulted from reworking and seaward transport of shelf deposits due to the coastline shifting landward.

1.6. Thesis overview

Recent research concerning patterns of mixed siliciclastic-carbonate sediment deposition on slopes of the northeast Australian margin clearly suggests that the system behaves differently than expected from generic models of continental margin evolution (Fig. 1.2C). Most notably, minimum and maximum siliciclastic fluxes to slopes of Queensland Trough appear to coincide with the last lowstand and postglacial

transgression, respectively, rather than the opposite, as predicted by conventional models. However, variations in the flux of siliciclastic and carbonate sediments to repositories east of the GBR remains somewhat enigmatic because of several outstanding key issues, including whether previously noted patterns of siliciclastic deposition are consistent through both space time, and how carbonate deposition is affected by sea level and climate changes during the late Quaternary. The subsequent three chapters of this thesis* aim to elucidate some of these issues and to develop a more thorough understanding of the evolution of the northeast Australian margin during the late Pleistocene and Holocene.

Firstly, only two cores that were examined in previous studies had appropriate radiocarbon age control to allow the quantification of siliciclastic fluxes to slopes of the northeast Australian margin since the last glacial lowstand. Moreover, both of these cores were taken from the upper slope in the northern part of the central GBR province, where the shelf is narrow and rainfall is high, but sediment discharge is low. As a consequence, the significance of these results for regional interpretations of margin evolution is equivocal, especially in areas where the shelf is wide and sediment discharge is high. Chapter 2 presents the results of an investigation intended to develop a more thorough understanding of siliciclastic sedimentation offshore the central GBR province, by examining cores from areas with disparate morphology, climate, and sedimentary sources, to those previously studied. The chapter is derived from a paper published in the journal *Geology* (v. 31, pp. 1013-1016) entitled: *Tropical view of Quaternary sequence stratigraphy: siliciclastic accumulation on slopes east of the Great Barrier Reef since the Last Glacial Maximum*, by Michael C. Page, Gerald R. Dickens and Gavin B. Dunbar.

* The reader should note that tables and figures in this thesis are numbered according to the chapter in which they are first referred to, and appear in sequence at the end of that chapter.

In the study presented in Chapter 2, bulk carbonate content and a total of 27 radiocarbon ages were determined in six cores from the upper to lower slope of the western Queensland Trough, situated between ~15 and 18°S. Deposition in this suite of cores has been influenced by a wide range of potential controls on off-shelf terrigenous fluxes, including varying shelf width, rainfall, and sediment discharge. The datasets that were generated enabled the quantification of siliciclastic and carbonate mass accumulation rates for each core since the last glacial maximum. Variations in sediment fluxes to slopes of Queensland Trough are discussed, with particular emphasis on the siliciclastic component, and the implications for terrigenous sediment transport and deposition on the northeast Australian margin in response to late Quaternary sea-level changes.

Secondly, previous studies have suggested that carbonate fluxes to slopes offshore the central GBR province were highest during the last postglacial transgression, at the same time as highest fluxes of siliciclastic sediment. Similarly to patterns of siliciclastic deposition during the latest Quaternary, this response is also not consistent with conventional models for continental margin evolution, and is confirmed by the mass accumulation rate records discussed in Chapter 2. Most previous literature concerning carbonate sedimentation on the slope of the northeast Australian margin has circumvented this issue, with the notable exception of Dunbar and Dickens (2003b), who concluded that although bulk carbonate fluxes to the slope were highest during transgression, highest fluxes of neritic components occurred during the Holocene highstand. This conclusion in itself fails to account for the unexpected record of carbonate accumulation rates on slopes east of the GBR during the last postglacial transgression. Chapter 3 presents the results of a study intended to address the anomalous history of carbonate deposition on slopes offshore the central GBR

province, and is derived from a manuscript intended for submission to the journal *Sedimentology* entitled: *Periplatform carbonate accumulation on slopes east of the Great Barrier Reef since the Last Glacial Maximum: Toward a coherent model for sedimentation in a tropical mixed siliciclastic-carbonate system*, by Michael C. Page and Gerald R. Dickens.

In this study presented in Chapter 3, six well-dated cores from the upper to lower slope of the western Queensland Trough, situated between ~15 and 18°S, were examined for downcore variations in carbonate mineralogy and Sr concentration. One core was also examined for variations in macroscopic sedimentary components. These datasets, coupled with previously determined records of bulk sediment accumulation rates, enabled the quantification of mass accumulation rates for individual carbonate components in each core since the last glacial maximum. Mechanisms for observed carbonate accumulation rate records are discussed in relation to sea-level changes over the last glacial-interglacial cycle, and a model is proposed for the latest Quaternary evolution of the central GBR province that accounts for both siliciclastic and carbonate components of slope sediments.

Thirdly, previously most research concerning sediment deposition on slopes of the northeast Australian margin has focused on Queensland Trough, offshore of the central GBR province. Accordingly, the deposition of mixed siliciclastic-carbonate sediments offshore of other regions of the northeast Australian margin during the Late Pleistocene and Holocene remains largely unconstrained. The significance of previous work is particularly unclear with respect to the southern GBR province, because this region is fundamentally different than the area to the north: the hinterland is located wholly within the dry tropics, the GBR platform is two to four times wider, and off-shelf sedimentation takes place on the shallowly submerged Marion Plateau. Chapter 4

presents the results of a study intended to investigate sedimentation offshore the southern GBR province, and is derived from a manuscript published in the journal *Marine Geology* (v. 219 pp. 27-45) entitled: *Sediment fluxes to Marion Plateau (southern Great Barrier Reef province) over the last 130 ky: New constraints on 'transgressive-shedding' off northeastern Australia*, by Michael C. Page and Gerald R. Dickens.

In this study presented in Chapter 4, one core from the western edge of Marion Plateau, immediately seaward and down-slope of the present GBR, was examined for downcore variations in bulk carbonate content, carbonate mineralogy, and bulk carbonate Sr concentration. Age models were developed based on three radiocarbon dates and high-resolution stable isotope stratigraphy throughout the core length. The combination of these datasets enabled the quantification of mass accumulation rates for siliciclastic and bulk carbonate components, as well as for individual carbonate minerals, from the last interglacial (marine isotope substage 5e), through the last glacial cycle and into the Holocene highstand. Variations in siliciclastic and carbonate fluxes to Marion Plateau are discussed with respect to over 130 ky of sea-level changes, and are compared to the observed record from Queensland Trough. A model is proposed for the observed patterns of mixed siliciclastic-carbonate sediment deposition offshore of the southern GBR province.

Appended after the main body of the thesis are two associated research papers. Appendix A contains a manuscript concerning the amino-stratigraphy of late Pleistocene–Holocene sediments east of the GBR, and stems from a manuscript prepared for submission to the journal *Quaternary Research* entitled: *High-resolution amino-stratigraphy of cores from Queensland Trough and Marion Plateau: insights into AAR kinetics in the western Coral Sea since the Last Glacial Maximum*, by

Michael C. Page, Michael J. O'Leary, Paul J. Hearty, and Darrell S. Kaufman. This study forms part of a pilot program evaluating the utility of amino acid racemization in single foraminifers as a geoscientific tool for investigations involving Quaternary marine sediments. Amino-stratigraphies were developed for five cores from the western slope of Queensland Trough, and for one core from the western edge of Marion Plateau. Downcore progressions in the D-alloisoleucine/L-isoleucine ratios of aspartic acid are discussed, and the kinetic pathway of racemization is modelled over the last 20 to 25 ky. The effects of different bottom water temperatures on racemization rates at the cored sites are investigated, and paleoceanographic implications of the study presented.

Appendix B contains a data report on the bulk carbonate content of sediments recovered from Ocean Drilling Program (ODP) Hole 1198A, drilled during ODP Leg 194 on Marion Plateau. The appendix is derived from a manuscript published in: Anselmetti, F.S., Isern, A.R., Blum, P., and Betzler, C. (Eds.), *Proceedings of the Ocean Drilling Program, Scientific Results, Leg 194* (Online), available from World Wide Web: http://www-odp.tamu.edu/publications/194_SR/004/004.htm, entitled: *Data Report: Variations in bulk carbonate content, Hole 1198A, 0–23.69 mbsf*, by Michael C. Page. The data report presents baseline information on the deposition of mixed siliciclastic-carbonate sediments on Marion Plateau, and discusses cyclic variations in bulk carbonate content and their potential relationship with sea-level changes since the mid-Pleistocene.

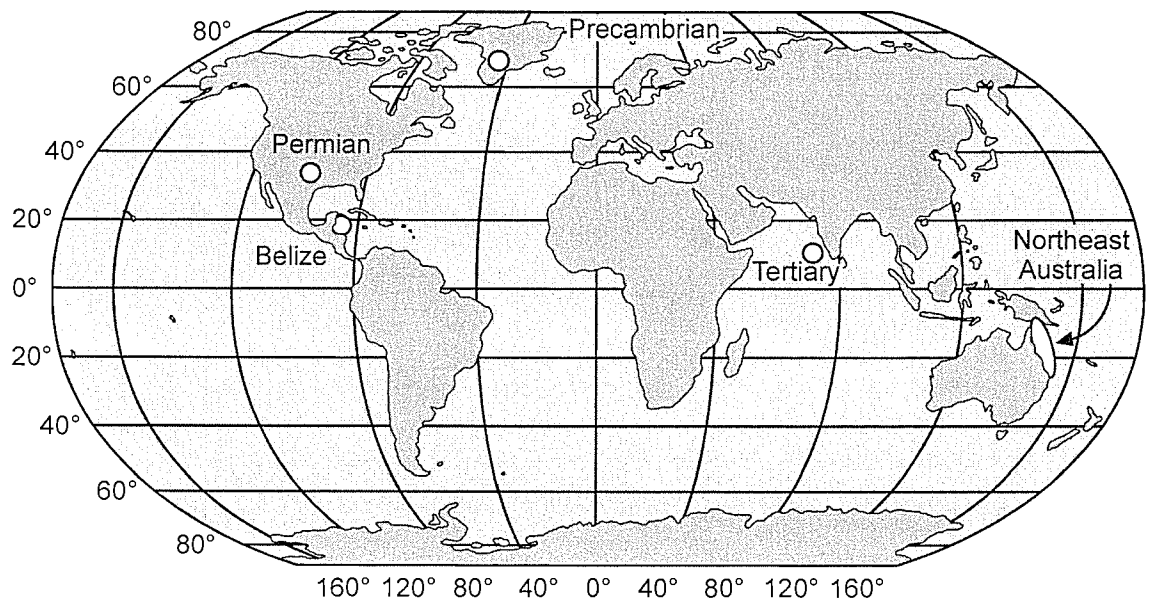


Figure 1.1: Global map showing the location of some modern and ancient examples of mixed siliciclastic-carbonate depositional systems. The regional name of modern examples is indicated, as is the age of examples in the geological record.

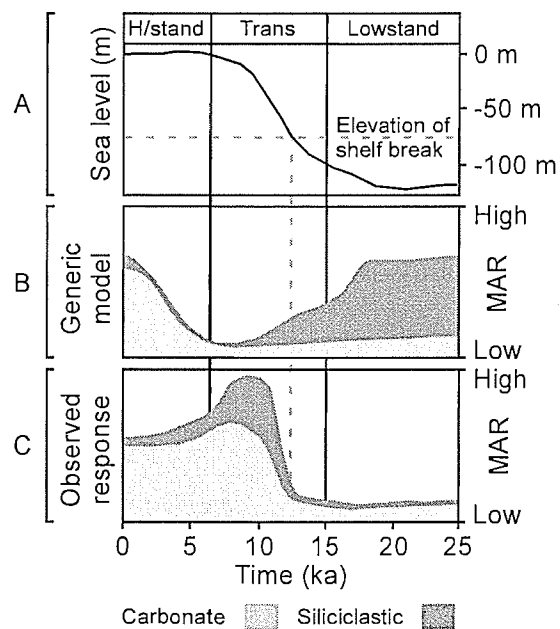


Figure 1.2: (A) Eustatic change since 25 ka. (B) Generic depositional model for sediment deposition on slopes of tropical mixed siliciclastic-carbonate systems. (C) Schematic representation of observed sedimentation patterns on slopes of the northeast Australian margin. H/stand – sea-level highstand. Trans – transgression. Lowstand – sea-level lowstand. MAR – mass accumulation rate.

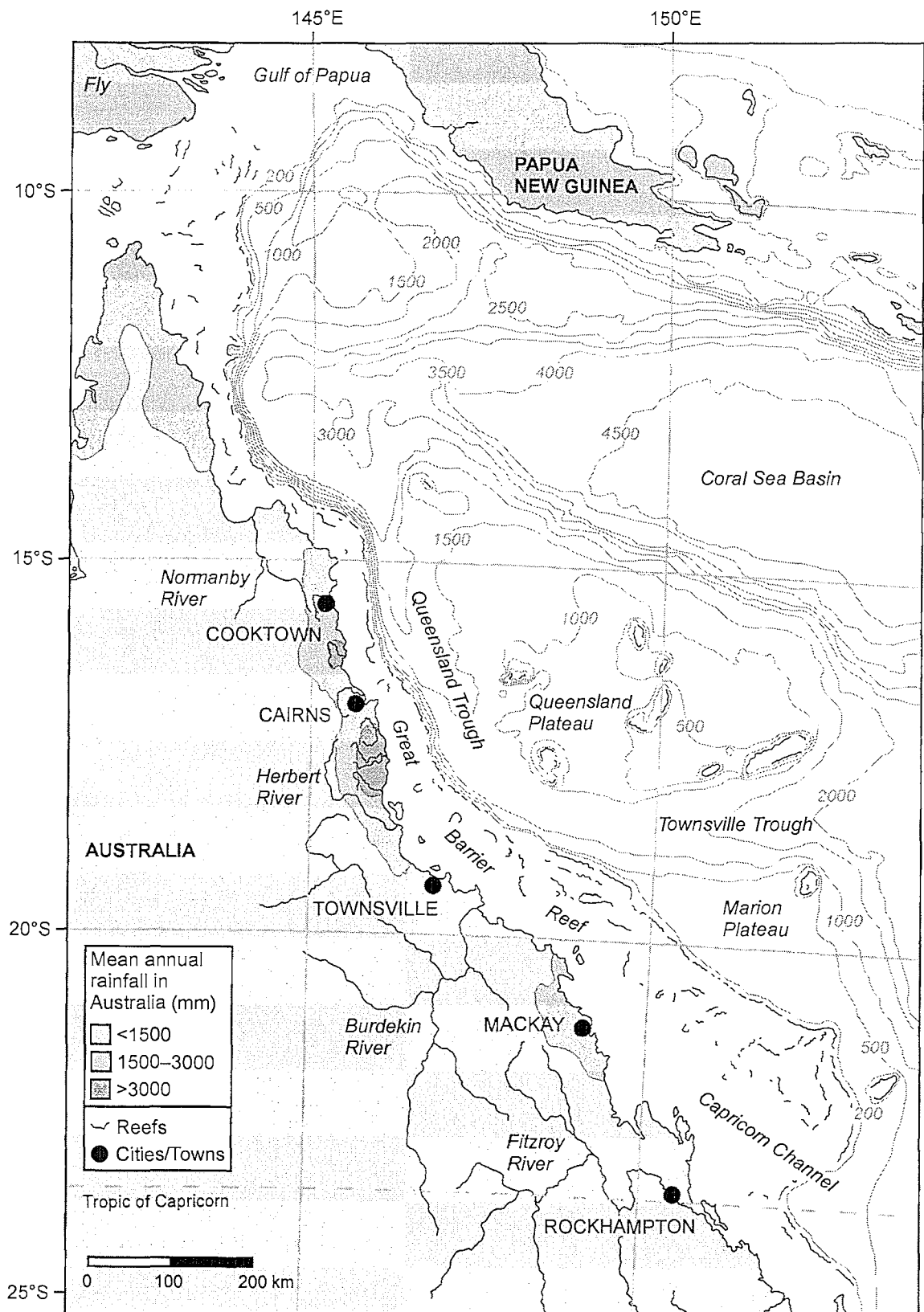


Figure 1.3: The northeast continental margin of Australia, including mean annual rainfall, the location of major rivers draining the hinterland, distribution of modern reefs of the Great Barrier Reef, and bathymetric features of the western Coral Sea.

CHAPTER 2

Tropical view of Quaternary sequence stratigraphy:
Siliciclastic accumulation on slopes east of the Great
Barrier Reef since the Last Glacial Maximum

Michael C. Page

School of Earth Sciences, James Cook University, Townsville, QLD 4811, Australia

Gerald R. Dickens

Department of Earth Sciences, Rice University, Houston, Texas 77005, USA

Gavin B. Dunbar

Antarctic Research Centre, Victoria University, Wellington, New Zealand

Adapted from a paper published in:

Geology

November 2003, Volume 31, Number 11, Pages 1013-1016

ABSTRACT

Generic models of continental-margin evolution predict that siliciclastic fluxes to slopes should be maximal and minimal during major sea-level lowstands and transgressions, respectively. Here we document the opposite for the northeast Australian margin, the largest extant mixed siliciclastic-carbonate depositional system. Cores from slopes of this margin consistently contain siliciclastic-rich intervals, ~0.3–1-m-thick, in the upper few meters. Radiocarbon dates of planktonic foraminifera show that this interval was deposited between 12 and 7 ka and represents greatly increased siliciclastic fluxes during transgression. This massive terrigenous discharge to slopes occurred along at least 450 km of the margin, irrespective of modern variations in bathymetry or climate. Although we cannot dismiss a significantly different early Holocene climate with greatly enhanced sediment discharge, available data instead suggest that rivers aggraded on the shelf during lowstand because of an extensive subaerially exposed reef system that formed a barrier to off-shelf sediment transport. This phenomenon may occur on other margins rimmed by reefs, requiring a major revision of concepts used to interpret mixed siliciclastic-carbonate systems.

2.1. INTRODUCTION

According to widely accepted paradigms (Vail et al., 1977; Walker, 1992), major eustatic fluctuations predictably change the composition and patterns of sediment deposition on slopes of passive continental margins. Siliciclastic accumulation should be (1) high during lowstand when rivers flow across exposed shelves and discharge directly onto the slope, (2) very low during transgression when river mouths rapidly retreat landward with flooding of the shelf, and (3) low to moderate during highstand when sediments prograde across the shelf (Fig. 1.2B). Implicit in this conventional wisdom is that rivers incise across exposed shelves during lowstands in an attempt to equilibrate with depositional base level (Miall, 1991; van Heijst and Postma, 2001). But what happens on tropical margins where rivers flow onto shelves rimmed by extensive carbonate reefs? During lowstands, subaerially exposed reefs would produce topographic highpoints, which might inhibit fluvial incision and result in sediment deposition on the shelf (Miall, 1991; Woolfe et al., 1998). Most literature has circumvented this issue. In particular, studies of slope environments in ancient mixed systems (e.g., Wilson, 1967; Dolan, 1989; Yang and Kominz, 2003) commonly interpret that highs in siliciclastic abundance correspond to sea-level lowstands. However, these interpretations usually stem from conventional models, which might be refined by examining in detail the relationship between sea level and sedimentation that is afforded by well-dated Quaternary successions.

The northeast Australian margin (Fig. 2.1) is the largest extant tropical mixed siliciclastic-carbonate depositional system. For >500 ky (e.g., Davies and McKenzie, 1993; International Consortium for Great Barrier Reef Drilling, 2001), rivers have discharged large masses of clay, quartz, and other weathered residue onto a shelf that hosts numerous carbonate reefs. Presently, these reefs collectively comprise the Great

Barrier Reef (GBR). East of the GBR, cores from the slope and basin and interpretations of seismic profiles show alternating siliciclastic-rich and carbonate-rich horizons in late Quaternary sediment (Harris et al., 1990; Davies and McKenzie, 1993; Glenn et al., 1993a; Dunbar et al., 2000; Dunbar and Dickens, 2003a). Following conventional models (Fig. 1.2B), siliciclastic-rich intervals on the slope have been interpreted as representing high siliciclastic accumulation rates during lowstands (Harris et al., 1990) or condensed sections formed during transgressions (Kronen and Glenn, 2000). Conversely, in the two cores with good age control (Ocean Drilling Program [ODP] Site 820, FR4/92 [RV *Franklin*, cruise 4/92] PC16, Fig. 2.1), the uppermost siliciclastic-rich interval clearly reflects increased siliciclastic accumulation rates during transgression between ca. 12 and 7 ka, whereas condensed sections formed during lowstand (Peerdeman and Davies, 1993; Dunbar et al., 2000, Fig. 1.2C). However, both cores come from the upper slope off a coastal region currently characterized by an unusually wet climate, but with minimal riverine inputs (Neil et al., 2002). Here we present and discuss results from six additional cores that form a 450 km transect along the slope of the northeast Australian margin (Fig. 2.1), and show that regardless of location, terrigenous sediment fluxes were highest during transgression.

2.2. LOCATION, SAMPLES, AND METHODS

Northeast Australia (Fig. 2.1) has distinct topographic differences that produce spatially variable rainfall and riverine discharge (Belperio, 1983; Neil et al., 2002). Between $\sim 15^{\circ}$ and 18° S, consistent, high rainfall results in relatively steady fluvial flow throughout the year, although with small sediment yields. By contrast, between $\sim 18^{\circ}$ and 20° S, sporadic rainfall leads to ephemeral fluvial systems but with relatively large annual sediment loads. The latter region includes the Burdekin River (Fig. 2.1), which

discharges >50% of the siliciclastic material to the margin (Belperio, 1983; Neil et al., 2002). Similar variability is evident in bathymetry. From south to north, shelf width progressively decreases and the slope steepens (Fig. 2.1).

Six cores were examined in this study (Fig. 2.1). These cores, from 1.8 to 4.5 m long and collected between 1985 and 1992 (Harris et al., 1990; Dunbar et al., 2000), were selected because they delineate a transect encompassing a range of potential controls on off-shelf siliciclastic fluxes (e.g., climate, bathymetry, sediment discharge). The southernmost core, 51GC43 (*RV Rig Seismic*, cruise 051), is located on the middle slope, 901 m below sea level (mbsl) and slightly northeast of the lowstand Burdekin system (Fielding et al., 2003). The northernmost core, FR5/90 PC27a, is located on the lower slope, 2163 mbsl, adjacent to an exceptionally narrow shelf. The remaining four cores, FR4/92 PC11, PC12, PC13, and PC14, are located on the middle slope, between 1320 and 1574 mbsl.

Sediment on the northeast Australian margin includes two basic components—terrigenous siliciclastics and biogenic carbonate—with only trace amounts of other material (Dunbar et al., 2000; Heap et al., 2001). Consequently, quantification of bulk carbonate content allows determination of siliciclastic abundance. Nominally 10 cm³ samples were taken every 5–10 cm down each core for determination of bulk carbonate content via the carbonate-bomb technique (Mueller and Gastner, 1971). Duplicate sample analyses and standard comparisons place the accuracy and precision of reported carbonate contents at $\pm 3\%$.

Ages were determined at 27 depths in the cores by radiocarbon analyses of pelagic planktonic foraminifera. Bulk samples were wet-sieved at 125 μm , and ~20 mg of *Globigerinoides sacculifer* and white *G. ruber* were picked from the coarse fraction after inspecting their preservation and rejecting specimens with secondary cements or

chamber infilling. Foraminifera were sonicated in Milli-Q ultrapure water to dislodge any remaining non-primary particles and collected by removing water and suspended fines with a pipette. Samples were analyzed by accelerator mass spectrometry (AMS) at the Australian Nuclear Science and Technology Organization (ANSTO). ANSTO reported ages as conventional ^{14}C years before present.

2.3. RESULTS

2.3.1. Carbonate Profiles

Bulk carbonate profiles (Fig. 2.2) are similar in all six cores. Carbonate contents (Table 2.1) are high at the surface, decrease across distinct dark grey intervals, and increase again at depth. Transitions between carbonate-rich and siliciclastic-rich intervals are gradational, apart from thin intervals at 1.01 m and 1.16 m in PC14, which have sharp lower boundaries, graded bedding, and abundant coarse-grained quartz, consistent with an interpretation that they are turbidites. Excluding turbidites, carbonate contents range from 83% to 29%, with maximum and minimum variation in PC13 (44%) and PC11 (39%). Thus, the dark grey intervals represent a nominal 40% increase in siliciclastic abundance. The siliciclastic-rich interval is thickest and deepest at PC27a and GC43, and thinnest and shallowest at PC11 and PC12. These observations agree with the general trend that siliciclastic-rich intervals thin away from the shelf (Dunbar et al., 2000).

2.3.2. Radiocarbon Ages

Extracted planktonic foraminifera give conventional ^{14}C ages (Table 2.2) between $22,100 \pm 140$ yr B.P. and 1680 ± 40 yr B.P. After corrections for atmospheric and marine reservoir effects using the CALIB 4.0 freeware program (Stuiver et al.,

1998), the dates of these samples are between 23,750 cal. yr B.P. (calibrated years before present) and 1250 cal. yr B.P. (Fig. 2.2). It is important to note that radiocarbon ages in each core increase with depth, as expected for primary pelagic material, but a trend not expected for reworked sediment. Equally important, radiocarbon ages in PC14 agree with age estimates from the oxygen isotope record of planktonic foraminifera at this site (Dunbar et al., 2000).

2.3.3. Timing and Accumulation of Siliciclastic-Rich Intervals

A dark grey, siliciclastic-rich horizon is evident in the upper 2 m of all cores. Across all sites, this horizon is dated between ca. 12 and 7 ka (Fig. 2.2). Given that sediment in these cores is essentially a two-component system, this horizon reflects a relative increase in the siliciclastic flux. An enhanced flux can be demonstrated by quantifying the mass-accumulation rate ($r_{ma,\alpha}$) of each component: $r_{ma,\alpha} = \alpha_{conc} \times \rho_{db} \times r_{bls}$, where α_{conc} is the amount (wt%) of component α , ρ_{db} is the dry bulk density including pore space, and r_{bls} is the bulk linear sedimentation rate, defined as the thickness of an interval divided by the time it represents. GC43, PC13, PC14 and PC27a were dated within the top 3 cm at 2460, 1250, 1940 and 1520 cal. yr B.P., respectively (Fig. 2.2). These “old surface ages” may reflect poor recovery of unconsolidated sediment at the seafloor. For cores without radiocarbon ages in the upper few centimeters, we assumed an average age of 1780 cal. yr B.P. for calculating the values of r_{bls} . The ρ_{db} was assumed to be $1.0 \text{ g}\cdot\text{cm}^{-3}$, typical for shallow seafloor sediments on the continental slope of northeastern Australia (Davies et al., 1991).

Mass-accumulation rates were determined for siliciclastic and carbonate components down each core (Fig. 2.3), and consistently show that the uppermost siliciclastic-rich intervals resulted from increased siliciclastic fluxes, up to six times

greater than before 12 ka. Notably, the maxima coincide with increased carbonate mass-accumulation rates, a response opposite to that predicted by generic models (e.g., Walker, 1992). As suspected by others (Peerdeman and Davies, 1993; Dunbar et al., 2000), siliciclastic-rich intervals represent periods of enhanced siliciclastic and carbonate fluxes, but with much larger increases in the former. A marked increase in the absolute abundance of high-Mg calcite within siliciclastic-rich intervals strongly suggests a neritic origin for the carbonate (Dunbar and Dickens, 2003b).

2.4. DISCUSSION

All cores studied have a prominent high in siliciclastic abundance in the upper 2 m, possibly corresponding to the first subsurface reflector on shallow seismic profiles and the uppermost siliciclastic-rich horizon in other sediment cores. Applying conventional concepts, this interval has been interpreted as representing the Last Glacial (Harris et al., 1990). However, our results unequivocally show that regardless of location, it was deposited during transgression (Lambeck and Chappell, 2001), when sea level relative to the northeast Australian margin rose above the shelf-slope break (Figs. 1.2A, 2.3).

Although recognizing that siliciclastic-rich intervals coincide with transgression, Glenn et al. (1993a) and Kronen and Glenn (2000) suggested that they represent sequence condensation. Their primary argument was that at ODP Site 821 these intervals contain “pristine” verdine, a mineral formed near the seafloor when sediment slowly accumulates in shallow, tropical waters (Odin and Sen Gupta, 1988). The data presented here and elsewhere (Peerdeman and Davies, 1993; Dunbar et al., 2000) are inconsistent with their interpretation. Possibly the verdine occurs just below the siliciclastic-rich intervals or is reworked from condensed sections upslope, which

would support work indicating condensed lowstand sections on the upper slope (Peerdeman and Davies, 1993; Dunbar et al., 2000).

The northeast Australian margin clearly behaves differently than predicted from generic models for continental-margin evolution. Tectonism and climate have increasingly been invoked as explanations for significant deviations from model expectations (e.g., Rankey, 1997; Galloway, 1998; Goodbred and Kuehl, 2000). There is no evidence or reason to suspect regional uplift on this passive margin at ca. 11–7 ka.

However, increased rainfall appears to characterize low-latitude regions of the Eastern Hemisphere during this time (Thomas and Thorp, 1995). Palynological records suggest that the precipitation rate west of Cairns (Fig. 2.1) rose from ~600 to 3000 mm/yr since 18 ka, with the majority of increase occurring between 11 and 7 ka (Kershaw, 1985). This increase may have dramatically escalated fluvial discharge to the coast, as argued to explain increased siliciclastic accumulation rates on shelves of other low-latitude margins in the early Holocene (Thomas and Thorp, 1995; Goodbred and Kuehl, 2000). For the northeast Australian margin, however, we note that (1) enhanced precipitation could have increased vegetation, consequently reducing riverine sediment loads (Neil et al., 2002), (2) the lowstand Burdekin River had channel characteristics similar to those of the modern system (Fielding et al., 2003), suggesting similar discharges, and (3) evidence for elevated early Holocene sediment deposition on the shelf is not apparent (Johnson and Searle, 1984; Harris et al., 1990; Heap et al., 2001).

Alternatively, we suggest that the mixed nature of the margin strongly influences siliciclastic transport and deposition. Specifically, during lowstands, reefs on the outer GBR shelf were subaerially exposed (Marshall and Davies, 1984; International Consortium for Great Barrier Reef Drilling, 2001), forming an extensive

chain of hills that would force rivers to aggrade on the outer shelf (Woolfe et al., 1998). Seismic profiles indicate that the Burdekin River failed to incise the outer 10 km of the GBR shelf, and thus did not grade to depositional base level when sea level was below the shelf edge during the Last Glacial (Fielding et al., 2003). Consequently, siliciclastic material might have “ponded” behind carbonate highs on the outer shelf during lowstand (Rankey et al., 1999), discharging to slopes and basins only after sea level rose above the shelf-slope break and waves, tidal currents, and cyclones could erode and remobilize sediment (Steckler et al., 1999; Dunbar et al., 2000). Notably, a major pulse in mangrove pollen marks the siliciclastic-rich interval at ODP Site 820 (Grindrod et al., 1999). The co-accumulation of terrigenous material, high-Mg calcite, and mangrove pollen on the slope during transgression may collectively signal the release of nearshore sediment when sea level on the shelf surpasses a critical depth.

The northeast Australian margin represents an excellent modern example of a tropical mixed siliciclastic-carbonate depositional system. Over the past 25 ky, maximum and minimum siliciclastic fluxes to slopes of this margin occurred during transgression and lowstand, respectively (Fig. 2.3). Although we do not fully understand the cause of this depositional behaviour, it diverges significantly from generic models of continental-margin evolution, as well as the record inferred from many ancient mixed systems. Furthermore, key hypotheses proposed to explain the latest Quaternary evolution of the northeast Australian margin, including the effect of subaerially exposed topographic highs on siliciclastic transport and deposition, have been identified on other mixed siliciclastic-carbonate margins in both the modern (Ferro et al., 1999) and ancient (Rankey et al., 1999) geological record. The patterns of slope sedimentation identified on the northeast Australian margin may also occur on other margins where rivers and reefs interact over space and time, and may constitute a

fundamental response of passive continental margins to sea-level changes. In particular, the role of transgressions in the development of continental slope sequences, especially along tropical mixed siliciclastic-carbonate margins, warrants further investigation.

ACKNOWLEDGMENTS

This research was supported through a James Cook University Earth Science Scholarship, an Australian Postgraduate Award, an AAPG Foundation Grant-In-Aid, the CRC Reef/Ken Woolfe Scholarship (to Page), and an Australian Research Council Small Grant (to Woolfe and Dickens). The Australian Nuclear Science and Technology Organisation provided AMS analysis under Australian Institute of Nuclear Science and Engineering grants 98/143R, 00/038, 01/042P, and 03/056. We thank Paul Hearty for his generous contribution of AMS analyses under grant 03/056. Thanks are also extended to Stephen Pekar, Eugene Rankey, and Andrew Heap, for reviews and constructive comments that improved this paper.

Core	Core depth (cm)	Carbonate content (wt %)	Core	Core depth (cm)	Carbonate content (wt %)
51GC43	5.5	72	FR4/92-PC11	12.0	78
	19.5	71		23.0	77
	37.0	67		28.0	76
	55.0	55		34.0	70
	66.0	54		39.0	68
	75.0	44		44.0	65
	84.0	44		52.0	51
	96.0	38		59.0	53
	106.0	30		67.0	72
	122.0	31		74.0	74
	134.0	34		83.0	76
	154.0	40		89.0	79
	171.0	44		93.0	78
	177.5	44		98.0	81
	182.5	40		102.0	83
	190.0	31		109.0	81
	193.5	33		116.0	78
	201.5	30		123.0	76
	207.5	35		129.0	74
	212.0	42		136.0	68
	220.5	29		142.0	75
	223.5	37		151.0	81
	232.5	47		159.0	82
	239.0	46		168.0	77
	253.5	70		177.0	68
				185.0	67
				193.0	69
				203.0	75
				212.0	76
				220.0	67
				228.0	66
				235.0	65
		242.0	65		
		252.0	68		
		262.0	74		
		273.0	77		
		285.0	73		
		294.0	71		
		303.0	72		
		310.0	54		
		317.0	59		
		327.0	45		
		335.0	65		
		344.0	45		
		352.0	51		
		361.0	66		
		373.0	77		
		378.0	77		
		382.0	62		
		389.0	54		
		397.0	45		

Core	Core depth (cm)	Carbonate content (wt %)	Core	Core depth (cm)	Carbonate content (wt %)
FR4/92-PC12	10.0	70	FR4/92-PC13	8.0	71
	17.0	69		22.0	57
	28.0	57		34.0	66
	38.0	49		45.0	64
	46.0	46		55.0	59
	53.0	44		66.0	47
	60.0	49		76.0	45
	67.0	61		83.0	59
	75.0	57		87.0	69
	85.0	64		95.0	71
	94.0	63		105.0	77
	102.0	65		115.0	82
	112.0	74		124.0	82
	120.0	73		132.0	76
	130.0	77		143.0	75
	137.0	69		153.0	71
	146.0	68		163.0	77
	154.0	67		172.0	78
	163.0	70		183.0	68
	170.0	64		193.0	66
	178.0	66		203.0	69
	184.0	75		213.0	73
	195.0	80		223.0	73
	207.0	83		233.0	70
	219.0	78		243.0	63
	225.0	72		253.0	62
	236.0	66		262.0	60
	247.0	72		273.0	64
	257.0	69		282.0	68
	265.0	74		292.0	74
	274.0	70		302.0	76
	285.0	57		312.0	69
	295.0	60		322.0	64
	305.0	68		332.0	69
315.0	63	342.0	63		
325.0	60	353.0	55		
335.0	59	363.0	38		
345.0	70	369.0	39		
		373.0	49		
		381.0	50		
		391.0	61		

Core	Core depth (cm)	Carbonate content (wt %)	Core	Core depth (cm)	Carbonate content (wt %)
FR4/92-PC14	21.0	67	FR5/90-PC27a	18.0	57
	30.0	64		30.0	61
	35.0	56		41.0	61
	41.0	61		53.0	61
	48.0	61		64.0	62
	56.0	56		76.0	49
	63.0	51		87.0	54
	71.0	41		98.0	52
	78.0	36		109.0	43
	86.0	45		119.0	44
	92.0	59		143.0	39
	98.0	45		154.0	47
	101.0	24		165.0	40
	102.5	58		176.0	48
	108.0	58		187.0	58
	110.5	64		198.0	59
	116.0	31		209.0	67
	119.0	69		220.0	59
	123.0	64		231.0	49
	131.0	71		242.0	48
139.0	76	253.0	52		
146.0	74	264.0	54		
154.0	76	273.0	57		
161.0	73	294.0	57		
167.0	69	305.0	62		
175.0	67	316.0	67		
182.0	68	327.0	68		
		338.0	76		
		349.0	74		
		360.0	65		
		371.0	75		
		382.0	78		
		393.0	71		

Table 2.1: Measured bulk carbonate content in cores 51GC43, FR4/92 PC11, FR4/92 PC12, FR4/92 PC13, FR4/92 PC14, and FR5/90 PC27a.

Lab code	Core depth (cm)	Conventional 14C age (yrs BP)	Error (yrs +/-)	Calibrated 14C age (yrs BP)	1 SIGMA error (yrs +/-)
<u>51GC43</u>					
OZF296	5	2760	40	2460	80
OZG452	31	5570	50	5930	40
OZG453	48	7810	60	8290	80
OZE893	75	8600	50	9010	160
OZE894	152	10370	50	11120	370
OZG454	171	12680	80	14130	420
OZF297	211	18230	140	21080	360
<u>FR4/92-PC11</u>					
OZF724	36	6490	50	6980	60
OZE875	60	9530	50	10280	90
OZF725	79	16180	90	18720	300
<u>FR4/92-PC12</u>					
OZF723	30	6660	50	7200	40
OZE876	59	9750	50	10460	150
<u>FR4/92-PC13</u>					
OZG455	5	1680	40	1250	30
OZF299	55	7690	50	8150	40
OZE874	79	10300	50	10990	380
OZF722	104	20550	140	23750	440
<u>FR4/92-PC14</u>					
OZF298	24	2330	40	1940	50
OZE808	75	9180	60	9820	150
OZE809	88	10980	60	12490	330
OZE810	109	14370	80	16640	250
<u>FR5/90-PC27a</u>					
OZG450	7	1960	40	1520	40
OZG451	52	4760	50	4990	70
OZD814	82	7160	90	7620	60
OZD815	156	9320	90	9910	230
OZD816	200	11250	160	12870	170
OZD817	224	12900	150	14340	580
OZG449	318	22100	140	N.A.	N.A.

Table 2.2: Results of accelerator mass spectrometry radiocarbon analyses and calibration of conventional ages for cores 51GC43, FR4/92 PC11, FR4/92 PC12, FR4/92 PC13, FR4/92 PC14, and FR5/90 PC27a. (N.A.–Beyond the range of calibration)

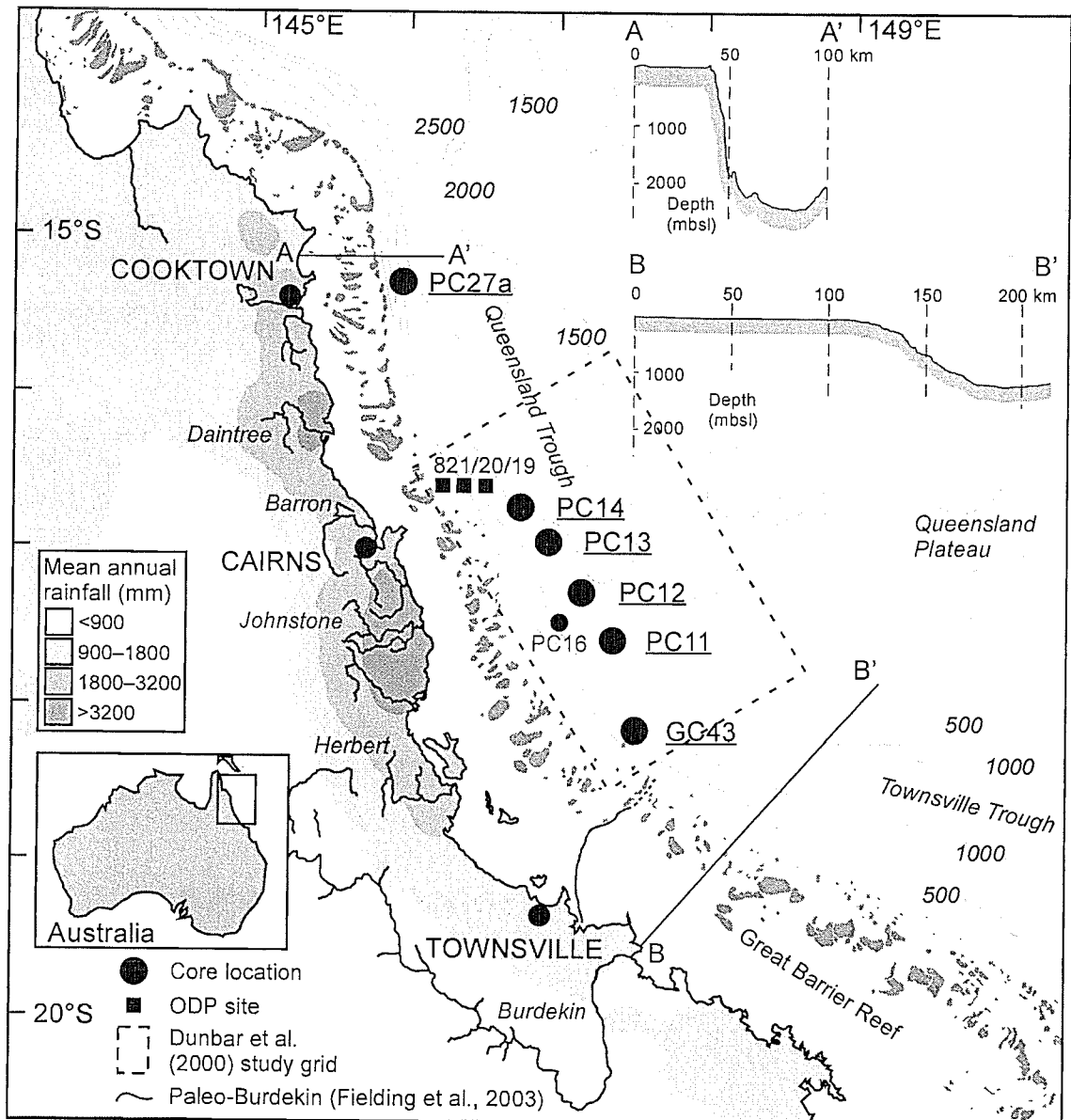


Figure 2.1: The northeast Australian margin between ~15 and 20°S, including mean annual rainfall, location of major rivers, distribution of modern reefs on the shelf, bathymetry (m) of the western Coral Sea, and location of cores FR5/90 PC27a, ODP Holes 819, 820 and 821, FR4/92 PC14, FR4/92 PC13, FR4/92 PC12, FR4/92 PC16, FR4/92 PC11, and 51GC43.

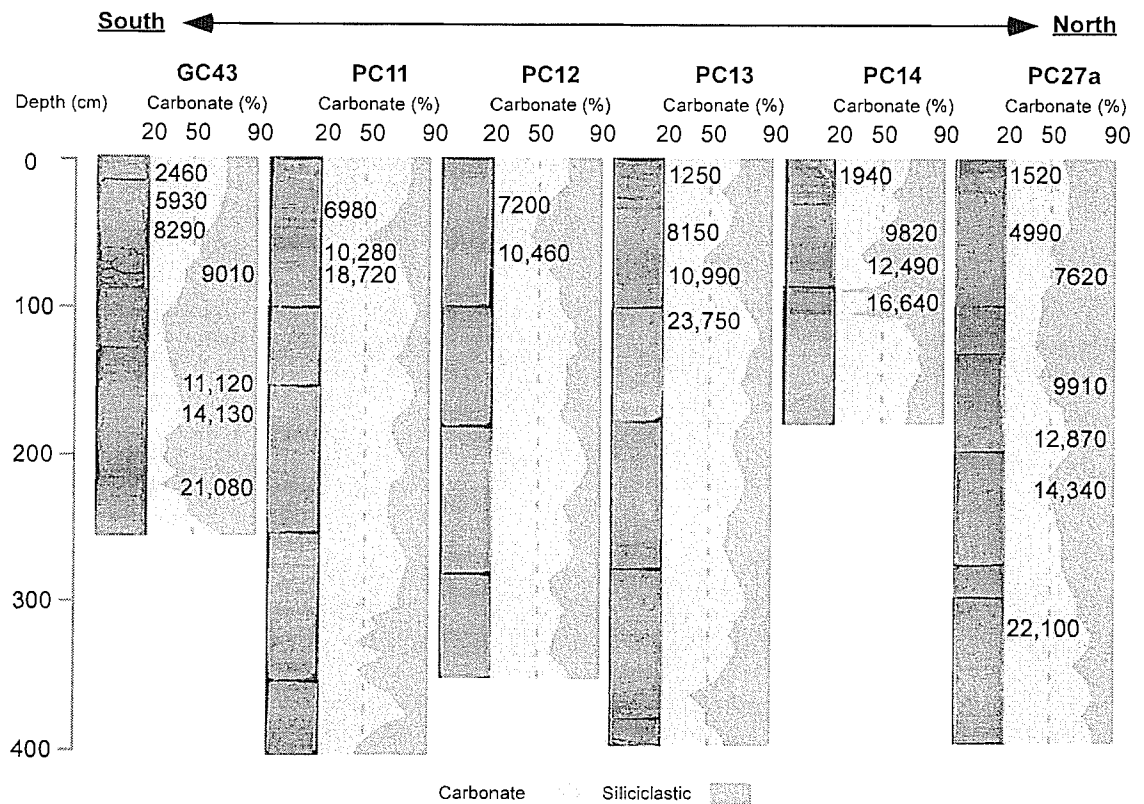


Figure 2.2: Downcore profiles of bulk carbonate content for cores 51GC43, FR4/92 PC11, FR4/92 PC12, FR4/92 PC13, FR4/92 PC14, and FR5/90 PC27a, and radiocarbon ages (calibrated years before present) of planktonic foraminifera.

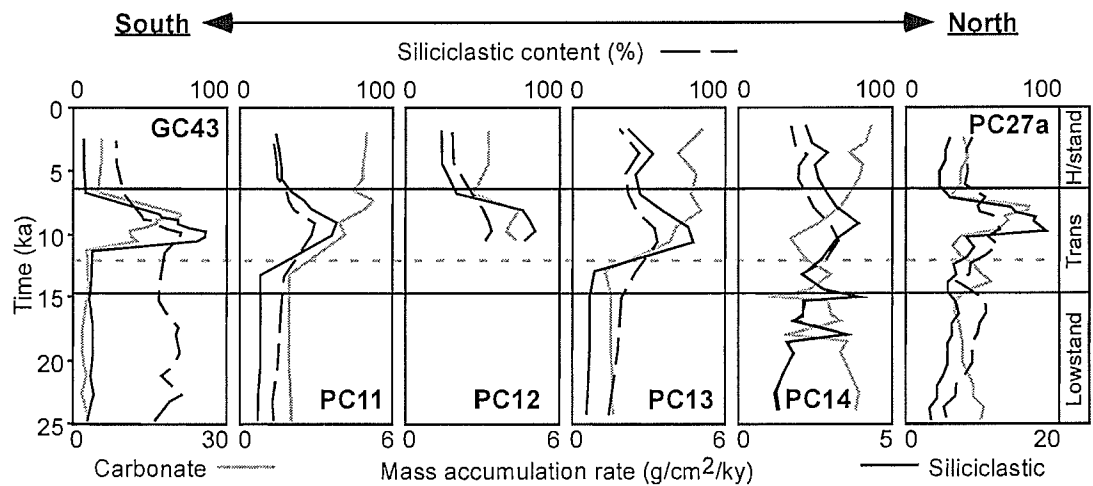


Figure 2.3: Mass-accumulation rates of siliciclastic and carbonate sediment in cores 51GC43, FR4/92 PC11, FR4/92 PC12, FR4/92 PC13, FR4/92 PC14, and FR5/90 PC27a. Dashed line approximates the time when sea level reached the shelf edge (ca. 12 ka). H/stand—sea-level highstand; Trans—sea-level transgression; Lowstand—sea-level lowstand.

CHAPTER 3

Periplatform carbonate accumulation on slopes east of the
Great Barrier Reef since the Last Glacial Maximum:
Toward a coherent model for sedimentation in a tropical
mixed siliciclastic-carbonate system

Michael C. Page

School of Earth Sciences, James Cook University, Townsville, QLD 4811, Australia

Gerald R. Dickens

Department of Earth Sciences, Rice University, Houston, Texas 77005, USA

Adapted from a paper intended for submission to:

Sedimentology

ABSTRACT

The northeast Australian margin, including the Great Barrier Reef, is the largest modern example of a tropical mixed siliciclastic-carbonate depositional system, where both rivers and reefs contribute large quantities of sediment. In contrast to generic models for these systems, during the late Quaternary maximum accumulation rates of siliciclastic and carbonate sediments on the slope occurred during transgression ca. 12–7 ka, rather than during the last glacial lowstand and Holocene highstand, respectively. Here we document changes in the relative abundance and mass accumulation rates (*MARs*) of low-Mg calcite (LMC), aragonite, and high-Mg calcite (HMC) in six well-dated cores from the upper to lower slope to investigate bulk carbonate accumulation rate patterns. In general, as a percent of total carbonate the relative abundance of LMC is highest away from the shelf and during lowstand, whereas the relative abundances of aragonite and HMC are highest close to the shelf and during highstand. Mostly, however, the *MARs* of individual carbonate minerals are in-phase with the *MARs* of both the bulk siliciclastic and carbonate components. Accumulation rates of LMC, aragonite, and HMC were low during lowstand, increased significantly during transgression, and tapered to moderate levels during highstand. The *MARs* of each of the carbonate components generally decrease away from the shelf, especially during transgression and highstand. Bulk carbonate strontium concentrations also suggest that most aragonite comes from neritic organisms. Thus, the high fluxes of aragonite and HMC to the slope during transgression are attributed to elevated neritic productivity when sea level began to flood the shelf. Analyses of sieved grains show that a significant fraction of LMC, particularly during transgression, is weathered reefal debris. The amplified *MAR* of LMC during transgression is therefore explained by the remobilisation of neritic carbonate from the outer shelf that had been subaerially

exposed and diagenetically altered during lowstand. Our work demonstrates that initiation and rapid expansion of shallow water coralgall communities was synchronous with massive off-shelf fluxes of siliciclastic sediment, and indicates that most new reef growth either occurred on bathymetric highs above muddy water, or was unaffected by high turbidity and high suspended sediment concentrations in the water column. The established depositional paradigm for tropical mixed systems, which has the highest accumulation rates of siliciclastic and carbonate sediment on slopes during sea-level highstand and lowstand, respectively, is not consistent with Late Quaternary sedimentation on slopes of the northeastern Australian margin, because important concepts (e.g., antecedent topography, shallow water sediment remobilisation) are not emphasized.

3.1. INTRODUCTION

The sedimentology of continental margins traditionally has been studied within the framework of idealized siliciclastic or carbonate systems, depending on whether rivers or shallow marine ecosystems dominate sediment supply (e.g., Posamentier and Vail, 1988; James and Kendall, 1992; Handford and Loucks, 1993; Schlager et al., 1994). For both cases, widely accepted paradigms predict how major fluctuations in sea level could affect sediment accumulation rates on continental slopes. These models suggest that siliciclastic accumulation rates should be: (1) high during lowstand, when rivers flow across exposed shelves and discharge directly onto the slope, (2) very low during transgression, when rivers rapidly retreat landward with flooding of the shelf, and (3) low to moderate during highstand, when sediments prograde across the shelf. In contrast, carbonate accumulation rates should be: (1) low during lowstand, when shallow marine accommodation space is restricted to a narrow zone on the upper slope, (2) moderate to high during transgression, when shallow marine accommodation space expands on to the shelf, and (3) high during highstand, when accommodation space is maximised on the flooded shelf.

Many continental margins at low latitudes receive significant amounts of both siliciclastic sediment from rivers and carbonate sediment from shallow marine sources such as reefs (cf. Mount, 1984). Sedimentologists commonly refer to these margins as tropical mixed siliciclastic-carbonate systems, and examples can be found off the modern coasts of northeast Australia (e.g., Davies et al., 1991) and Belize (e.g., Jones and Desrochers, 1992), or in the rock record (e.g., Permian strata in west Texas and New Mexico: Borer and Harris, 1991). Most literature discussing tropical mixed systems suggests that continental slopes record major eustatic changes in a manner predicted by depositional models for end-member siliciclastic and carbonate systems

(e.g., Wilson, 1967; Dolan, 1989; Harris et al., 1990; Foreman et al., 1991; Tucker and Chalcraft, 1991; James and Kendall, 1992; Kronen and Glenn, 2000). Accordingly, highs in siliciclastic accumulation rates on the slope should mark lowstands, highs in carbonate accumulation rates should mark highstands, and condensed intervals with low accumulation rates of both components should mark major transgressions (Fig. 1.2B). Crucially, much of this work has been based on stratigraphic sections in the ancient rock record, where accumulation rates are difficult to quantify.

The northeast continental margin of Australia (Fig. 3.1), including the Great Barrier Reef (GBR), represents the largest extant tropical mixed siliciclastic-carbonate system (Belperio and Searle, 1988; Neil et al., 2002). Recent investigations of well-dated late Quaternary sediment cores from slopes east of the GBR have revealed fundamental inconsistencies with widely accepted models for mixed system evolution (Figs. 1.2C, 3.2). Most notably, over the last 25 ky, both siliciclastic and carbonate accumulation rates on the slope were lowest during lowstand ca. 25–12 ka, when the shelf was exposed, highest during transgression ca. 12–7 ka, when sea level rose above the shelf, and moderate during highstand ca. 7 ka to present, when the shelf was flooded (Peerdeman and Davies, 1993; Dunbar et al., 2000; Dunbar and Dickens, 2003a; Page et al., 2003; Page and Dickens, 2005).

Two end-member models, emphasizing either antecedent topography or climate, have been proposed to account for the unexpected patterns of siliciclastic deposition on slopes of the northeast Australian margin (Dunbar and Dickens, 2003a; Page et al., 2003; Page and Dickens, 2005). The anomalous history of carbonate deposition, however, lacks a sufficient explanation (Dunbar and Dickens, 2003b; Page et al., 2003). In this paper, we quantify variations in the relative abundance and accumulation rates of low-Mg calcite (LMC), aragonite, high-Mg calcite (HMC), and bulk Sr in six cores

from the slope of the northeast Australian margin. This work establishes a clear baseline for understanding the distribution and flux of carbonate minerals on this margin over space and time. We demonstrate that the high carbonate accumulation rates on the continental slope during transgression were most pronounced near the shelf and resulted from increased fluxes of all carbonate minerals. We explain these observations, as well as the changes in accumulation rates of siliciclastic material, through changes in sediment production and the remobilisation of sediment on the shelf during transgression. The results of this study illustrate a new model for sediment dynamics on a tropical mixed siliciclastic-carbonate margin, which may be applicable to the study of other mixed siliciclastic-carbonate systems throughout the geological record.

3.2. BACKGROUND

The continental margin of northeast Australia between 15 and 18.5° S latitude (Fig. 3.1) can be divided into four large physiographic regions (Scott, 1993): (1) a hinterland of steep mountains and broad coastal plains, (2) a broad, low-gradient shelf rimmed by the extensive chain of barrier reefs and bathymetric highs of the GBR, (3) the Queensland Trough (QT), a north-south trending rift-basin with water depths exceeding 2100 m, and (4) the Queensland Plateau, a detached carbonate platform with isolated reefs. Distinct variations in bathymetry are evident from south to north: shelf width decreases, reef density increases, the continental slope steepens, and the QT deepens.

Sediments on the northeast Australian margin comprise two basic components (e.g., Harris et al., 1990; Dunbar et al., 2000; Heap et al., 2001): (1) terrigenous siliciclastics such as quartz, clays and other weathered residue, and (2) marine biogenic

carbonates composed of LMC, aragonite, and HMC. As such, the carbonate content of bulk sediment reflects the relative abundance of both components (Heap et al., 2001). Carbonate contents of surface sediment vary across the margin, reflecting in part proximity to sediment sources. Carbonate contents are lowest on the inner-shelf, where a siliciclastic sediment prism occurs between the 5 and 25 m isobaths, increase across the middle shelf, and reach nearly 100% adjacent to coral reefs on the outer shelf (Belperio, 1983; Dunbar and Dickens, 2003b). East of the GBR, carbonate contents of surface sediment steadily decline toward the north along the axis of QT, dropping to below 50% about 100 km northeast of Cooktown (Dunbar et al., 2000; Sutherland, 2000; Dunbar and Dickens, 2003b). This pattern primarily represents elevated terrigenous accumulation rates in the northern QT (rather than diminished carbonate accumulation rates), although the source to sink pathway for the siliciclastic material remains enigmatic (Dunbar et al., 2000; Francis et al., 2003).

Surface distributions of carbonate minerals also display clear spatial trends across the outer GBR shelf and within QT (Dunbar and Dickens, 2003b). As a percent of total carbonate, aragonite and HMC contents decrease steadily with increasing distance from the GBR (and scattered reefs on the Queensland Plateau), whereas LMC content does the opposite. Additionally, bulk sediment Sr concentrations strongly co-vary with the relative abundance of aragonite, systematically decreasing away from reefs (Sutherland, 2000; Dunbar and Dickens, 2003b). These surface patterns are consistent with partitioning between neritic and pelagic carbonate (Sutherland, 2000; Dunbar and Dickens, 2003b), similar to that in sediment around the Bahamas (e.g., Boardman and Neumann, 1984; Heath and Mullins, 1984; Boardman et al., 1986; Droxler et al., 1988; Milliman et al., 1993). Close to reefs, carbonate is dominated by debris from corals and algae, which generally precipitate Sr-rich aragonite, and benthic foraminifera, which

precipitate HMC. Away from areas of neritic production, carbonate is dominated by tests of planktonic foraminifera and coccolithophorids, which precipitate Sr-poor LMC, and pteropods, which precipitate Sr-poor aragonite (e.g., Milliman, 1974).

Sediment cores from QT show that carbonate content changes in accordance with the last glacial-interglacial oscillation in sea level (e.g., Peerdeman and Davies, 1993; Dunbar et al., 2000; Dunbar and Dickens, 2003a; Page et al., 2003). The bulk carbonate content of sediment is moderate to high during lowstand, low during transgression, and moderate to high during highstand. This pattern reflects variations in the fluxes of both siliciclastic and carbonate components over time (Fig. 3.2). Crucially, both siliciclastic and carbonate accumulation rates in QT were lowest during lowstand, highest during transgression, and moderate during highstand (Dunbar et al., 2000; Dunbar and Dickens, 2003a; Page et al., 2003).

Most studies of late Quaternary sediment cores from QT have focussed on the unexpected behaviour of the siliciclastic component, rather than the anomalous patterns of carbonate sedimentation. As a notable exception, Dunbar and Dickens (2003b) examined variations in the relative abundances of carbonate mineral phases down a series of QT cores (Fig. 3.1) and found that as a percent of total carbonate the abundances of aragonite and HMC were generally lowest during lowstand, moderate during transgression, and highest during highstand. Similar records in the Bahamas have been explained by 'highstand shedding' (e.g., Kier and Pilkey, 1971; Boardman and Neumann, 1984; Boardman et al., 1986; Schlager et al., 1994), where the production and discharge of neritic carbonate increases with flooding of the shelf, because a greater proportion of seafloor is within the photic zone (Fig. 1.2B). Such an explanation is problematic for late Quaternary sediment in QT, however, because net carbonate accumulation rates on the slope were highest immediately after sea level

crossed the shelf-slope break (i.e., transgression) rather than during highstand when neritic carbonate was most abundant (Figs. 1.2C, 3.2; Page et al., 2003). Unfortunately, most cores examined by Dunbar and Dickens (2003b) were insufficiently dated and too far from the GBR platform to fully constrain the flux of carbonate components to QT over time, and critical assumptions regarding the uniformity of LMC accumulation rates on the slope may have been incorrect. Thus, the late Quaternary record of carbonate sedimentation on the northeast Australian margin remains unclear. It is this record that we examine further herein.

3.3. SAMPLES AND ANALYTICAL METHODS

Sediment cores from six sites on the western slope of QT between 15 and 18.5°S were examined in this study (Fig. 3.1). They include Ocean Drilling Program (ODP) Hole 820A (cores 1H through 2H-1), *RV Franklin* piston cores 5/90 PC27a, 4/92 PC11, 4/92 PC13 and 4/92 PC16, and *RV Rig Seismic* gravity core 051 GC43. The locations of these cores lie between 5 and 57 km east of the modern 120 m isobath, range in water depth from 280 to 2163 m below sea level (mbsl), and encompass major physiographical variations along the margin (Fig. 3.1). Importantly, all cores except PC27a lie well above the regional aragonite compensation depth of ~1750 m (Correge, 1993), and none of the cores contain calcareous turbidites (Peerdeman and Davies, 1993; Dunbar et al., 2000; Page et al., 2003). Further documentation of the cores is provided elsewhere (Table 3.1).

Other than wide spatial coverage, the cores were selected because they had been studied previously (Peerdeman and Davies, 1993; Dunbar et al., 2000; Dunbar and Dickens, 2003a, b; Page et al., 2003). Bulk carbonate contents have already been determined at nominally 10 to 20 cm intervals down cores at ODP Hole 820A

(Peerdeman and Davies, 1993), PC16 (Dunbar et al., 2000), and GC43, PC11, PC13 and PC27a (Page et al., 2003). Between three and nine samples of planktonic foraminifera also have been dated by accelerator mass spectrometry (AMS) at all six sites (Fig. 3.3). After converting radiocarbon ages to calibrated years before present (cal BP), the combination of these data enabled the construction of carbonate accumulation rate records along slopes of QT (Fig. 3.2).

Carbonate mineralogy (Fig. 3.3, Table 3.2) was determined on 51 samples of bulk sediment from cores at ODP 820A, GC43, PC27a, PC13, and PC11 by X-ray diffraction (XRD) using a Siemens D5000 X-ray diffractometer at the James Cook University Advanced Analytical Centre (JCU-AAC). Nominally 10 cm³ of sediment were freeze-dried to remove pore fluids and crushed by hand using a ceramic mortar and pestle. Sub-samples of the powder were then placed into cavity mounts on glass smear slides and analysed by XRD using the Cu K α line at 30kV and 20mA. Samples were rotated during analysis to minimize preferred orientation and examined between 1.3° 2 θ and 65° 2 θ at a rate of 0.5° 2 θ •min⁻¹. For each sample the absolute abundances of all minerals including LMC, aragonite, and HMC were quantified with Siroquant v. 2.0, which quantifies mineral abundances by iteratively adjusting multiple synthetic XRD profiles to match the measured XRD patterns (Taylor, 1991). Errors in individual mineral abundances are difficult to assess, in part because the sum of all quantified phases must total 100%, regardless of the number of phases considered. However, the sum of LMC, aragonite, and HMC is consistently within $\pm 15\%$ of the measured bulk carbonate content (Table 3.2), which is consistent with previous studies that have utilised these methods (e.g. Dunbar and Dickens 2003b), and suggests that most primary siliciclastic phases were accounted for during mineral quantification, and that errors are small (<5%) for each carbonate mineral. The above sample preparation and

analysis are the same as those described by Dunbar (2000) and Dunbar and Dickens (2003b). Consequently, 10 samples from PC16, and 1 sample each from PC27a, PC13, and PC11 were incorporated into this study (Table 3.2).

Carbonate Sr concentration was determined for 51 samples of crushed bulk sediment (Table 3.3) using a Varian Liberty Series II sequential inductively coupled plasma atomic emission spectrometer (ICPAES) at the JCU-AAC. Sub-samples of material used for XRD analyses were weighed and digested with 5 mL of 10% HNO₃, which dissolves carbonate phases but not siliciclastic minerals. The solute was then analysed using a wavelength of 407.771 nm and Sr concentrations were determined by standard comparison to laboratory solutions of known Sr concentration. Repeated analysis of laboratory Sr solutions places the accuracy of reported values at $\pm 10\%$.

To gain a better understanding of carbonate grains, bulk sediment samples were taken every 10 to 20 cm down core GC43 and wet-sieved at 250 μm . The coarse fraction was examined under binocular microscope and representative samples of sediments were photographed (Fig. 3.4). Samples deposited during transgression and highstand contain large (>1000 μm) irregular clasts of carbonate. Nine of these clasts were extracted from the samples using an insect brush and tweezers and examined for their mineralogy using a Bruker-AXS General Area Detector Diffraction System (GADDS) at the JCU-AAC. Instrument conditions were 40 kV and 52 mA and samples were analysed for one minute at 2θ between 23 and 58°. Mineralogy was determined by assessing the diffraction patterns against the commercially available International Centre for Diffraction Data database.

3.4. COMPOSITIONAL VARIATION

3.4.1. Carbonate Mineralogy (XRD)

The samples exhibit a wide range in the absolute abundance of individual carbonate minerals. Some variability reflects differences in siliciclastic dilution because the total carbonate content varies between 30 and 82% (Table 3.2). Siliciclastic dilution can be accounted for by recalculating carbonate mineral abundances relative to the total carbonate content. The simplest normalization is:

$$ra_M = qa_M / (qa_{LMC} + qa_{aragonite} + qa_{HMC})$$

where ra_M is the relative abundance of carbonate phase M (LMC, aragonite or HMC), and qa is the quantified abundance of each carbonate phase. Even after “removing” the siliciclastic component, the ra of the three primary carbonate phases vary significantly across the sample suite (Table 3.2): LMC (16 – 94%), aragonite (6 – 47%) and HMC (0 – 45%). In general, these variations correspond to distinct patterns over space and time (Figs. 3.3, 3.5A).

The shelf-slope break on the northeast Australian margin typically is placed at 70 to 80 m below present sea level (Maxwell, 1968; Larcombe et al., 1995). For the purposes of this paper, the definition of the shelf includes all subaqueous areas shallower than the 120 m isobath, because this nominal depth approximates the extent of the photic zone and hence of neritic productivity (James and Kendall, 1992; Jackson, 1997), and presumably the limit of aragonite and HMC precipitation. The distances between the 120 m isobath and individual cores have changed over the last 25 ky in response to variations in global ice volume and sea level (Fig. 1.2A; Table 3.1). Nonetheless, the relative abundance of carbonate minerals has adhered to a basic spatial pattern: ra_{LMC} generally increases with distance from the shelf, whereas $ra_{aragonite}$ and ra_{HMC} generally decrease with distance from the shelf (Fig. 3.5A). The notable exceptions (which are discussed in greater detail in section 3.6.6) are PC16, which consistently has a depressed ra_{LMC} and an elevated ra_{HMC} given its distance from the

shelf, and PC27a, which has depressed $ra_{\text{aragonite}}$ and ra_{HMC} during lowstand. Notwithstanding these exceptions, and directly relating to the overall spatial trends, LMC is usually the most prevalent carbonate mineral in the studied cores, with aragonite and HMC in successively lower amounts. Some sediment intervals from ODP 820A, PC16, and GC43, all within 25 km of the modern 120 m isobath, are exceptions (Figs. 3.3, 3.5A). In particular, most sediments examined from ODP 820A have $>40\%$ $ra_{\text{aragonite}}$ and $>35\%$ ra_{HMC} , so that LMC is the least abundant carbonate mineral.

Apart from the spatial trends, the relative abundance of carbonate minerals changes temporally in general correspondence with the last glacial-interglacial sea level cycle (Figs. 3.3, 3.5A). In all cores, ra_{LMC} is highest during lowstand, decreases throughout the transgression, and is lowest during highstand. The relative abundance of aragonite is essentially the opposite, being lowest during lowstand, and peaking during the Holocene highstand. Temporal trends in ra_{HMC} are less distinct. Most cores show peaks in ra_{HMC} during transgression (as also noted by Dunbar and Dickens, 2003b), but these are relatively minor and no consistent pattern is evident.

The magnitudes of downcore variations in carbonate mineralogy are related to physiography (Figs. 3.3, 3.5A). Cores far from the shelf have greater changes in the relative abundance of minerals over time compared to cores proximal to the shelf. For example, between ~21 and 2.5 ka, ra_{LMC} , $ra_{\text{aragonite}}$, and ra_{HMC} vary by 30, 20, and 10%, respectively, in PC11 (57 km east of the modern 120 m isobath), but only by 3, 10, and 13%, respectively, in GC43 (12 km east of the 120 m isobath).

3.4.2. Strontium concentrations

Marine organisms can precipitate aragonite with a wide range of Sr. In general, however, neritic organisms (e.g., corals and algae) produce aragonite with ≥ 7500 ppm

Sr, whereas pelagic organisms (e.g., pteropods) produce aragonite with ≤ 1500 ppm Sr, similar to Sr concentrations in HMC and LMC (Milliman, 1974; Bathurst, 1975; Boardman and Neumann, 1984; Droxler et al., 1988).

The samples examined in this study exhibit considerable variation in the extractable Sr content of bulk sediment, which ranges from 620 to 2630 ppm (Table 3.3). The extractable Sr content of individual samples is calculated relative to the initial mass of bulk sediment. However, because of the sample preparation techniques employed in this study (i.e. only carbonate minerals were in solution), the extractable Sr content relates only to the bulk carbonate fraction of the sample. Consequently, these values need to be corrected to account for differences in the abundance of siliciclastic and bulk carbonate components (Table 3.3), according to:

$$Sr_{\text{carbonate}} = Sr_{\text{extractable}} \times (100 \div W_{\text{carbonate}})$$

where $Sr_{\text{carbonate}}$ is the corrected Sr content of the bulk carbonate fraction, $Sr_{\text{extractable}}$ is the extractable Sr content relative to the initial bulk mass, and $W_{\text{carbonate}}$ is the weight percent of bulk carbonate in the sample.

Corrected Sr content of the samples (Table 3.3) ranges from 1610 ppm (1.24 mbsf, PC13) to 3900 ppm (6.36 mbsf, ODP 820A). The relationship between $Sr_{\text{carbonate}}$ and $ra_{\text{aragonite}}$ can be examined by plotting these variables on an aragonite-Sr mixing diagram (Fig. 3.6). When all data are considered together, a linear best fit indicates a strong correlation between $Sr_{\text{carbonate}}$ and $ra_{\text{aragonite}}$ ($r^2 = 0.74$), suggesting that most aragonite accumulating on slopes of QT is Sr-rich aragonite. Independent of the linear best fit, the relationship between $Sr_{\text{carbonate}}$ and $ra_{\text{aragonite}}$ in almost 80% of the samples plots above the theoretical mixing line for samples that contain equal parts Sr-rich aragonite and Sr-poor aragonite (50/50 line; Fig. 3.6). Notably, of the 13 samples that plot on, or below, the 50/50 mixing line, and therefore contain the most significant

quantities of Sr-poor aragonite, most are from sediment deposited during the last glacial lowstand, when the shelf was exposed and neritic accommodation space was lowest.

3.4.3. Carbonate Grains

Some downcore mineralogical changes in GC43 can be linked to macroscopic compositional changes. Within lowstand intervals (Figs. 3.4A–B), the carbonate sand fraction is dominated by clean, well-preserved tests of planktonic and benthic foraminifers. Pteropods are also relatively abundant, but coralline algae are relatively uncommon. These observations are consistent with the observation that LMC was most abundant during lowstand, and Sr-poor aragonite was most significant before 12 ka. Within transgressive intervals (Figs. 3.4C–H), the percent carbonate sand is visually less compared to lowstand intervals, partly reflecting vastly increased abundance of terrigenous mud (Page et al., 2003). Nevertheless, planktonic and benthic foraminifers remain abundant within the carbonate sand fraction. Pteropods appear less common, but coralline algae are more common, and coarse shell fragments (possibly molluscan in origin) are numerous. Most notably, however, a conspicuous component of the carbonate sand fraction within sediments deposited during transgression comprises carbonate clasts up to $>1000\ \mu\text{m}$ (Figs. 3.4C–H). Within highstand intervals (Figs. 3.4I–J), the carbonate sand fraction is generally similar to that deposited during transgression. Planktonic and benthic foraminifers are abundant, coralline algae and shell fragments are common, and pteropods are present in varying abundance. Highstand intervals also contain substantial, albeit lesser quantities of carbonate clasts. With the notable exception of the carbonate clasts, macroscopic changes in the carbonate sediments deposited within GC43 are similar to those described at ODP

820A (Peerdeman and Davies, 1993), suggesting that these observations might be consistent with other locations on the slope.

The anomalous carbonate clasts have two distinct types: (1) aggregates of small cemented particles, some of which include a recognisable nucleus (Figs. 3.4C & H), or (2) clasts of recrystallised carbonate (Fig. 3.4F-J). The two types can also occur together, for example, where recrystallised grains are coated by aggregates of cemented particles (Fig. 3.4D, 3.4E). Nevertheless, mineralogical analysis reveals that regardless of texture the clasts are composed exclusively of LMC. The sedimentary textures and mineralogy of the carbonate clasts are not consistent with primary biogenic carbonate, but do appear to be consistent with secondary alteration of biogenic carbonate under subaerial and/or meteoric conditions (e.g., James and Choquette, 1990; Bathurst, 1993). Pre-Holocene carbonate sediments with similar diagenetic characteristics have also been recorded previously on the GBR shelf (Orme et al., 1978; Johnson et al., 1984). These observations suggest that the carbonate clasts were probably formed by diagenesis and erosion of neritic carbonate on the shelf during lowstand.

3.5. MASS ACCUMULATION RATES

Mass accumulation rates (*MARs*) are a measure of the quantities of a given sedimentary component accumulating over discrete intervals of time. Calculating *MARs* is fundamental to understanding the patterns of sediment deposition on slopes east of the GBR, because *MARs* enable variations in the flux of individual components to be assessed quantitatively and independently of co-occurring components. Mass accumulation rates ($\text{g/cm}^2/\text{ky}$) can be calculated according to:

$$MAR_x = W_x \times LSR \times DBD$$

where W_X is the fractional weight percent of component X, LSR is the bulk linear sedimentation rate (cm/ky), defined as the net thickness of sediment accumulated over a given interval of time, and DBD is the dry bulk density (g/cm^3) including pore space.

Bulk siliciclastic and carbonate $MARs$ have been determined previously for late Quaternary sediment at GC43, PC27a, PC13, and PC11 (Page et al., 2003). For these cores, $LSRs$ were calculated between successive radiocarbon dates, and a DBD of $1.0 g/cm^3$ was assumed because this is typical for shallow slope sediments in QT (Davies et al., 1991). The same approach was used to calculate siliciclastic and carbonate $MARs$ down cores from PC16 and ODP 820A (Fig. 3.2). Late Quaternary MAR records from QT (including at PC16 and ODP 820A) consistently show highs for both siliciclastic and carbonate components during transgression ca. 12–7 ka (Figs. 1.2C, 3.2). This is not an artefact of misplaced age datums because all cores examined from QT show this general record despite the use of different radiocarbon age datums, and the radiocarbon ages have been confirmed with other dating techniques, most notably oxygen isotope stratigraphy (Dunbar and Dickens, 2003a; Page and Dickens, 2005). In the simplest sense, the time interval between similarly spaced samples decreases significantly during transgression (Fig. 3.3).

In a similar way, $MARs$ of individual carbonate minerals can be determined down each core according to:

$$MAR_M = ra_M \times MAR_{\text{carbonate}}$$

where MAR_M is the mass accumulation rate of carbonate mineral M (LMC, aragonite, or HMC), and other terms are as defined above. Mass accumulation rates of individual carbonate minerals vary significantly down individual cores, and among different cores (Fig. 3.7). In general, however, these variations conform to distinct patterns over space and time (Figs. 3.5B, 3.7).

Similar to spatial variations in their relative abundance, $MAR_{\text{aragonite}}$ and MAR_{HMC} generally decrease with increasing distance from the shelf, even during sea-level lowstand (Fig. 3.5B). In this regard, it is noteworthy that $MAR_{\text{aragonite}}$ and MAR_{HMC} at the deepest location, PC27a, always lie on the trends delineated by the shallower cores, suggesting that dissolution is not significantly affecting carbonate mineralogical records in late Quaternary sediment on the slope of QT. Thus, sediment near the shelf has high relative abundances of aragonite and HMC because these phases are accumulating relatively fast. By contrast, the spatial patterns of ra_{LMC} and MAR_{LMC} are dissimilar, with the latter either fairly uniform across the margin, or higher closer to the shelf (Fig. 3.5B). Thus, sediment distal to the shelf in QT has a high relative abundance of LMC because other phases are accumulating relatively slowly.

In all cores, the MAR of all carbonate minerals changed markedly over time in concert with variations in sea level (Fig. 3.7). However, the magnitudes of these changes among cores were also largely dependant on distance from the shelf.

During sea-level lowstand, $MAR_{\text{aragonite}}$ and MAR_{HMC} were lowest in all cores, and among cores the MAR s of each carbonate mineral were most similar during this time (Fig. 3.5B). For example, during lowstand, the $MAR_{\text{aragonite}}$ at ODP 820A (the core closest to the shelf) was about 7 times higher than at PC11 (the core farthest from the shelf), whereas during transgression and highstand, $MAR_{\text{aragonite}}$ at ODP 820A was about 14 times higher than at PC11. These observations are consistent with an interpretation of reduced supply of neritic carbonate from the shelf. Generally, MAR_{LMC} was also lowest during lowstand and early transgression, but was fairly uniform across QT, suggesting carbonate deposition from pelagic sources. The only exception was PC27a, which records elevated MAR_{LMC} during lowstand.

During transgression, *MARs* for all three carbonate phases increased significantly in all cores examined (Fig. 3.7). Aragonite and HMC *MARs* during transgression were typically 2 to 6 times greater than during lowstand, with peaks over some intervals including order-of-magnitude increases. The average MAR_{LMC} also rose by a factor of ~2 to 7.5, except at PC27a, where it at a similar level from lowstand through transgression. Aragonite *MARs* generally increased the most between lowstand and transgression, and the increases in all carbonate mineral *MARs* were generally most pronounced in cores proximal to the shelf. For example, $MAR_{aragonite}$ increased by 6 times at ODP 820A, but by only 3 times at PC11.

The *MAR* of bulk carbonate drops in all slope cores of QT from the transgression to present (Fig. 3.7). In general, this corresponds to a decrease in the *MARs* of all carbonate phases, although there are a few exceptions (e.g., $MAR_{aragonite}$ and MAR_{LMC} are highest during highstand in PC13). Decreases in the *MARs* of carbonate minerals were generally greater in cores closer to the shelf (Fig. 3.5B). Hence, the spatial differences in carbonate accumulation rates observed on the modern seafloor were more pronounced during transgression.

3.6. DISCUSSION

3.6.1. Origin and problem of carbonate abundance and accumulation patterns

Prominent changes in bulk carbonate content characterize late Quaternary sediment sections deposited on the upper to lower slope of QT. In particular, a distinct dark-grey siliciclastic-rich interval occurs within the upper few metres of all cores examined from this region (e.g., Harris et al., 1990; Peerdeman and Davies, 1993; Dunbar et al., 2000; Kronen and Glenn, 2000; Dunbar and Dickens, 2003a; Page et al., 2003). Applying conventional concepts for tropical mixed siliciclastic-carbonate

depositional systems, this interval has been interpreted as representing high siliciclastic accumulation rates and low carbonate accumulation rates during the last glacial lowstand and early transgression ca. 25–12 ka (e.g., Harris et al., 1990; Kronen and Glenn, 2000). Recent studies using radiocarbon dating (Dunbar et al., 2000; Dunbar and Dickens, 2003a; Page et al., 2003) have confirmed that the siliciclastic-rich interval is time correlative along the margin, and indeed represents anomalously high rates of siliciclastic accumulation on the slope. However, this horizon unequivocally formed during transgression ca. 12–7 ka, and coincided with periods of peak carbonate accumulation rates (Figs. 1.2C, 3.2). The bulk carbonate content of this interval is low only because the depositional flux of siliciclastic material increased more than that of carbonate (Dunbar and Dickens, 2003a; Page et al., 2003).

The relative abundances of different carbonate minerals also change markedly in late Quaternary sediment of QT. These changes generally correspond in time to variations in siliciclastic and bulk carbonate accumulation rates, as well as variations in sea level (Fig. 3.3). With few exceptions, LMC is most abundant during lowstand, and aragonite and HMC become more abundant with rising sea level, especially near the shelf (Fig. 3.5A). This result is consistent with, but amplifies, previous findings (Dunbar et al., 2000; Dunbar and Dickens, 2003b) that showed that the relative abundance of neritic carbonate on the slope is lowest during lowstand and higher during transgression and highstand. The generally high Sr content of sediment and the strong down-core correlations between Sr content and aragonite content (Fig. 3.6) are also consistent with previous work (Dunbar et al., 2000; Sutherland, 2000; Dunbar and Dickens, 2003b), and suggest that the aragonite chiefly comes from neritic organisms on the shelf.

Downcore changes in carbonate mineralogy might be interpreted according to conventional concepts for carbonate depositional systems (e.g., Boardman et al., 1986; Posamentier and Vail, 1988; James and Kendall, 1992; Schlager et al., 1994) where (1) low relative abundance of neritic components reflects decreased carbonate productivity when the shelf was exposed, and (2) high relative abundance of neritic components reflects increased carbonate productivity when the shelf was flooded. Indeed, this concept of 'highstand shedding' (cf. Schlager et al., 1994) has been proffered previously for patterns of late Quaternary carbonate deposition in QT (Dunbar and Dickens, 2003b).

Mass accumulation rates, however, show that temporal variations in the relative abundance of carbonate minerals have a more complicated origin. Apart from a few exceptions, *MARs* of all carbonate minerals were (1) lowest during lowstand, (2) highest during transgression, and (3) moderate to high during highstand (Fig. 3.7). Furthermore, peak *MARs* of all carbonate minerals during transgression were most pronounced in cores closest to the shelf (Fig. 3.5B). Thus, the shelf appears to supply aragonite, HMC, and LMC, especially during transgression. Somewhat analogous to the aforementioned siliciclastic dilution of bulk carbonate, the absolute abundance of LMC is low during transgression only because the depositional fluxes of aragonite and HMC rose more than the depositional flux of LMC.

Conventional models for sediment deposition on tropical mixed siliciclastic-carbonate margins are not consistent with the late Quaternary evolution of the northeast Australian margin, because they do not predict the high accumulation rates of siliciclastic and carbonate components, including LMC, to slopes during transgression. We suggest, however, that the slope records can be explained fairly simply when two facts concerning the adjacent shelf are stressed.

3.6.2. Changes on the shelf and a solution to slope accumulation

Drill cores through reefs of the GBR (Fig. 3.8) show that Holocene carbonate and active coral reefs constitute relatively thin strata at the top of reef profiles. Underlying these Holocene sections, much of the reef structures consist of a series of dissolution horizons, formed when the reefs were subaerially exposed during lowstands, and older carbonate deposits representing reef growth during past highstands. The “solution unconformities” between Pleistocene and Holocene strata commonly lie between 10 and 25 m below modern reef tops (Davies and Hopley, 1983; Johnson et al., 1984; Marshall and Davies, 1984; International Consortium for Great Barrier Reef Drilling, 2001; Webster and Davies, 2003), which represents a palaeorelief of at least 35 to 50 m above the adjacent coastal plain, and demonstrates that the GBR comprised an extensive bathymetric high on the shelf during the last lowstand. Although active reefs and the Holocene section consist mostly of aragonite, the older sections have been extensively recrystallised to LMC, probably when they were exposed to meteoric water during lowstand (Johnson et al., 1984; Marshall and Davies, 1984; International Consortium for Great Barrier Reef Drilling, 2001).

Seismic profiles across the shelf show numerous channels that formed when rivers traversed the shelf during the last lowstand (Johnson and Searle, 1984; Fielding et al., 2003). However, even the biggest of these paleo-channel systems (that of Burdekin River) did not traverse all the way to the shelf-slope break (Fielding et al., 2003). Evidently, rivers lacked sufficient stream power to cross the broad, low gradient, reef-silled shelf of northeastern Australia during the last lowstand (Fielding et al., 2003). Nevertheless, there is very little siliciclastic material on the modern middle to outer shelf (Johnson and Searle, 1984; Harris et al., 1990). Sediment loads of lowstand

river systems were probably deposited on the shelf and subsequently eroded and removed during transgression (Dunbar et al., 2000; Dunbar and Dickens, 2003a; Page et al., 2003).

These observations from the shelf are crucial to understanding the accumulation rate records on the slope because they imply:

- (1) Erosion and weathering of reefs during lowstand, creating an abundant source of diagenetic LMC that could be mobilized during transgression,
- (2) An absence of riverine delivery of sediment to slopes during lowstand, and,
- (3) Prominent topographic highs on the outer shelf that could be colonized by corals during transgression.

Taking these interpretations, we propose the following basic evolution for the northeast Australian margin over the last 25 ky (Fig. 3.9).

3.6.3. Lowstand ca. 25–12 ka

Deposition of all sedimentary components was slowest in QT before sea level crossed the shelf-slope break ca. 12 ka (Fig. 3.7). Reduced stream power and low shelf gradients caused fluvial avulsion behind subaerially exposed reefs and deposition of siliciclastic sediment on the shelf (e.g., Dunbar et al., 2000; Dunbar and Dickens, 2003a; Page et al., 2003). Because reefs comprising the main GBR were inactive, the production and shedding of neritic carbonate was at a minimum and aragonite and HMC accumulation rates in QT were low. We note, though, that aragonite and HMC accumulation rates did not drop to zero and still displayed a slight increase toward the shelf (Fig. 3.5B), suggesting that some neritic production existed, presumably on the upper slope (Fig. 3.9). During this time the ra_{LMC} and the number of pelagic tests in

sediment were most pronounced (Figs. 3.3, 3.4) because the accumulation rates of all other components were low.

3.6.4. Transgression ca. 12–7 ka

Sea level rose above the shelf edge of the northeast Australian margin ca. 12 ka (Fig. 3.7; Larcombe et al., 1995; Lambeck and Chappell, 2001). Around this time, all sedimentary components accumulated at greater rates on slopes of QT, especially in areas close to the shelf. Siliciclastic fluxes peaked because of either vastly increased precipitation on the continent (Kershaw, 1985, 1994; Wyrwoll and Miller, 2001), which increased fluvial runoff and overall terrestrial sediment supply to the margin (Thomas et al., 2001; Thomas, 2003), or shallow water on the shelf (with accompanying waves and currents) eroded and remobilised fluvial siliciclastic sediments deposited on the shelf during lowstand (Dunbar et al., 2000; Dunbar and Dickens 2003; Page et al., 2003; Fig. 3.9). The immense influx of LMC to the slope during transgression was also most pronounced near the shelf (Fig. 3.5B) and included eroded carbonate clasts (Fig. 3.4), most likely representing weathered and diagenetically altered reefal material that was remobilised in shallow water (along with siliciclastic sediment) and transported to slopes of QT.

The accumulation rates of aragonite and HMC escalated dramatically during transgression all along slopes of QT (Fig. 3.7). We suggest that this represents a sudden increase in neritic production associated with a major increase in accommodation space (Jones and Desrochers, 1992). Using bathymetric cross sections (Fig. 3.10), straightforward reconstructions of sea level rise show that almost immediately upon flooding of the shelf ca. 12 ka, the area of seafloor within 120 m of the sea surface increased several fold, and continued to expand until sea level stopped rising ca. 6 ka

(Larcombe et al., 1995; Lambeck and Chappell, 2001). Certainly, an increase in shallow marine accommodation space of this magnitude can lead to major reef growth and/or the development of vast *Halimeda* bioherms (James and Bourge, 1992; Hallock, 2001).

Somewhat surprisingly, however, initial reef building and/or bioherm development on the northeast Australian margin was synchronous with immense off-shelf fluxes of siliciclastic sediment (Figs. 1.2C, 3.2). Suspended sediment concentrations and turbidity on the shelf must have been high. These conditions are purportedly the least suitable for the development of both coral reefs and algal bioherms (James and Bourge, 1992; Hallock, 2001), but seemingly did not affect the rapid expansion of these organisms on the northeast Australian margin during the earliest Holocene. Perhaps the simplest explanation is that these organisms developed on top of pre-existing highs and were physically separated in the water column from siliciclastic sediments that were being transported in intermediate or bottom nepheloid layers (e.g. Pak et al., 1980; Walsh and Nittrouer, 1999). Alternatively, the detrimental effects of high terrigenous inputs and turbidity on sustained reef growth may generally be overestimated (e.g., Larcombe and Woolfe, 1999; Smithers and Larcombe, 2003).

3.6.5. Highstand ca. 7 ka–present

The accumulation rates of all sedimentary components in QT have moderated during the Holocene highstand (Fig. 3.7). Siliciclastic fluxes have dropped significantly toward the present, probably for two reasons (Fig. 3.9). First, riverine sources have moved landward so that newly delivered terrestrial sediment is trapped on the inner shelf (Belperio, 1983; Larcombe and Carter, 2004). Secondly, however, siliciclastic repositories on the outer and middle shelf were depleted during the transgression and

now lie below normal wave-base reworking. Fluxes of LMC also have decreased because altered reef detritus on the shelf is depleted and isolated from normal wave-base. A similar rate of LMC accumulation in all but the most shelf-proximal cores suggests LMC accumulating on the slope during highstand is predominantly sourced from pelagic organisms. Decreased fluxes of aragonite and HMC suggest that neritic productivity has dropped, arguably because accommodation space has ceased to increase, or more likely diminished, as reefs and associated sediments continue to expand and sea level remains relatively stable. This is evidenced by the cessation of vertical reef growth on the GBR between 4 and 6 ka, with lateral growth predominating since (Fig. 3.8: Davies and Hopley, 1983; Johnson et al., 1984; Ryan et al., 2001; Webster and Davies, 2003). This change in reef growth, and the decreased flux of neritic carbonate to the slope of QT, may be related to a drop in overall global carbonate production in the late Holocene (Ryan et al., 2001).

3.6.6. Discrepancies

The observed sediment accumulation rate records in our cores form a mostly cohesive dataset and we have highlighted the generalities. We note, however, that there are some discrepancies in the details. The most striking is the record of LMC deposition at PC27a (Figs. 3.5B, 3.7), where MAR_{LMC} was very high during the last lowstand, rather than at lowest levels similar to the other sites. Notably, the accumulation rates of neritic carbonate at PC27a are consistent with those at other sites, and with the proximity of PC27a to the shelf, suggesting that this is not the result of misplaced age datums or erroneous mineralogical data. A possible explanation lies in the fact that the slope adjacent to PC27a is amongst the steepest within QT (Fig. 3.10). Perhaps high gradients on the upper and middle slope were not conducive to

sedimentation and promoted down-slope transport and sediment deposition at the toe-of-slope, especially during lowstand when sea level (and thus a shallow, high-energy environment) was below the shelf edge. Unfortunately, no sedimentologic evidence was observed in PC27a to either support or refute this possibility, and thus, barring further investigation, the MAR_{LMC} at PC27a during the lowstand remains enigmatic.

Other discrepancies within the dataset concern the $MARs$ of LMC and aragonite at PC13, which, unlike the other sites, are slightly higher during highstand compared to transgression (Fig. 3.7). However, the significance of these departures from the trends displayed by the other cores appears nominal. For example, at PC11 the $MARs$ of all carbonate minerals are also very similar during transgression and highstand, and like PC13, PC11 is also distal to the shelf. During transgression and highstand, MAR_{LMC} at PC13 and PC11 were around 2 to 3 $g/cm^2/ky$, and during highstand, similar MAR_{LMC} also occur at most other sites (apart from at the most shelf-proximal core, i.e. ODP 820A). The uniformity of these results is consistent with predominantly pelagic-driven deposition of LMC during highstand, and suggests this was also the case at distal locations in QT during transgression. Similarly to how the grain size of neritic carbonate is likely to influence records of aragonite and HMC deposition at sites distal to the shelf, it is possible that fluxes of LMC did not increase as much at distal sites because the bulk of LMC clasts sourced from the shelf were too coarse to be transported long distances.

3.7. CONCLUSIONS

1. The deposition of sedimentary successions on slopes of QT since the LGM does not conform with generic models for the evolution of tropical mixed siliciclastic-carbonate systems (Fig. 1.2B) because (i) minimum and maximum

siliciclastic fluxes occurred during lowstand and transgression, respectively, and (ii) carbonate fluxes were in-phase with siliciclastic fluxes (Figs. 1.2C, 3.2).

2. The distribution of carbonate minerals across QT is mostly consistent with partitioning of material sourced from neritic and pelagic organisms. The relative abundance of aragonite and HMC decreases with increasing distance from the shelf (Fig. 3.5A), and the relative abundance of LMC is essentially the opposite. In general, the relative abundance of LMC is low near the shelf because aragonite and HMC accumulate relatively fast, and is high away from the shelf because aragonite and HMC accumulate relatively slowly.
3. The distribution of carbonate minerals down cores from QT (Fig. 3.3) appears consistent with conventional models for carbonate systems. The relative abundance of aragonite and HMC was lowest during lowstand and increased progressively with increasing sea level, reaching a peak in the late Holocene. The relative abundance of LMC was essentially the opposite and decreased with rising sea level.
4. The accumulation rates of carbonate minerals down cores from QT (Fig. 3.7) are not consistent with conventional models for carbonate sedimentation on slopes (i.e. 'highstand shedding'). During lowstand, the accumulation rates of aragonite and HMC were low, but slightly higher closer to the shelf (Fig. 3.5B), and the accumulation rates of LMC were uniform across most of QT. During transgression, accumulation rates of *all* carbonate minerals reached their highest levels, and accumulation rates of *all* carbonate minerals were higher closer to the shelf. Notably, this included numerous LMC clasts (Fig. 3.4), but the relative abundance of LMC decreased because the accumulation rates of aragonite and HMC increased by more. During highstand, the accumulation

rates of aragonite and HMC tapered to more moderate levels, but remained higher in cores closer to the shelf. The accumulation rates of LMC also decreased and were generally similar throughout QT, but the relative abundance of LMC was lowest because the accumulation rates of aragonite and HMC decreased by less.

5. Conventional models are not consistent with the evolution of the northeast Australian margin during the Late Pleistocene and Holocene, because important factors such as antecedent topographic profiles, carbonate diagenesis, and shallow-water sediment remobilisation are not emphasised. Taking these factors, we propose a coherent model (Fig. 3.9) for the observed patterns of mixed siliciclastic-carbonate sediment deposition in QT since the LGM:

- (i) During lowstand ca. 25–12 ka, rivers aggraded behind topographic barriers (e.g., exposed reefs), depositing sediment onto the shelf and starving the slope. Coevally, subaerial exposure and erosion of Pleistocene reefs altered neritic carbonate and produced LMC clasts. Neritic accommodation space and production of aragonite and HMC was severely restricted (Fig. 3.10). Sedimentation in QT was dominated by pelagic LMC.
- (ii) During transgression ca. 12–7 ka, sea level flooded the shelf and ‘lowstand’ siliciclastic deposits and LMC clasts were remobilised in shallow, high-energy environments, and transported to the slope. Rapid increases in accommodation space (Fig. 3.10) maximised neritic productivity and shedding of aragonite and HMC. Holocene reef and/or bioherm development was initiated (and indeed flourished) regardless of high turbidity and suspended sediment concentrations.

- (iii) During highstand ca. 7 ka to present, new fluvial inputs were restricted to an inner shelf sediment wedge. Remnant deposits of terrigenous material and LMC clasts on the middle and outer shelf were depleted and isolated from normal wave base reworking. Accommodation space stabilised and then diminished as deglaciation ceased and reefs caught up with sea level. Production and shedding of aragonite and HMC reduced toward the present.

Although diverging from conventional models for sediment deposition on tropical mixed siliciclastic-carbonate margins in several key aspects, the above evolution for the northeast Australian margin over the latest Quaternary is consistent with general trends in all data from QT, and a growing amount of data from the adjacent shelf (for a review see Larcombe and Carter, 2004). One might suggest that the northeast Australian margin is, for whatever reason, a special case, and that other tropical mixed systems, both modern and ancient, might behave according to conventional paradigms. However, similar relationships between physiography, fluvial evolution, and sediment transport and deposition have been identified on shelves of other mixed siliciclastic-carbonate systems (e.g., Ferro et al., 1999; Rankey et al., 1999). Consequently, our results may equally apply, in whole or in part, to the evolution of other passive continental margins throughout the geological record, especially tropical mixed siliciclastic-carbonate systems with barrier reefs.

ACKNOWLEDGEMENTS

An Australian Postgraduate Award, AAPG Foundation Grant-In-Aid and CRC Reef-Ken Woolfe Scholarship supported this research. Thanks are extended to Raphael

Wust for helpful discussion of the data and manuscript and to the Ocean Drilling Program who provided samples for this research.

Core	Latitude	Longitude	Water Depth (m)	Distance to 120 m isobath	
				Present (km)	LGM (km)
FR5/90-PC27a	15° 17.4'S	145° 56.8'E	2163	16	15
ODP 820A	16° 38.2'S	146° 18.2'E	280	5	1
FR4/92-PC13	16° 57.1'S	146° 55.2'E	1507	35	31
FR4/92-PC16	17° 25.9'S	146° 53.5'E	1043	24	18
FR4/92-PC11	17° 34.3'S	147° 20.9'E	1320	57	51
51GC43	18° 07.9'S	147° 28.6'E	901	12	6

Table 3.1: Location and other information pertaining to sediment cores FR5/90 PC27a, ODP 820A, FR4/92 PC13, FR4/92 PC16, FR4/92 PC11, and 51GC43.

Core	Sample code	Core depth (cm)	Depth (cm bsf)	Age (cal BP)	Bulk CO ₃ content ^{^^} (%)	LMC (qa) ra (%)	Aragonite (qa) ra (%)	HMC (qa) ra (%)
FR5/90-PC27a	2656 - 24 [^]	0	0	980	n.d.	(31) 46	(26) 38	(11) 16
	5343 - 17	20	20	2520	57	(38) 54	(24) 34	(9) 13
	5343 - 18	52	52	4990	61	(42) 57	(22) 30	(10) 14
	5343 - 19	82	82	7620	52	(37) 57	(21) 32	(7) 11
	5343 - 20	150	150	9910	45	(34) 61	(15) 27	(7) 13
	5343 - 21	194	194	12870	59	(52) 67	(11) 14	(15) 19
	5343 - 22	218	218	14340	59	(54) 79	(6) 9	(8) 12
	5343 - 23	294	294	20240	57	(67) 94	(4) 6	(0) 0
	5343 - 24	347	347	24350	74	(67) 77	(15) 17	(5) 6
	5343 - 25	400	400	28470	77	(67) 85	(11) 14	(1) 1
	5343 - 26	450	450	32360	61	(67) 86	(10) 13	(1) 1
ODP 820A	5675 - 17	6	6	1030	69	(16) 21	(34) 44	(27) 35
	5675 - 18	206	206	4610	65	(17) 24	(30) 43	(23) 33
	5675 - 19	326	326	6760	57	(12) 22	(22) 41	(20) 37
	5675 - 20	406	406	7870	54	(13) 22	(25) 42	(21) 36
	5676 - 21	576	576	9680	39	(10) 22	(19) 41	(17) 37
	5675 - 22	616	616	10910	43	(8) 20	(17) 41	(16) 39
	5675 - 23	636	636	12500	40	(7) 16	(20) 47	(16) 37
	5675 - 24	656	656	14090	42	(9) 17	(23) 44	(20) 38
	5675 - 25	686	686	16470	48	(14) 22	(27) 42	(24) 37
	5675 - 26	725	725	31750	78	(17) 29	(19) 32	(23) 39
	5675 - 27	746	746	41200	77	(16) 28	(19) 33	(23) 40
FR4/92-PC13	2656 - 27 [^]	0	0	560	n.d.	(38) 59	(19) 30	(7) 11
	4675 - 07	8	8	1660	71	(41) 55	(26) 35	(8) 11
	5309 - 15	34	34	5250	66	(40) 58	(19) 28	(10) 14
	5309 - 10	55	55	8150	58	(35) 56	(15) 24	(13) 21
	4675 - 08	76	76	10640	45	(32) 62	(13) 25	(7) 13
	5309 - 11	83	83	13030	59	(48) 65	(16) 22	(10) 14
	5309 - 12	87	87	15070	69	(54) 74	(9) 12	(10) 14
	4675 - 09	95	95	19160	71	(66) 81	(7) 9	(8) 10
	5309 - 13	105	105	24260	77	(74) 86	(6) 7	(6) 7
	5309 - 14	124	124	33950	82	(74) 87	(7) 8	(4) 5
	FR4/92-PC16	2612 - 36*	13	0	30	n.d.	(26) 33	(29) 36
2126 - 01*		34	21	1740	76	(28) 35	(29) 36	(24) 30
2126 - 02*		60	47	3930	73	(26) 37	(23) 33	(21) 30
2173 - 10*		106	86	6960	65	(24) 34	(21) 30	(25) 36
2126 - 03*		146	126	8530	53	(17) 31	(17) 31	(20) 37
2126 - 04*		191	171	10330	42	(14) 28	(15) 30	(21) 42
3083 - 01*		231	208	12020	30	(15) 36	(14) 33	(13) 31
2173 - 11*		251	228	12930	55	(21) 36	(15) 25	(23) 39
3083 - 02*		271	248	15750	49	(30) 52	(11) 19	(17) 29
2612 - 28*		284	261	17720	56	(19) 27	(22) 31	(30) 42

Core	Sample code	Core depth (cm)	Depth (cm bsf)	Age (cal BP)	Bulk CO ₃ content ^{^^} (%)	LMC (<i>qa</i>) <i>ra</i> (%)	Aragonite (<i>qa</i>) <i>ra</i> (%)	HMC (<i>qa</i>) <i>ra</i> (%)
FR4/92-PC11	2384 - 31 [^]	10	0	1780	n.d.	(49) 59	(23) 28	(11) 13
	4675 - 01	12	2	2180	78	(43) 51	(25) 30	(16) 19
	5343 - 01	23	13	4380	77	(61) 66	(21) 23	(10) 11
	5343 - 02	34	24	6580	70	(59) 66	(21) 23	(10) 11
	5343 - 03	44	34	8080	65	(51) 62	(20) 24	(11) 13
	4675 - 02	59	49	10140	53	(37) 58	(17) 27	(10) 16
	5675 - 16	67	57	13390	72	(61) 73	(12) 14	(11) 13
	5343 - 04	74	64	16500	74	(57) 66	(20) 23	(9) 10
	5343 - 05	83	73	20500	76	(73) 81	(9) 10	(8) 9
	4675 - 03	98	88	27160	81	(66) 78	(9) 11	(10) 12
	5343 - 06	109	99	32050	81	(70) 83	(8) 10	(6) 7
	51GC43	4675 - 16	5.5	5.5	2530	72	(32) 39	(31) 38
5343 - 07		37	37	6760	67	(36) 43	(28) 34	(19) 23
5343 - 08		55	55	8480	55	(28) 39	(24) 33	(20) 28
4675 - 17		84	84	9260	44	(19) 37	(19) 37	(14) 27
4675 - 18		134	134	10630	34	(14) 33	(15) 36	(13) 31
5343 - 09		154	154	11440	40	(18) 34	(16) 30	(19) 36
5343 - 10		171	171	14130	44	(22) 37	(19) 32	(19) 32
5343 - 11		182.5	182.5	16130	40	(25) 43	(17) 29	(16) 28
4675 - 19		193.5	193.5	18040	33	(25) 53	(12) 26	(10) 21
5343 - 12		212	212	21250	42	(21) 36	(16) 28	(21) 36
4675 - 20		239	239	25940	46	(22) 37	(19) 32	(18) 31

qa – quantified abundance; *ra* – relative abundance

n.d. – no data

[^] Data from Dunbar (2000)

* Data from Dunbar and Dickens (2003b)

^{^^} Bulk carbonate data from Page et al. (2003), except data for ODP 820A (Peerdeman and Davies, 1993) and data for FR4/92 PC 16 (Dunbar et al., 2000)

Table 3.2: Bulk carbonate content and carbonate mineral abundances in sediment cores FR5/90 PC27a, ODP 820A (1H, 2H-1), FR4/92 PC13, FR4/92 PC16, FR4/92 PC11, and 51GC43.

Core	Sample code	Core depth (cm)	Depth (cmbsf)	Age (cal BP)	Bulk CO ₃ content [^] (%)	Sr content measured* (ppm)	Sr content corrected* (ppm)	Aragonite <i>ra</i> (%)
FR5/90-PC27a	5516-001	20	20	2520	57	1700	2930	34
	5516-002	52	52	4990	61	1705	2840	30
	5516-003	82	82	7620	52	1790	3510	32
	5516-004	150	150	9910	45	940	2140	27
	5516-005	194	194	12870	59	1480	2510	14
	5516-006	218	218	14340	59	1020	1700	9
	5516-007	294	294	20240	57	1100	1930	6
	5516-008	347	347	24350	74	1800	2430	17
	5516-009	400	400	28470	77	1650	2200	14
	5516-010	450	450	32360	61	1440	2360	13
ODP 820A	5675-017	6	6	1030	69	2630	3870	44
	5675-018	206	206	4610	65	2380	3660	43
	5675-019	326	326	6760	57	2140	3750	41
	5675-020	406	406	7870	54	1890	3500	42
	5675-021	576	576	9680	39	1240	3180	41
	5675-022	616	616	10910	43	1250	2910	41
	5675-023	636	636	12500	40	1520	3900	47
	5675-024	656	656	14090	42	1360	3090	44
	5675-025	686	686	16470	48	1780	3710	42
	5675-026	725	725	31750	78	1910	2450	32
	5675-027	746	746	41200	77	2090	2710	33
FR4/92-PC13	4675 - 07	8	8	1660	71	2020	2850	35
	5309 - 15	34	34	5250	66	1830	2770	28
	5309 - 10	55	55	8150	58	1580	2680	24
	4675 - 08	76	76	10640	45	980	2180	25
	5309 - 11	83	83	13030	59	1440	2400	22
	5309 - 12	87	87	15070	69	1260	1830	12
	4675 - 09	95	95	19160	71	1160	1630	9
	5309 - 13	105	105	24260	77	1360	1770	7
	5309 - 14	124	124	33950	82	1320	1610	8
	FR4/92-PC11	5516-011	12	2	2180	78	2240	2870
5516-012		23	13	4380	77	2350	3050	23
5516-013		34	24	6580	70	1920	2740	23
5516-014		44	34	8080	65	1580	2430	24
5516-015		59	49	10140	53	1260	2380	27
5675-016		67	57	13390	72	1670	2320	14
5516-016		74	64	16500	74	1400	1890	23
5516-017		83	73	20500	76	1260	1660	10
5516-018		98	88	27160	81	1450	1790	11
5516-019		109	99	32050	81	1500	1850	10

Core	Sample code	Core depth (cm)	Depth (cmbst)	Age (cal BP)	Bulk CO ₃ content [^] (%)	Sr Sr _{extractable} [*] (ppm)	Sr Sr _{carbonate} [*] (ppm)	Aragonite <i>ra</i> (%)
51GC43	5516-037	5.5	5.5	2530	72	2140	2970	38
	5516-038	37	37	6760	67	1860	2780	34
	5516-039	55	55	8480	55	1580	2870	33
	5516-040	84	84	9260	44	1180	2680	37
	5516-041	134	134	10630	34	850	2500	36
	5516-042	154	154	11440	40	1240	3100	30
	5516-043	171	171	14130	44	1100	2500	32
	5516-044	182.5	182.5	16130	40	1040	2600	29
	5516-045	193.5	193.5	18040	33	620	1880	26
	5516-046	212	212	21250	42	940	2240	28
	5516-047	239	239	25940	46	1220	2650	32

[^] Bulk carbonate data from Page et al. (2003), except data for ODP 820A (Peerdeman and Davies, 1993)

^{*} Sr_{extractable} – relative to the total bulk mass of the sample; Sr_{carbonate} – relative to the mass of the bulk carbonate fraction of the sample

ra – relative abundance as a percentage of total carbonate

Table 3.3: Measured and corrected (for siliciclastic dilution) strontium concentration down sediment cores FR5/90 PC27a, ODP Hole 820A (1H to 2H-1), FR4/92 PC13, FR4/92 PC11, and 51GC43.

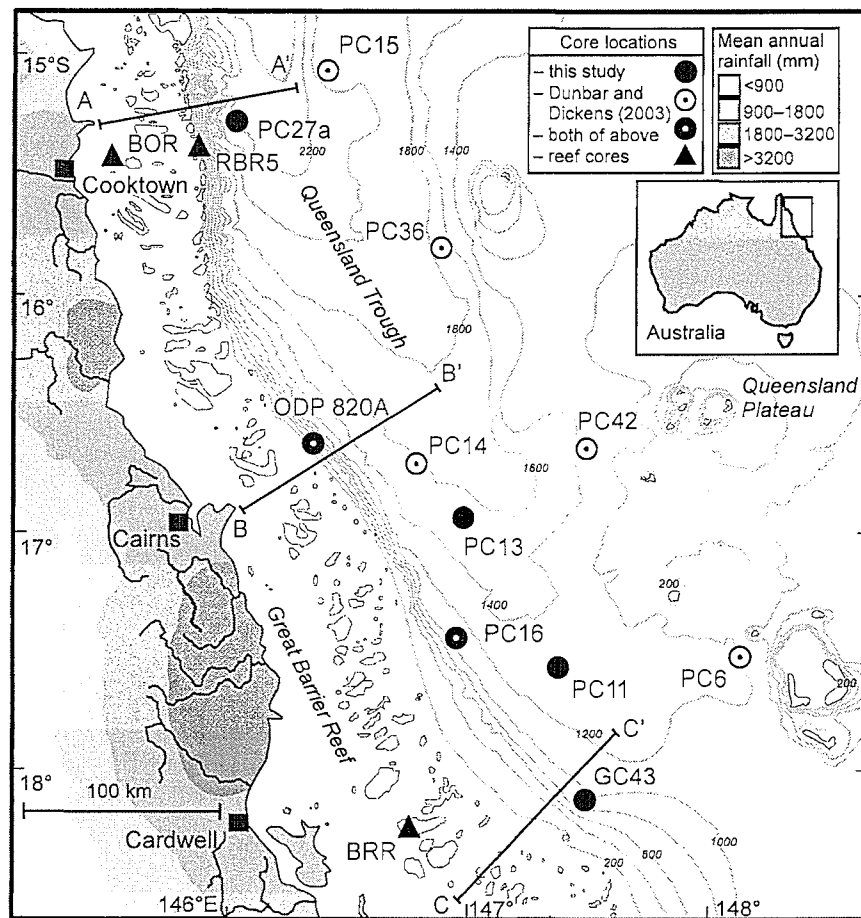


Figure 3.1: The central portion of the northeast Australian margin, bathymetry (m) of the Coral Sea, and mean annual rainfall on the continent. Circles indicate cores examined from Queensland Trough. Triangles indicate cores through reefs on the shelf (BRR – Britomart Reef, Johnson et al., 1984; RBR5 – Ribbon Reef 5, BOR – Boulder Reef, International Consortium for Great Barrier Reef Drilling, 2001). Transects A–A’, B–B’ and C–C’ appear as cross-sections on **Fig. 3.10**.

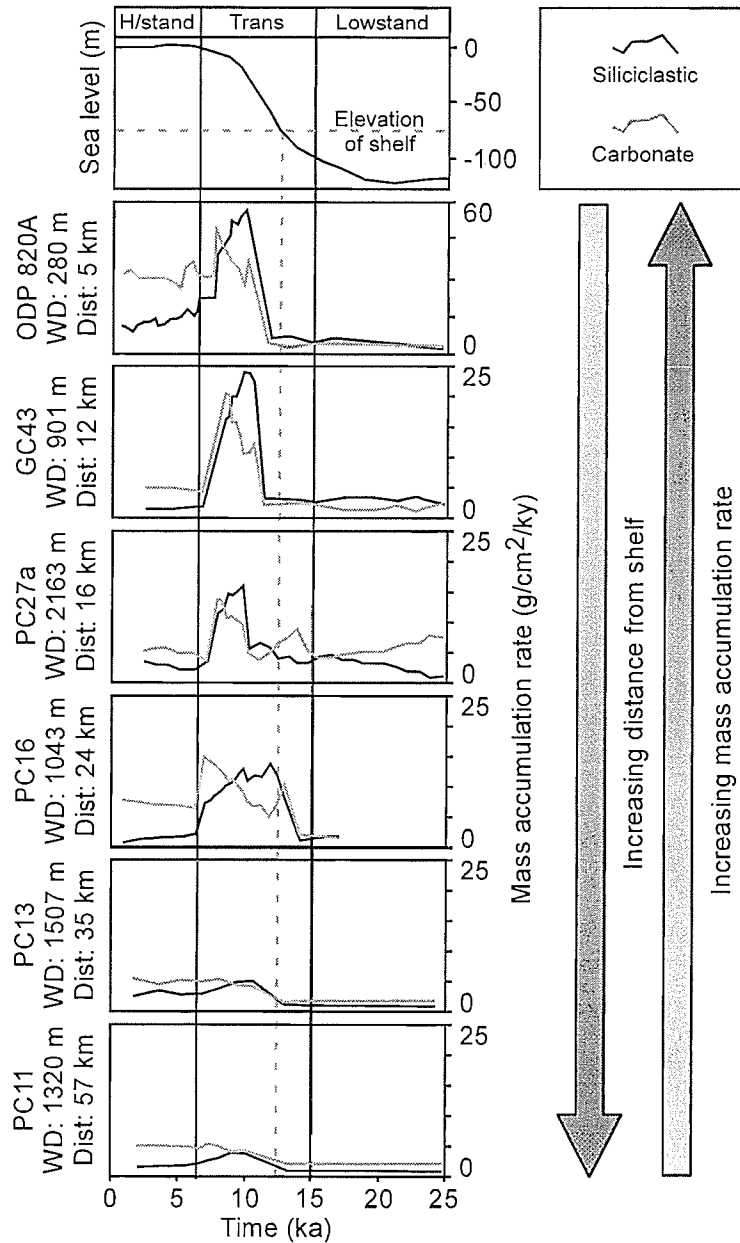


Figure 3.2: Mass accumulation rates of bulk siliciclastic and bulk carbonate components in cores from ODP 820A, 51GC43, FR5/90 PC27a, FR4/92 PC16, FR4/92 PC13, and FR4/92 PC11 (modified after: Peerdeman and Davies, 1993; Dunbar et al., 2000; Page et al., 2003). H/stand – sea-level highstand. Trans – transgression. Lowstand – sea-level lowstand. WD – water depth. Dist – distance offshore of the 120 m isobath. Note the different Y-scale for ODP 820A.

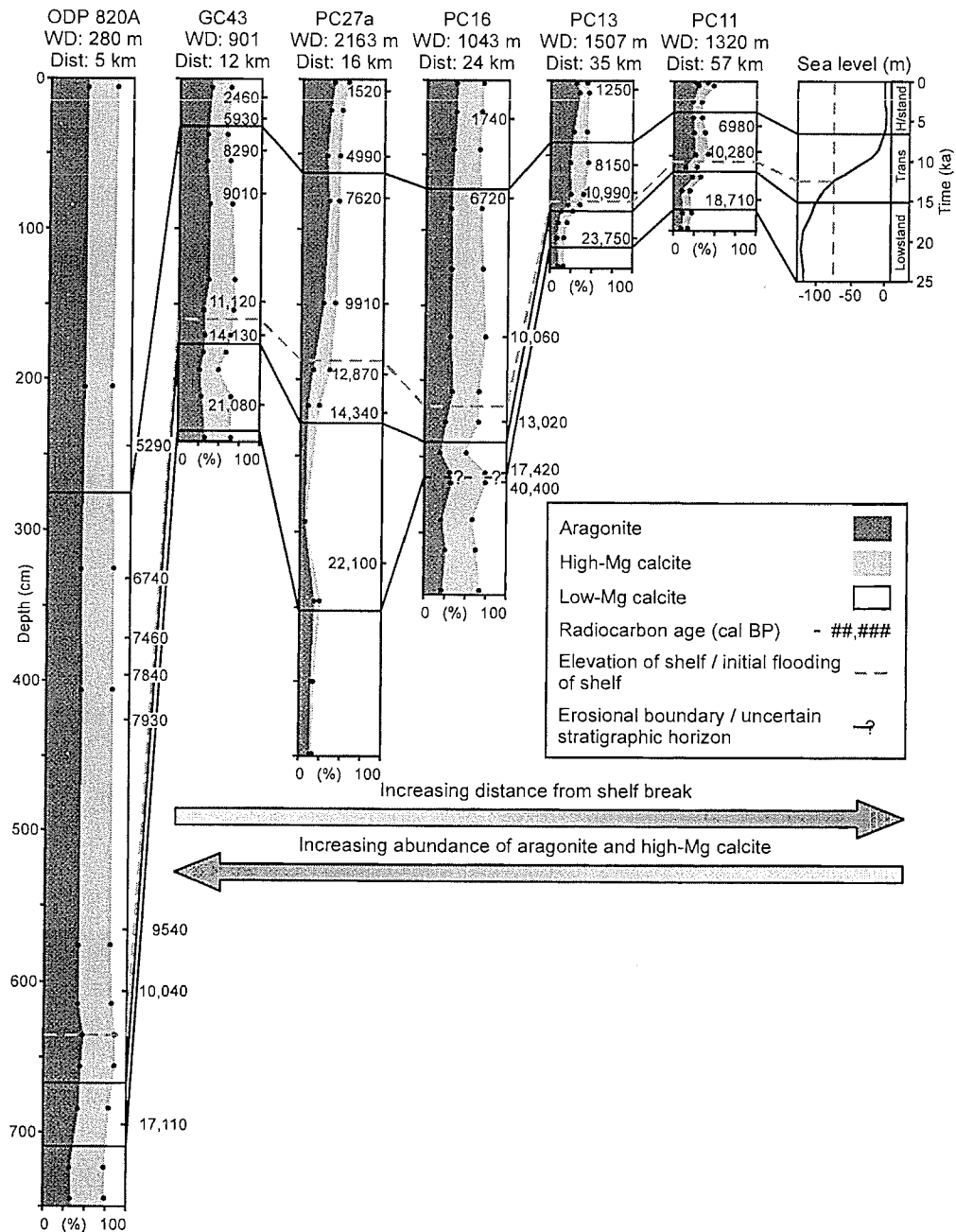
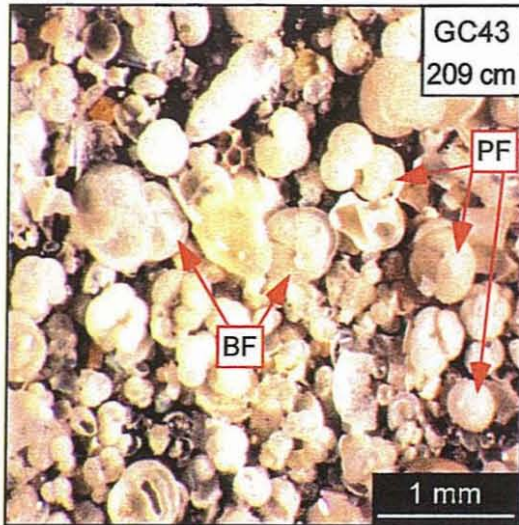
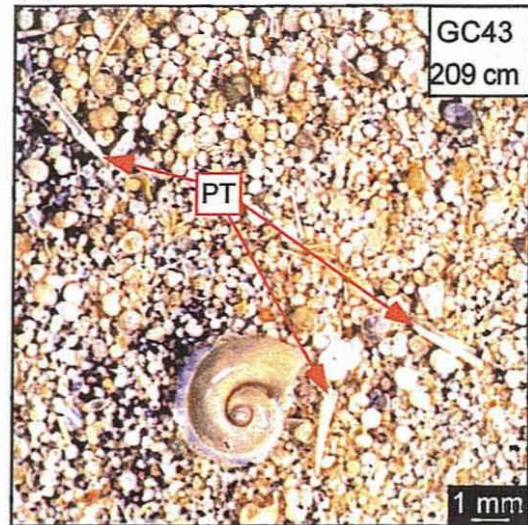


Figure 3.3. Downcore profiles of carbonate mineralogy and radiocarbon ages (modified from Peerdeman and Davies, 1993; Dunbar et al., 2000; Page et al., 2003) for ODP Hole 820A, 51GC43, FR5/90 PC27a, FR4/92 PC16, FR4/92 PC13, and FR4/92 PC11. Original age models for ODP 820A and PC16 (based on conventional radiocarbon ages) have been calibrated with the CALIB 4.3 freeware (Stuiver et al., 1998) to maintain consistency with the age models of Page et al. (2003). H/stand – sea-level highstand. Trans – transgression. Lowstand – sea-level lowstand. WD – water depth. Dist – distance offshore of the 120 m isobath.

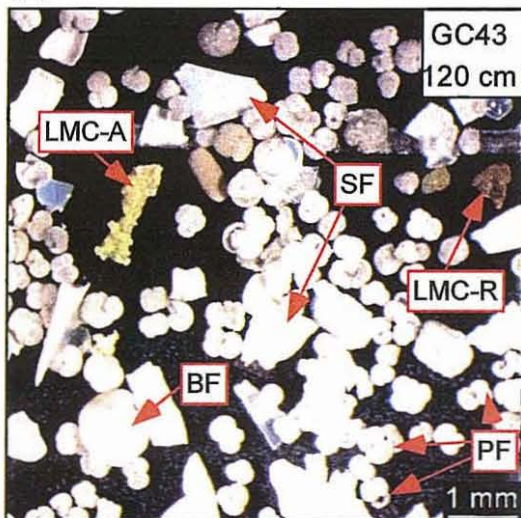
(A)



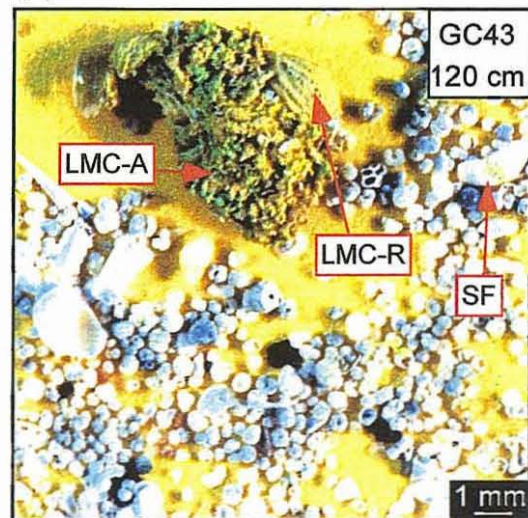
(B)



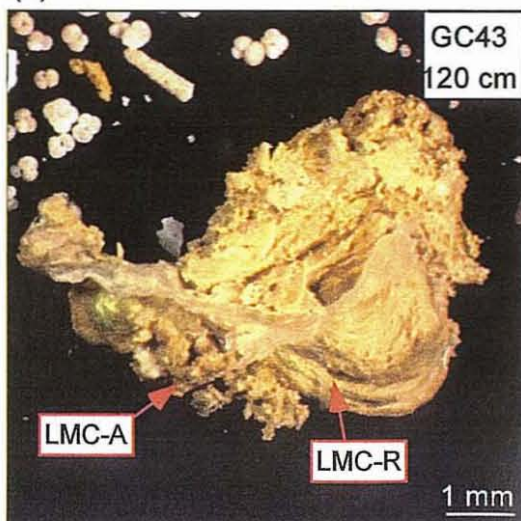
(C)



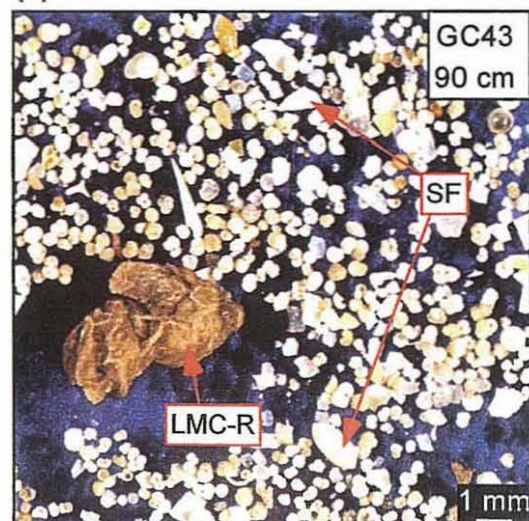
(D)



(E)



(F)



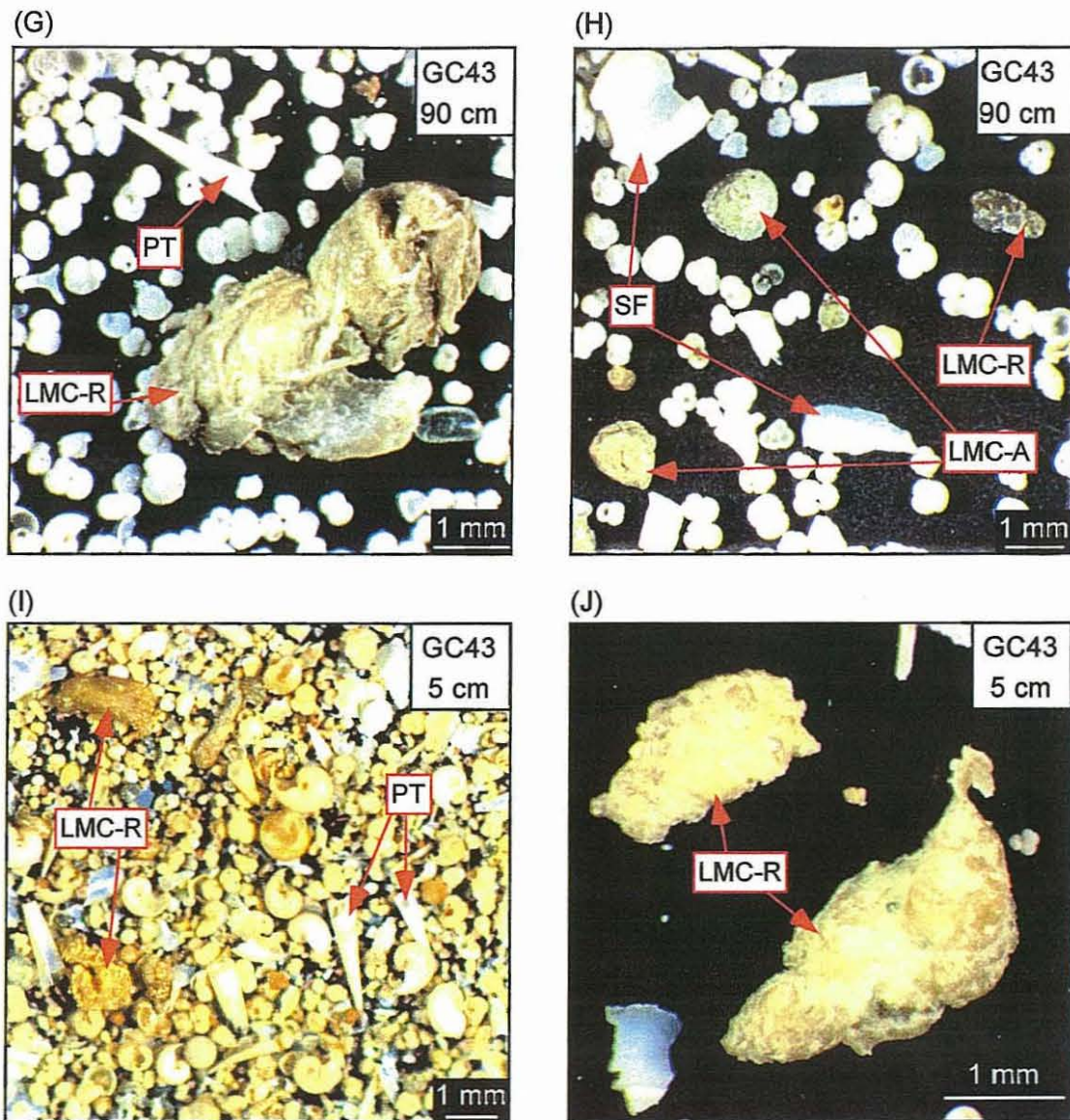


Figure 3.4: The sand-sized fraction of sediment deposited in core 51GC43 during:
 (A–B) The last glacial lowstand, ~21 ka (209 cmbsf), planktonic (PF) and benthic (BF) foraminifers are the dominant components, pteropods (PT) are also common;
 (C–E) The postglacial transgression, ~11 ka (120 cmbsf) and (F–H) ~9 ka (90 cmbsf), foraminifera are abundant, shell fragments (SF) and LMC clasts are common, LMC clasts occur as both cemented aggregates (LMC-A) and recrystallised grains (LMC-R);
 (I–J) The Holocene highstand, ~2.5 ka (5 cmbsf), foraminifers are abundant and shell fragments are common, LMC clasts are present in minor quantities.

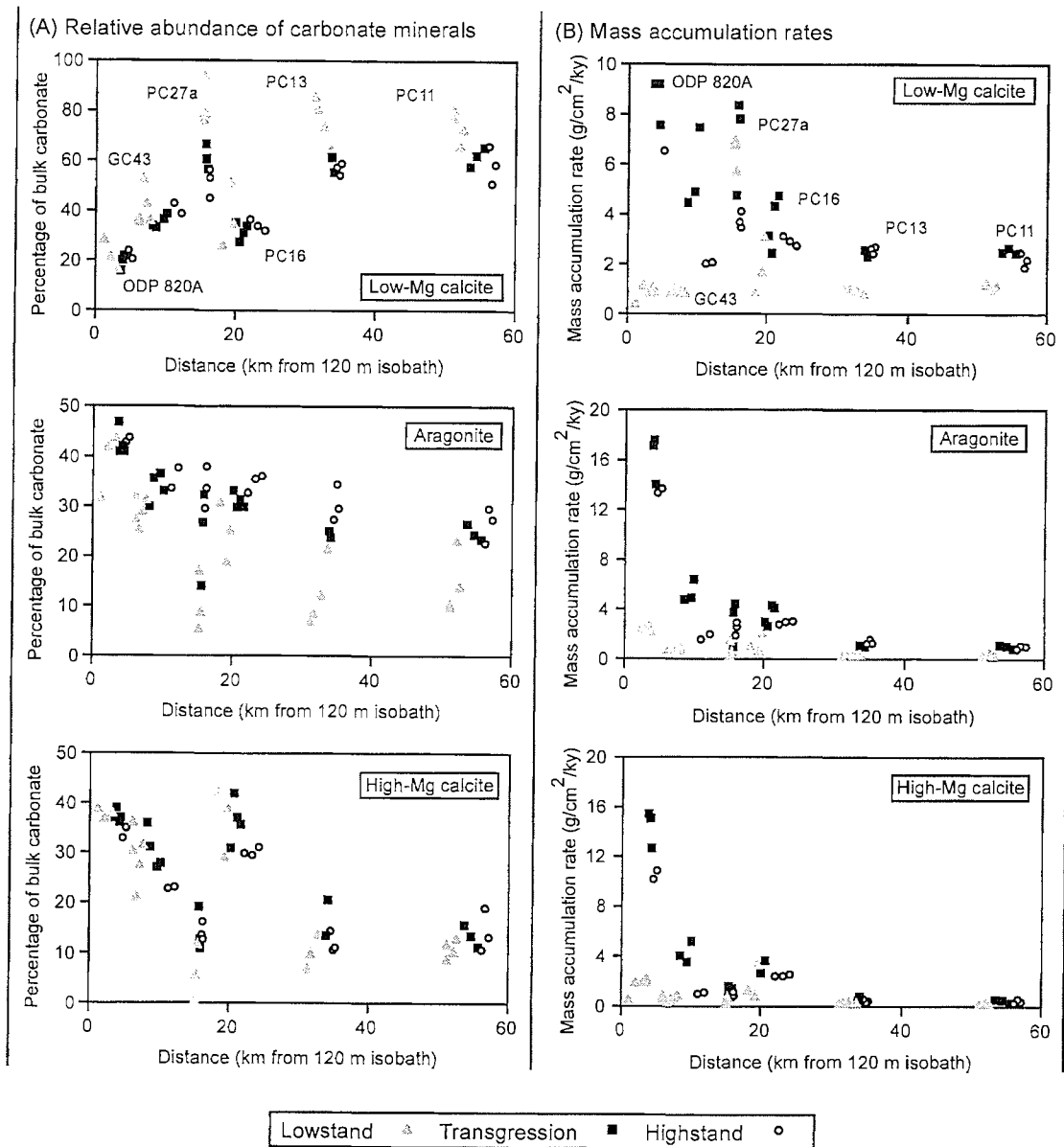


Figure 3.5: Relative abundances (A) and mass accumulation rates (B) of low-Mg calcite, aragonite, and high-Mg calcite during lowstand, transgression, and highstand, in cores from ODP Hole 820A, 51GC43, FR5/90 PC27a, FR4/92 PC16, FR4/92 PC13, and FR4/92 PC11, plotted against distance from the 120 m isobath. With increasing distance from the shelf, the relative abundance of LMC generally increases, and the relative abundances of aragonite and HMC generally decrease. Note, however, that with increasing distance from the shelf, the mass accumulation rates of all carbonate minerals generally decrease.

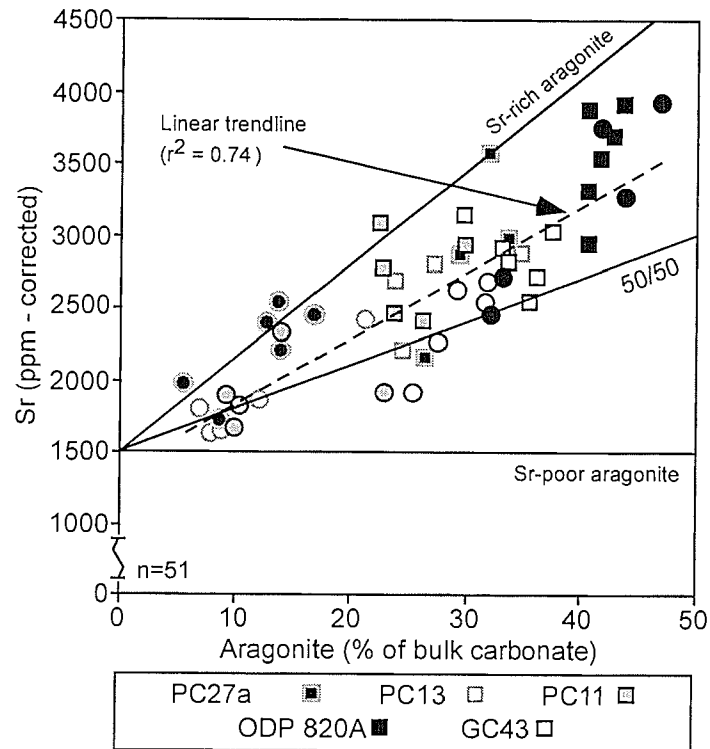


Figure 3.6: Strontium concentration versus the percentage of aragonite in the bulk carbonate fraction of sediment from cores FR5/90 PC27a, ODP 820A (1H to 2H-1), FR4/92 PC13, FR4/92 PC11, and 51GC43. Circles represent samples deposited prior to 12 ka; squares represent samples deposited after 12 ka. Assuming that Sr-rich aragonite contains 7500 ppm Sr, and that Sr-poor aragonite contains 1500 ppm Sr, samples in which the aragonite present in the bulk carbonate fraction is composed entirely of Sr-rich aragonite should plot along the solid line marked Sr-rich aragonite, and samples in which the aragonite present in the bulk carbonate fraction is composed entirely of Sr-poor aragonite should plot along the solid line marked Sr-poor aragonite. Samples in which the aragonite present in the bulk carbonate fraction is composed of equal parts Sr-rich aragonite and Sr-poor-aragonite should plot along the solid line marked 50/50. The linear trendline ($y = 45.5x + 1391$; $r^2 = 0.74$) indicates that more than 50% of the aragonite present in most samples is composed of Sr-rich aragonite.

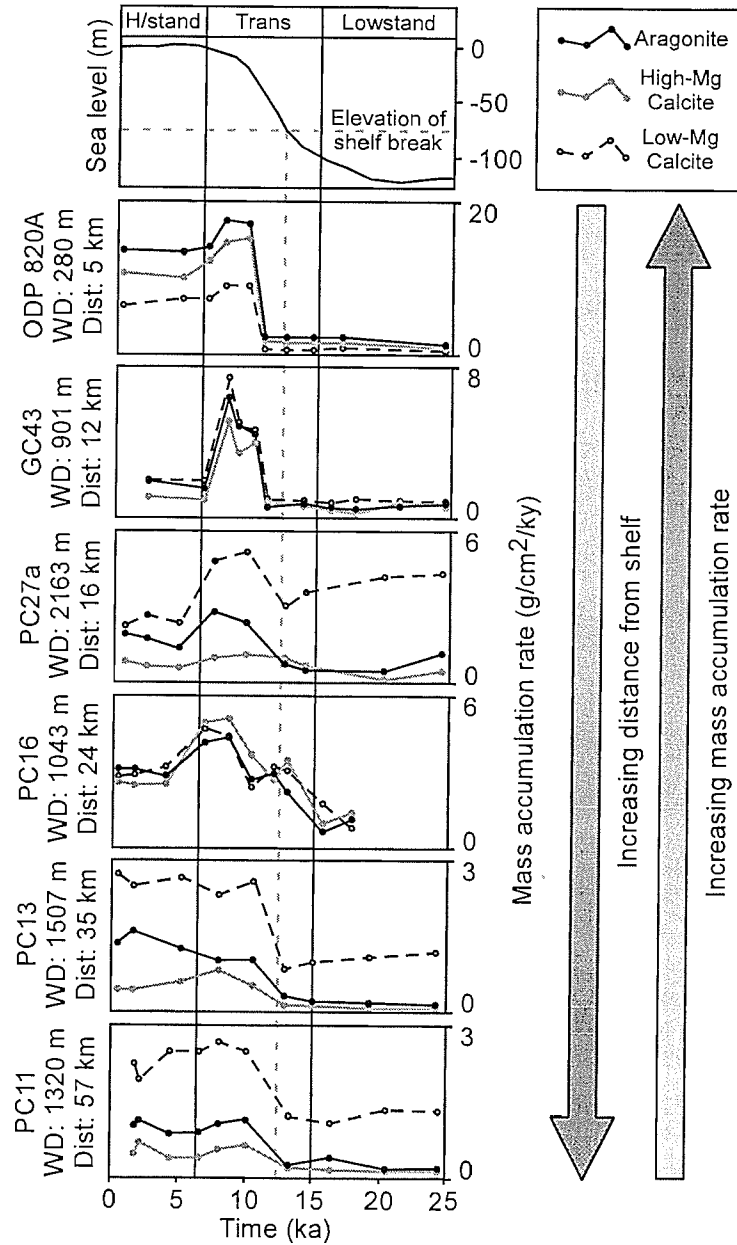


Figure 3.7: Mass accumulation rates of low-Mg calcite, aragonite and high-Mg calcite in cores from ODP Hole 820A, 51GC43, FR5/90 PC27a, FR4/92 PC16, FR4/92 PC13, and FR4/92 PC11. H/stand – sea-level highstand. Trans – transgression. Lowstand – sea-level lowstand. WD – water depth. Dist – distance offshore of the 120 m isobath.

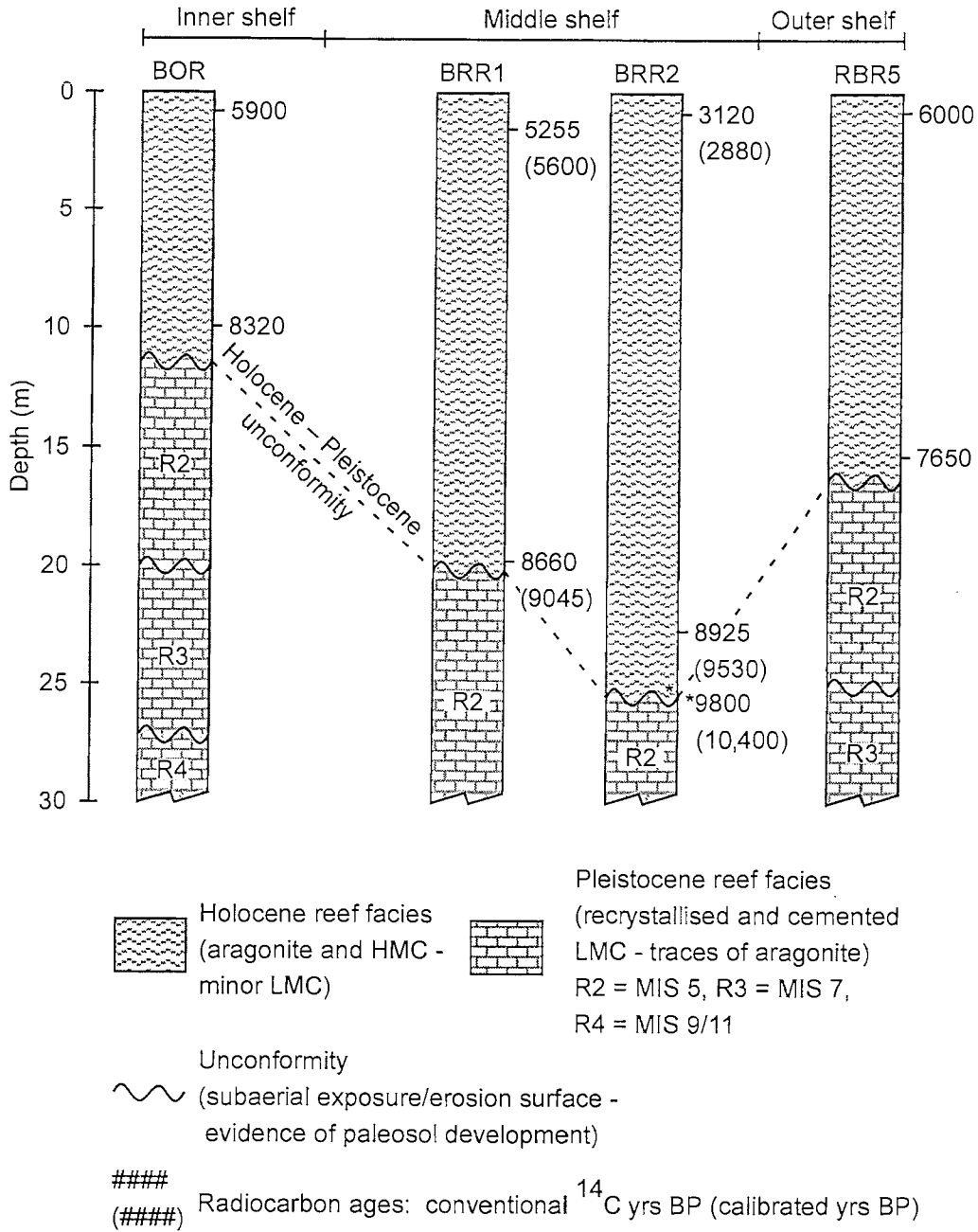


Figure 3.8: General stratigraphy of cores through individual reefs on the Great Barrier Reef (modified from: Johnson et al., 1984; International Consortium for Great Barrier Reef Drilling, 2001; Webster and Davies, 2001) the location of which are shown on **Fig. 3.1**. Holocene reefs are founded upon Pleistocene substrates that have been subaerially exposed and altered from aragonite (and high-Mg calcite) to low-Mg calcite, and are separated by erosional ('solution') unconformities. The lowermost age for BRR2 is estimated based on the distance between the lowermost radiocarbon age and the underlying solution unconformity, and published growth rates for Britomart Reef (Johnson et al., 1984).

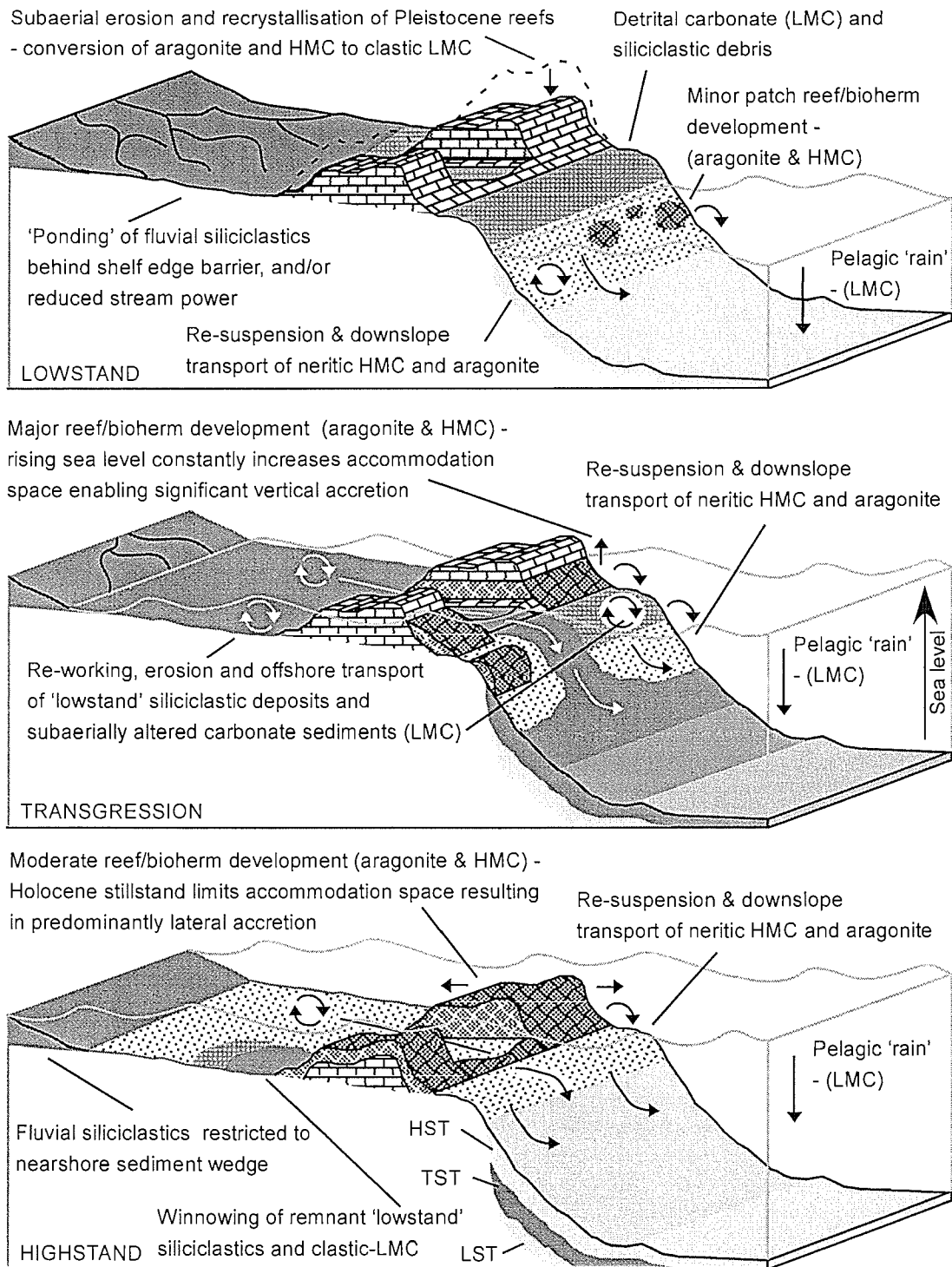


Figure 3.9: Schematic model of sedimentary processes and off-shelf fluxes on the northeast Australian margin since the Last Glacial Maximum.

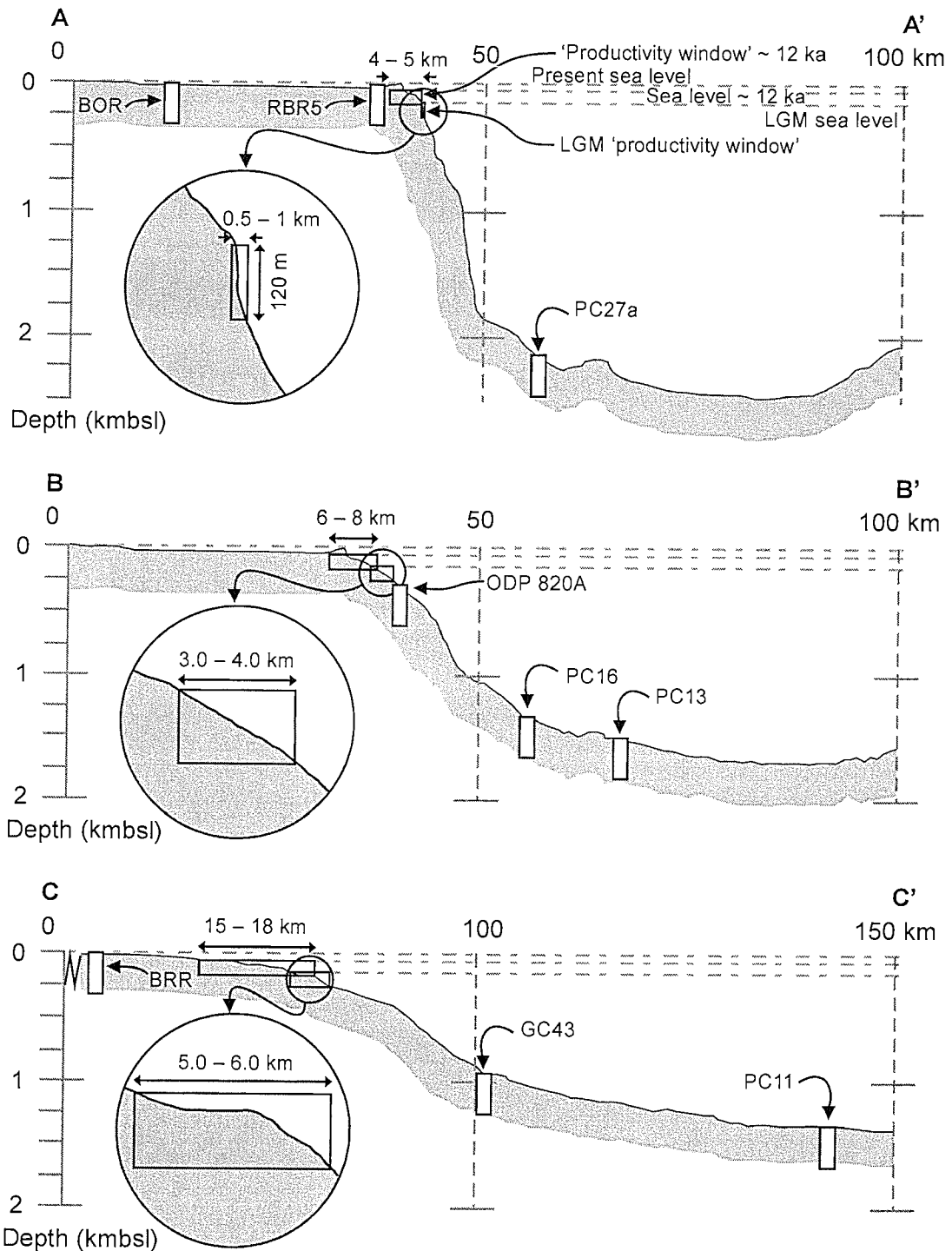


Figure 3.10: Bathymetric profiles across the shelf-slope break of the northeast Australian margin (location of transects shown on **Figure 3.1**) and the approximate position of cores in Queensland Trough and on the shelf. Note that the areas of seafloor within 120 m of the sea surface during lowstand ('LGM productivity window') increase by up to an order of magnitude almost immediately upon sea level rising above the shelf break during transgression.

CHAPTER 4

Sediment fluxes to Marion Plateau (southern Great Barrier Reef Province) over the last 130 ky: New constraints on 'transgressive-shedding' off northeastern Australia

Michael C. Page

School of Earth Sciences, James Cook University, Townsville, QLD 4811, Australia

Gerald R. Dickens

Department of Earth Sciences, Rice University, Houston, Texas 77005, USA

Adapted from a paper published in:

Marine Geology

May 2005, Volume 219, Pages 27-45

ABSTRACT

Generic models predict siliciclastic and carbonate fluxes to continental slopes of tropical mixed systems will be out-of-phase over cycles of sea-level change. Siliciclastic and carbonate fluxes should be highest during lowstands and highstands, respectively, and condensed sections should form during transgressions. Recent studies have documented the opposite response for slopes along portions of the largest modern tropical mixed system, the northeast Australian margin; siliciclastic and carbonate fluxes are in-phase and highest during transgressions. An outstanding issue is the extent of this response through space and time, because studies to date have mostly focussed on sedimentation over the last 40 ky in Queensland Trough, offshore from a narrow shelf and a wet tropical hinterland in the central GBR province. Here we investigate mixed sediment deposition over the last 130 ky in a core from Marion Plateau, offshore from a wide shelf and a dry tropical hinterland in the southern GBR province. Bulk carbonate content and carbonate mineralogy were determined downcore, and foraminiferal oxygen isotopes and radiocarbon ages were used to constrain ages and accumulation rates. Carbonate content and mineralogy vary predictably with changes in sea level over the last 130 ky; bulk carbonate and aragonite are more abundant during highstands and less abundant during lowstands. However, component mass accumulation rates reveal that highest off-shelf fluxes of all material (siliciclastic, low-Mg calcite, aragonite, and high-Mg calcite) occurred during transgressions. Sedimentation consistently diverges from conventional models in all cores examined to date from slopes of the northeast Australian margin, regardless of core location and modern differences in climate and physiography between the southern and central GBR provinces. These unconventional patterns of sediment deposition could result from changes in climate, particularly increased precipitation during deglaciations, although

this does not explain elevated fluxes of low-Mg calcite. Alternatively, fluvial sediments and diagenetically altered carbonate aggraded on the shelf during lowstands, and were eroded and transported to the slope during transgressions.

4.1. INTRODUCTION

The northeast Australian continental margin, extending from southern Papua New Guinea to central Queensland (Fig. 4.1), represents the largest modern example of a tropical mixed siliciclastic-carbonate depositional system (cf. Mount, 1984). Unlike most extant and well-studied margins surrounding Europe and North America, rivers discharge significant quantities of terrigenous siliciclastic material onto a shelf hosting an extensive number of carbonate producing reefs, known collectively as the Great Barrier Reef (GBR). This system has been broadly similar for at least 500 kyr (Davies et al., 1991; International Consortium for Great Barrier Reef Drilling, 2001), although the location and magnitude of riverine discharge and carbonate production have undoubtedly varied with changes in late Quaternary climate and sea level.

The deposition of siliciclastic and carbonate sediment on slopes of the northeast Australian margin presents an intriguing problem for marine geoscientists. Late Quaternary sedimentary successions east of the GBR are characterised by alternating siliciclastic-rich and carbonate-rich horizons (e.g., Harris et al., 1990; Glenn et al., 1993a), which reflect changes in the shedding of various components from the shelf. Following accepted sediment deposition models for tropical mixed systems (Fig. 1.2B), which are largely based on inference (e.g., Wilson, 1967; Dolan, 1989; James and Kendall, 1992), these horizons were originally interpreted as representing low carbonate/high siliciclastic accumulation rates during sea-level lowstands, high carbonate/low siliciclastic accumulation rates during sea-level highstands, and condensed intervals during sea-level transgressions (Harris et al., 1990; Glenn et al., 1993a; Kronen and Glenn, 2000).

Recent investigations on well-dated sediment cores, however, clearly demonstrate that this is not the case for slopes of the central portion of the northeast Australian

margin, at least over the last 40 kyr (Peerdeman and Davies, 1993; Dunbar et al., 2000; Dunbar and Dickens, 2003a; Page et al., 2003, Page and Dickens, 2005). Along slopes of Queensland Trough (Fig. 4.1) siliciclastic and carbonate accumulation rates have been in-phase since before the last glacial maximum (LGM; Fig. 1.2C). Accumulation rates of both components were lowest during the last glacial lowstand ca. 25–12 ka, highest during transgression ca. 12–7 ka, and at relatively moderate levels during highstand ca. 7 ka to present (Page et al., 2003). Results from Ocean Drilling Program (ODP) Site 820 suggest a similar depositional response also accompanied sea-level change during the penultimate glacial-interglacial transition (Peerdeman and Davies, 1993), or marine isotope stage (MIS) 6 to MIS 5e. These results represent a fundamental departure from conventional wisdom for the evolution of tropical mixed siliciclastic-carbonate depositional systems.

All cores from slopes off northeastern Australia that have been examined previously for late Quaternary sediment fluxes have come from Queensland Trough between ~15° and 18°S (Fig. 4.1). These cores lie offshore of the central GBR province, where a relatively narrow to moderately wide (<100 km) shelf is flanked by a mostly wet tropical hinterland. As such, these cores may not be representative of the entire northeast Australian margin, because it is possible that exceptions to previously documented sedimentation patterns might exist due to different boundary conditions elsewhere on the margin.

In this study, we examine late Quaternary siliciclastic and carbonate sediment fluxes on Marion Plateau, east of the southern GBR province at ~20.8°S, where a very broad (~200 km) reef-rimmed shelf extends from a dry tropical hinterland. The purpose of this study was to investigate sediment deposition east of the GBR at a location where climatic and physiographic boundary conditions are different to those that exist in the

central GBR province. However, despite modern differences in climate and physiography, patterns of late Quaternary sediment deposition on Marion Plateau parallels that in Queensland Trough: maximum siliciclastic and carbonate fluxes to the slope occurred during sea-level transgression ca. 11 to 8 ka. These results suggest that sedimentation all along slopes of the northeast Australian margin deviates from that predicted by conventional models, probably because of climate or antecedent topography. Increased precipitation during the last postglacial transgression may have increased sediment delivery to slopes east of the GBR, and/or exposure of the GBR during the last glacial lowstand may have resulted in fluvial aggradation and sediment deposition behind topographic highs on the outer shelf, which could be reworked and transported to the slope during transgression.

4.2. LOCATION, SAMPLES AND METHODS

4.2.1. The northeast Australian margin

The continental margin of northeast Australia between $\sim 15^\circ$ and 23° S latitude (Fig. 4.1) can be divided into four general but distinct physiographic regions: (1) a continental hinterland variously dissected by ephemeral and entrenched rivers, (2) a low-gradient shelf rimmed by an extensive barrier reef system, the GBR, (3) relatively steep slopes seaward of the GBR, and (4) basins and plateaux of the open ocean. The dimensions and characteristics of these regions, however, vary significantly with latitude, as does climate.

The central GBR province, from nominally 15 to 19° S, is flanked by a wet tropical hinterland where numerous, relatively small rivers flow steadily throughout the year, albeit with low sediment yields (Neil et al., 2002). This area also receives large quantities of terrestrial siliciclastic sediment from the highly ephemeral Burdekin

River, which drains a dry tropical interior and discharges to the coast at ~19.5°S (Fig. 4.1). These rivers debouch onto a shelf that narrows in width from ~100 km at 19°S to ~50 km at 15°S. Reef density also increases to the north (Maxwell, 1968). Beyond the shelf, water depths increase rapidly down a steep slope into Queensland Trough, a north-south trending rift basin up to 2800 m deep (Scott, 1993).

Patterns of late Quaternary sediment deposition in Queensland Trough have been fairly well documented (Peerdeman and Davies, 1993; Dunbar et al., 2000; Dunbar and Dickens, 2003b, 2003a; Page et al., 2003, Page and Dickens, 2005). Importantly and in contrast to expectations from widely accepted sequence stratigraphic paradigms (e.g., Vail et al., 1977; van Wagoner et al., 1988), these studies clearly demonstrate that siliciclastic and carbonate accumulation rates on slopes were much higher when sea level transgressed the shelf than when sea level was at lowstand or highstand. An outstanding issue is whether this unexpected record of sedimentation occurs to the north and south where modern physiography and climate are different.

The southern GBR province, from nominally 19 to 24°S, lies offshore the dry tropics and predominantly receives terrestrial siliciclastic sediment from ephemeral fluvial systems, the most significant being Fitzroy River (Neil et al., 2002). The shelf is very broad, up to 200 km wide, and reefs are generally patchier and less continuous than those to the north (Fig. 4.1), defining a wide, expansive network on the outer shelf (Maxwell, 1968). Further offshore, the upper slope is gradual and less steep than offshore of the central GBR province, terminating at 300-500 m water depth on Marion Plateau, a shallow block of subsided continental crust (Ewing et al., 1970). Although Marion Plateau is the focus of ODP Leg 194 research, late Quaternary sediment deposition on the slope offshore of the southern GBR province remains poorly

documented, generally due to poor recovery of surface sediments and low temporal resolution in available cores.

4.2.2. Core GC10

Core GC10 was collected by gravity corer on *RV Franklin* cruise 03/99 during site survey operations for ODP Leg 194. The core is located 320 metres below sea level (mbsl) at approximately 20.8°S latitude and 152.3°E longitude, or about 22 km east of the seaward edge of the modern GBR (Fig. 4.1). Other than an apparently unrecovered top, the core contains one of the most complete records of late Quaternary sedimentation on slopes east of the southern GBR province. Similar to cores from slopes of Queensland Trough, the sedimentary succession consists mostly of pelagic and neritic biogenic carbonates, and lesser quantities of hemipelagic siliciclastic material (Heck et al., 2004).

Forty-eight samples of nominally 10 cm³ volume were extracted from GC10 at 5–6 cm resolution between 0 and 1.1 mbsf (metres below sea floor), and 10 cm resolution between 1.1 and 3.7 mbsf. All analyses were performed on aliquots of this sample suite, excepting radiocarbon analyses for which separate samples of ~10 cm³ were required.

4.2.3. Analytical methods

Biogenic carbonate and terrigenous siliciclastic material account for nearly all mass of bulk sediment along the northeast Australian margin (Harris et al., 1990; Heap et al., 2001). Quantification of bulk carbonate thus renders accurate values for siliciclastic abundance (Heap et al., 2001). Carbonate content in GC10 was determined using the ‘Karbonate-Bombe’ technique (Mueller and Gastner, 1971). Bulk samples

were freeze-dried to remove water and crushed with a mortar and pestle. Between 200 and 300 mg of powdered sediment were weighed and reacted with excess 10% HCl in a closed vessel attached to a water-filled, volumetrically calibrated titration tube. The quantity of evolved CO₂ was then determined via displacement of the liquid. Duplicate analyses and comparisons with commercial standard carbonate place the precision and accuracy of reported carbonate contents at $\pm 3\%$. Bulk carbonate contents measured here also compare favourably with data obtained from GC10 using coulometric techniques (Heck et al., 2004).

Periplatform carbonate sediments contain neritic and pelagic components that can be distinguished by their mineralogy and Sr content (Milliman, 1974; Boardman and Neumann, 1984; Milliman et al., 1993). Neritic carbonate is typically dominated by Sr-rich aragonite (>7500 ppm Sr) and high-magnesium calcite (HMC) (<2000 ppm Sr), whereas pelagic carbonate is dominated by Sr-poor aragonite (<1500 ppm Sr) and low-magnesium calcite (LMC) (<2000 ppm Sr). To determine the origin of carbonate in GC10 the mineralogy of 45 samples was determined by X-ray diffraction (XRD) of crushed bulk sediment using a Siemens D5000 X-ray diffractometer at the James Cook University Advanced Analytical Centre (JCU-AAC). All samples were analysed at 30kV and 20mA between 1.3° and 65° at 0.5° min⁻¹. Samples were rotated during analysis to minimize preferred orientation. Relative abundance of the three primary phases of biogenic carbonate were quantified with Siroquant v2.0 (Taylor, 1991). Comparison of the quantified abundance of carbonate minerals with the bulk carbonate content of each sample indicates a maximum error of $\pm 5\%$ for each phase.

Strontium content of 41 samples was determined at the JCU-AAC using a Varian Liberty Series II inductively coupled plasma atomic emission spectrometer (ICP-AES). Bulk samples averaging 200 mg were weighed, digested in 5 ml of 10%

HNO₃ to dissolve the carbonate fraction, and analysed at a wavelength of 407.771 nm. Strontium concentrations in solution were determined by comparison to known values in laboratory prepared standards. Repeated analysis of standard Sr solutions places the accuracy of reported solid phase Sr content at $\pm 10\%$. Strontium values were then corrected to account for siliciclastic dilution.

Planktonic foraminifera from late Quaternary sediment of the northeast Australian margin display variations in oxygen isotope composition that primarily reflect changes in seawater chemistry associated with well-dated changes in global ice volume (Peerdeman and Davies, 1993; Dunbar et al., 2000). Oxygen isotopes were thus analysed on 48 multi-specimen samples of the white form of the pelagic planktonic foraminifera *Globigerinoides ruber* to construct a stratigraphic record for GC10. Bulk sediment samples were wet sieved at 350 and 250 μm and dried at 50°C for 2–3 hours. Fifteen to twenty-five tests were hand-picked from the sieved fraction after examination under binocular microscope and rejection of specimens with secondary cements or chamber infilling. The species and size fraction was chosen to maintain consistency with stable isotope data published for other sediment cores in the region (Peerdeman and Davies, 1993; Dunbar et al., 2000; Dunbar and Dickens, 2003a). Isotopic ratios were determined at the University of Wollongong using a Micromass multi-preparation unit attached to a Prism III mass spectrometer calibrated against NBS 18 and NBS 19 standards. All isotopic ratios are reported in standard delta notation with respect to Pee Dee Belemnite (PDB). Repeated analysis of standards indicated internal reproducibility of $<0.1\%$. Sieved samples were also examined for the pink form of *G. ruber* using a binocular microscope. In the Pacific Ocean pink *G. ruber* disappeared ~ 120 ka (Thompson et al., 1979), so its last occurrence provides a robust chronostratigraphic datum off northeast Australia (e.g., Dunbar et al., 2000).

Primary chronological control within GC10 was provided by accelerator mass spectrometry (AMS) radiocarbon analysis of pelagic planktonic foraminifera from four discrete depths, 0.01, 0.28, 0.68 and 0.99 mbsf. Bulk samples were wet sieved at 125 μm in Milli-Q ultrapure water and dried at 50°C for ~24 hours. Approximately 15 mg of *Globigerinoides sacculifer* and white *G. ruber* were picked from the coarse fraction after inspecting preservation quality under binocular microscope and rejecting specimens with secondary cements or chamber infilling. Foraminifera were sonicated to dislodge any remaining non-primary particles and collected by removing water and suspended fines with a pipette. This procedure was repeated until the water remained clear upon sonication. The foraminifera were subsequently dried at 50°C for ~24 hours. Samples were analysed by AMS at the Australian Nuclear Science and Technology Organisation (ANSTO) and ages were reported as conventional ^{14}C years before present. These ages were calibrated using CALIB v4.3 (Stuiver et al., 1998) to correct for both atmospheric and marine reservoir effects.

4.3. RESULTS

4.3.1. Bulk carbonate content

Bulk carbonate content in GC10 ranges between 92% at 2.13 mbsf and 81% at 0.49 mbsf (Fig.4.2; Table 4.1). In general, carbonate content is high (>85%) above 0.25 mbsf, from 0.65 to 1.39 mbsf, and from 1.78 to 3.58 mbsf. Therefore, given the two-component nature of the sediment, the absolute abundance of siliciclastic material varies between approximately 8 and 19%, and is relatively high (>15%) from 0.25 to 0.65 mbsf, from 1.39 to 1.78 mbsf, and below 3.58 mbsf. Bulk carbonate content in GC10 is also partly reflected in sediment colour (Fig. 4.2). Intervals of high carbonate content are generally light whereas intervals of high siliciclastic content are generally

dark. The exception is at the top of the core where carbonate-rich sediment has a reddish hue, presumably because surrounding pore waters and the trace amounts of Fe-bearing minerals have become oxidized.

4.3.2. Carbonate mineralogy

To account for siliciclastic dilution, the absolute abundance of carbonate minerals in bulk sediment can be normalized so that their sum equals 100% (Fig. 4.2; Table 4.2). Normalized LMC varies from 56% at 0.78 mbsf to 38% at 2.22 mbsf, and is generally highest between 0.3 and 1.0 mbsf, and below 3.5 mbsf. Conversely, normalized aragonite varies from 38% at 1.92 mbsf to 20% at 0.78 mbsf, and is generally highest above 0.3 mbsf, and between 1.0 and 3.0 mbsf. In fact, LMC and aragonite display a strong negative relationship when all data are considered ($r^2 = 0.78$). This inverse relationship downcore is consistent with changes in the source of carbonate from neritic (aragonite) to pelagic (LMC) organisms (Boardman and Neumann, 1984; Dunbar and Dickens, 2003b).

Normalized HMC ranges from 31% at 0.28 mbsf to 19% at 2.02 mbsf. Thus, HMC varies less down the core compared to the other carbonate phases. Moreover, variations in HMC show little correlation to LMC ($r^2 = 0.11$) or aragonite ($r^2 = 0.02$). A poor relationship between the relative abundances of HMC and other carbonate phases also occurs in sediment cores from Queensland Trough (Dunbar and Dickens, 2003b).

4.3.3. Strontium content

Strontium concentrations of the carbonate fraction (Fig.4.2; Table 4.2) range from 3465 ppm at 2.42 mbsf to 2294 ppm at 0.54 mbsf. Throughout the core, Sr concentrations in carbonate display a strong positive relationship with normalized

aragonite abundance ($r^2 = 0.70$). Indeed, all samples plot along a mixing line defined by Sr-poor calcite and Sr-rich aragonite end-members, the latter characterized by corallgal material. We conclude, therefore, that the majority of aragonite within GC10 is of neritic origin (cf. Milliman, 1974; Boardman and Neumann, 1984; Milliman et al., 1993), consistent with similar findings from slopes of Queensland Trough (Dunbar and Dickens, 2003b, Page and Dickens, 2005).

4.3.4. Chronostratigraphy

An age model for GC10 was constructed by aligning variations in the measured foraminiferal $\delta^{18}\text{O}$ record (Table 4.3) to those in the well-dated SPECMAP $\delta^{18}\text{O}$ record (Martinson et al., 1987); Figs. 4.2, 4.3). Although the magnitude of isotope variations differ in the two records (perhaps because of changes in surface water temperature), a good correlation can be made using Analyseries v1.1 software (Paillard et al., 1996). According to this correlation, GC10 represents sediment deposition from ~130 to 6 ka. The 'old surface age' at the top of GC10 likely reflects poor recovery of unconsolidated sediment at the seafloor, which is common for piston and gravity cores from slopes of the northeast Australian margin (e.g., Dunbar et al., 2000; Page et al., 2003).

The age model for GC10 can be validated through three independent means. First, the four AMS radiocarbon dates (Figs. 4.2, 4.3; Table 4.4) provide ages consistent (± 0.07 to ± 3.2 ky) with those derived from oxygen isotope stratigraphy. Second, $\delta^{18}\text{O}$ decreases by ~1.8‰ between 0.65 mbsf and the core top. This drop is close to that observed between the LGM and Holocene at other locations on the northeast Australian margin (Peerdeman and Davies, 1993; Dunbar et al., 2000; Dunbar and Dickens, 2003a). Similarly, $\delta^{18}\text{O}$ increases by ~2.1‰ between 3.13 and 0.65 mbsf. This rise is similar to that occurring between MIS 5e and MIS 2 (LGM) at locations in

Queensland Trough (Peerdeman and Davies, 1993; Dunbar et al., 2000). Further, the relatively heavy $\delta^{18}\text{O}$ value (-0.8‰) at the base of the core (3.64 mbsf) is consistent with a return to full glacial conditions (MIS 6), as also suggested by Heck et al. (2004). Third, the pink form of *Globigerinoides ruber* is absent in GC10 above 3.03 mbsf (Figs. 4.2, 4.3), indicating that sediments at the base of GC10 were deposited prior to 120 ka (MIS 5e).

4.4. MASS ACCUMULATION RATES

4.4.1. Calculation

Mass accumulation rates (r_{ma}) of siliciclastic and carbonate components were determined according to: $r_{\text{ma-}\alpha} = \alpha_{\text{conc}} \times \rho_{\text{db}} \times r_{\text{s}}$, where α_{conc} is the amount (%) of component α , ρ_{db} is the dry bulk density including pore space, and r_{s} is the bulk sedimentation rate. Values of α_{conc} for siliciclastic and bulk carbonate come from this study (Table 4.1). The ρ_{db} was assumed to be 1.0 g cm^{-3} , typical of shallow sediments on Marion Plateau (Shipboard Scientific Party, 2002) and the slope of Queensland Trough (Davies et al., 1991). The r_{s} was calculated as a continuous sedimentation rate (Fig. 4.3) using Analyseries v1.1 (Paillard et al., 1996) by applying an ‘increasing cubic spline’ function to the $\delta^{18}\text{O}$ age model. For calculating r_{ma} of LMC, aragonite, and HMC, the normalized abundance of each mineral (Table 4.2) was used for α_{conc} in conjunction with the r_{s} of bulk carbonate.

A calculated r_{ma} depends strongly on r_{s} so it is important to consider the validity of the chosen age–depth model (e.g., Grant and Dickens, 2002). In the present case, where r_{s} is determined using the $\delta^{18}\text{O}$ curve, r_{s} is highest during transgressions (Figs, 4.4, 4.5; Table 5). As an end-member alternative, linear sedimentation rates can be derived from the radiocarbon ages, at least for the last 41 kyr (Fig. 4.3). This approach

also gives maximum r_s during transgression. Since the last lowstand, sedimentation rates at GC-10, and all along slopes of the Queensland Trough (Page et al., 2003), were highest during transgression irrespective of the age–depth curves used.

4.4.2. Last Glacial Maximum (~25 ka) to mid Holocene (~6 ka)

Mass accumulation rates of siliciclastic and carbonate components in GC10 have co-varied since the LGM (Fig. 4.4A). Mass accumulation rates were lowest during lowstand and early transgression (MIS 2) ca. 25–11 ka, averaging $0.4 \text{ g cm}^{-2} \text{ ky}^{-1}$ for siliciclastic material, and $2.1 \text{ g cm}^{-2} \text{ ky}^{-1}$ for carbonate. During transgression, ca. 11–8 ka, $r_{\text{ma-siliciclastic}}$ and $r_{\text{ma-carbonate}}$ averaged 1.3 and $6.9 \text{ g cm}^{-2} \text{ ky}^{-1}$, respectively, and reached maxima of 2.0 and $10.4 \text{ g cm}^{-2} \text{ ky}^{-1}$ at ~9 ka. These rates represent a 4–5 fold increase for each component and occurred when rising sea level reached ~60 m below present (Larcombe et al., 1995) and flooded the shelf of the southern GBR province (Figure 4.4; Maxwell, 1968). From ~8 ka until the mid-Holocene highstand ~6 ka (MIS 1), $r_{\text{ma-siliciclastic}}$ and $r_{\text{ma-carbonate}}$ dropped, averaging $1.1 \text{ g cm}^{-2} \text{ ky}^{-1}$ and $7.5 \text{ g cm}^{-2} \text{ ky}^{-1}$, respectively.

Mass accumulation rates of LMC, aragonite, and HMC were in-phase with $r_{\text{ma-carbonate}}$ over the last 25 ky (Fig. 4.4B). For all carbonate minerals, r_{ma} were lowest ca. 25–11 ka, at a peak ca. 11–8 ka, and moderate ca. 8–6 ka. Of the three carbonate minerals $r_{\text{ma-LMC}}$ was always the highest, averaging 1.1, 3.8, and $3.2 \text{ g cm}^{-2} \text{ ky}^{-1}$ during lowstand, transgression, and highstand, respectively. Mass accumulation rates of aragonite and HMC were very similar to each other, averaging 0.4, 2.3, and $2.2 \text{ g cm}^{-2} \text{ ky}^{-1}$ for aragonite and 0.5, 2.3, and $2.0 \text{ g cm}^{-2} \text{ ky}^{-1}$ for HMC, during lowstand, transgression, and highstand, respectively. Thus, aragonite accumulation rates were slightly lower than those of HMC during the lowstand and early transgression, and

slightly greater than those of HMC during transgression and highstand. Peak $r_{\text{ma-aragonite}}$ ($3.0 \text{ g}\cdot\text{cm}^{-2}\text{ky}^{-1}$) and $r_{\text{ma-HMC}}$ ($3.2 \text{ g}\cdot\text{cm}^{-2}\text{ky}^{-1}$) occur ~ 9.1 ka, and, within the limitations of the age model, lag peak $r_{\text{ma-LMC}}$ ($4.3 \text{ g}\cdot\text{cm}^{-2}\text{ky}^{-1}$) by ~ 0.5 ky.

4.4.3. Last Interglacial (~ 130 ka) to Last Glacial Maximum (~ 25 ka)

The interval of time spanning the Last Interglacial (MIS 5/6 boundary) ca. 130 ka to the LGM (MIS 2) ca. 25 ka is defined here as the penultimate glacial-interglacial cycle (PG-IC). Without radiocarbon dates, age control down GC10 is less constrained for this cycle. Nevertheless, $r_{\text{ma-siliciclastic}}$ and $r_{\text{ma-carbonate}}$ also appear to have co-varied throughout the PG-IC (Fig. 4.5A), with prominent peaks in both components ca. 130–127 ka during the transgression following MIS 6 (Lambeck and Chappell, 2001). Average $r_{\text{ma-siliciclastic}}$ and $r_{\text{ma-carbonate}}$ during this time were 1.6 and $10.7 \text{ g}\cdot\text{cm}^{-2}\text{ky}^{-1}$, respectively, which are broadly similar to those during the transgression following the LGM and 4–5 times higher than during the highstand that follows in MIS 5e.

Throughout the remainder of the PG-IC, $r_{\text{ma-siliciclastic}}$ and $r_{\text{ma-carbonate}}$ display three small peaks at ~ 86 ka near the MIS 5a/5b boundary, at ~ 59 ka near the MIS 3/4 boundary, and at ~ 26 ka near the end of MIS 3. Accumulation rates during these periods represent 40 to 60% increases over background levels during the PG-IC. On the whole, however, $r_{\text{ma-siliciclastic}}$ was very low throughout the PG-IC, averaging only $0.4 \text{ g}\cdot\text{cm}^{-2}\text{ky}^{-1}$ during MIS 5 and 4, and $0.2 \text{ g}\cdot\text{cm}^{-2}\text{ky}^{-1}$ during MIS 3. These variations were again in-phase with $r_{\text{ma-carbonate}}$, which averaged $2.8 \text{ g}\cdot\text{cm}^{-2}\text{ky}^{-1}$ during MIS 5, $2.5 \text{ g}\cdot\text{cm}^{-2}\text{ky}^{-1}$ during MIS 4, and $1.5 \text{ g}\cdot\text{cm}^{-2}\text{ky}^{-1}$ during MIS 3.

Similar to the last glacial-interglacial cycle, mass accumulation rates of LMC, aragonite, and HMC, were also in-phase with each other throughout the entire PG-IC (Fig. 4.5B) and generally follow the accumulation rate patterns of bulk sediment. All

carbonate phases have highest fluxes during MIS 5, moderate fluxes during MIS 4, and lowest fluxes during MIS 3, and LMC consistently has the highest accumulation rates. However, during periods of relatively high $r_{\text{ma-carbonate}}$ the mass accumulation rate of aragonite approaches that of LMC.

4.5. DISCUSSION

Core GC10 is located in a periplatform setting offshore of the southern GBR province (Fig. 4.1) and records the variable deposition of siliciclastic and carbonate material since 130 ka (Fig. 4.2). In general, there are three carbonate-rich horizons ($\text{CaCO}_3 > 85\%$), which correlate with interglacial periods (MIS 5 and 1), as well as the MIS 3 interstadial period, and three siliciclastic-rich horizons ($\text{CaCO}_3 < 85\%$), which correlate with glacial periods (MIS 2, 4 and 6). According to conventional depositional models for tropical mixed siliciclastic-carbonate margins (Fig. 1.2B) this should be interpreted as representing high carbonate fluxes to the slope during highstand, high siliciclastic fluxes to the slope during lowstand, and limited deposition during transgression. Our results do not support such an interpretation. Instead, carbonate and siliciclastic accumulation rates have been in-phase throughout the last 130 ky, and deposition of both components was highest during sea-level transgressions, lowest during sea-level lowstands, and moderate during sea-level highstands (Figs. 1.2C, 4.5).

The relative abundance of carbonate minerals and Sr also changes down GC10. In particular, relative abundance of aragonite and Sr content co-vary with bulk carbonate content and antithetically with relative abundance of LMC; both aragonite and Sr are generally more abundant during interglacial periods and less abundant during glacial periods. These results might be interpreted according to conventional facies models for carbonate margins (e.g., Boardman et al., 1986; Posamentier and

Vail, 1988; James and Kendall, 1992; Schlager et al., 1994), especially considering that the most recent phase of reef growth on the outer GBR began ca. 9 ka (Davies and Hopley, 1983; Johnson et al., 1984). During flooding of the shelf, the area of neritic productivity within the photic zone increases and greater amounts of Sr-rich aragonite debouch from the shelf; during exposure of the shelf, however, the area of shallow marine carbonate productivity decreases and less Sr-rich aragonite reaches the slope. Indeed, there is only one problem with such an interpretation of GC10: the highs in the relative abundance of aragonite and accumulation rates of aragonite also coincided with elevated LMC accumulation rates. Fluxes of both aragonite and LMC increased when the shelf was flooded, but the latter by a lesser amount. Thus, along with increased production of neritic carbonate during transgression, there was an accompanying source of LMC, which is not to be expected considering LMC is sourced predominantly from pelagic environments.

The accumulation rates of siliciclastic and carbonate material in GC10 on Marion Plateau cannot be explained by conventional models for the deposition of sedimentary successions on passive continental margins. In terms of timing, however, the observed patterns of sediment deposition are the same as those found on slopes of Queensland Trough (e.g., Peerdeman and Davies, 1993; Dunbar et al., 2000; Dunbar and Dickens, 2003a, b; Page et al., 2003). Despite the modern differences in local physiography and climate between the central and southern GBR provinces, both regions behave differently than expected from conventional models, with minimum and maximum off-shelf fluxes of all components occurring during lowstand and transgression, respectively. These results suggest that the similarities between the regions, such as the presence of a barrier reef system on the outer shelf, are greater influences on the recent evolution of the margin than climate and local physiography.

When comparing the sedimentary successions on Marion Plateau and Queensland Trough, however, it is important to stress two obvious differences in the respective patterns of sediment deposition during the late Quaternary. First, although cores from both areas record lows in bulk carbonate content during transgression, the magnitude varies substantially. Bulk carbonate content decreases from ~80 to 40% in cores from slopes of Queensland Trough (Page et al., 2003), but only from ~92 to 81% in GC10 (Fig. 4.2). Second, there is a difference in the proportion of siliciclastic and carbonate material accumulating on the seafloor. In Queensland Trough, sediment fluxes within uppermost sediment generally decrease with distance from the shelf (Dunbar et al., 2000; Page et al., 2003), so that at 24 km from the outer GBR, $r_{\text{ma-siliciclastic}}$ and $r_{\text{ma-carbonate}}$ reach maxima of ~13 and 14 $\text{g cm}^{-2}\text{ky}^{-1}$, respectively (Fig. 4.6). Thus, at a similar distance from the shelf, $r_{\text{ma-siliciclastic}}$ in GC10 is 6 to 10 times lower than in cores from Queensland Trough, but $r_{\text{ma-carbonate}}$ is broadly comparable (Figs. 4.6, 4.7; Table 4.5). Throughout the late Quaternary, sedimentation on Marion Plateau has been influenced by lower $r_{\text{ma-siliciclastic}}$, but similar $r_{\text{ma-carbonate}}$, when compared to sedimentation on slopes of Queensland Trough.

Two hypotheses have been proposed to explain patterns of siliciclastic deposition in Queensland Trough. We refer to these as the ‘climate model’ and the ‘physiography model’, although they are not mutually exclusive. In the ‘climate model’, fluvial discharge to the coast changed markedly over time because of variations in precipitation and vegetation. Coincident with northern hemisphere glaciations, northern Australia became exceptionally arid (Kershaw, 1985; Wyrwoll and Miller, 2001). This would have reduced stream power, as suggested in the wet tropics of north Queensland by pre-Holocene alluvial fan deposition at the base of mountain scarps (Thomas et al., 2001; Thomas, 2003). Presumably, therefore, wet tropical rivers carried

very little siliciclastic material to the coast during sea-level lowstands. Increased precipitation in northern Australia during the early Holocene (Wyrwoll and Miller, 2001), as perhaps evidenced in the wet tropics of north Queensland by palynological changes (Kershaw, 1985, 1994) and incision of the alluvial fan complexes (Thomas et al., 2001; Thomas, 2003), then significantly increased siliciclastic delivery to the margin. Curiously, however, no significant early Holocene deposits have been identified on the GBR shelf (Johnson and Searle, 1984; Harris et al., 1990; Heap et al., 2001) as are evident on other low-latitude shelves from this time .

According to the alternative ‘physiographic model’ the mixed nature of the margin strongly influenced siliciclastic transport and deposition. Specifically, during sea-level lowstands, the GBR was subaerially exposed (Marshall and Davies, 1984; International Consortium for Great Barrier Reef Drilling, 2001) and represented topographic highpoints across the outer shelf that forced rivers to aggrade before reaching the LGM shoreline (Woolfe et al., 1998; Fielding et al., 2003), and siliciclastic material to ‘pond’ behind karstified reefs (e.g., Rankey et al., 1999). When sea level rose above the shelf edge during transgressions, waves, currents, and cyclones could remobilise this sediment and release it to the slope (Steckler et al., 1999; Dunbar et al., 2000; Dunbar and Dickens, 2003a; Page et al., 2003).

Compelling evidence for major shifts in late Quaternary precipitation have not yet been suggested for the dry tropics adjacent to the southern GBR province, thus we cannot fully evaluate the merits of the ‘climate model’ to explain the observed sedimentation in GC10 on Marion Plateau. However, if intensified rainfall occurred in the dry tropics ca. 11-7 ka, fluvial sediment yields might have increased substantially because of greater erosion in this region of relatively low vegetative cover. For example, sediment yields from north Queensland rivers have increased

disproportionately in the dry tropics in response to modern land use practices (Neil and Yu, 1995; Neil et al., 2002). With available information, however, our results are not consistent with the 'climate model' because siliciclastic fluxes increased less during transgression in GC10 than in cores offshore the wet tropics (Fig. 4.6).

There are, however, good reasons to suggest that the 'physiographic model' applies to the southern GBR province (Fig. 4.8). First, the very broad shelf and expansive reef network may have prevented rivers from reaching the continental slope during lowstands, especially considering the generally ephemeral nature of dry tropical rivers, and the increased aridity (Wyrwoll and Miller, 2001) and reduced stream power during the last glacial. Second, the Capricorn Channel, an elongated depression beginning on the middle shelf at ~21°S, and deepening to the south (Figs. 4.1, 4.8), may have promoted fluvial incision parallel to the coast in the southern GBR province during lowstands (Maxwell, 1968). Third, the relatively complex combination of sea-level changes over the last 130 ky (Fig. 4.5) and bathymetric profiles across the southern GBR province (viz. the middle shelf is deeper than the outer shelf; Fig. 4.8) would have resulted in large parts of the middle shelf remaining flooded when fluvial systems were attempting to prograde across the shelf. Therefore, it is probable that rivers entering the southern GBR province discharged sediment on to the middle shelf during lowstands, effectively providing a siliciclastic source that could be reworked and mobilised offshore during transgressions.

The 'physiographic model' also explains the relatively low siliciclastic fluxes at GC10 compared to similarly located cores in the Queensland Trough (Fig. 4.6). Smaller fluxes of siliciclastic material reached Marion Plateau because (1) fluvial aggradation occurred further from the slope, and (2) some siliciclastic sediment was transported south via the Capricorn Channel.

Increased accumulation rates of aragonite and HMC all along slopes of the northeast Australian margin during transgressions (Fig. 4.7) is consistent with generic models for stratal evolution of tropical carbonate systems (e.g., Boardman and Neumann, 1984; Boardman et al., 1986; Coniglio and Dix, 1992; James and Bourge, 1992; Schlager et al., 1994). However, the coincident rise in LMC accumulation rates are not expected from these models because neritic organisms produce very little LMC (Milliman, 1974; Hallock, 2001), so flooding of the shelf should not escalate LMC production. We suspect that the influx of LMC to the slope during transgression reflects off-shelf transport of altered neritic carbonate (Fig. 4.8), analogous to siliciclastic reworking in the 'physiographic model'. During sea-level lowstands, the GBR was subaerially exposed: reefal aragonite on the outer shelf was diagenetically altered to LMC and erosion reduced the elevation of Pleistocene reefs by at least 15 to 20 m (Johnson et al., 1984; Marshall and Davies, 1984; International Consortium for Great Barrier Reef Drilling, 2001). These processes may have supplied LMC clasts to an outer shelf coastal plain. When sea level initially flooded the shelf during transgression, high-energy, shallow water conditions on the outer shelf reworked the coastal plain, as well as perhaps eroding more LMC clasts from Pleistocene reefs, and transported this material to the slope. To bolster this idea, clasts of LMC might be identified in sediments deposited during transgression on Marion Plateau, as have been found on the slope of Queensland Trough (Fig. 3.4).

All cores examined to date from slopes off northeastern Australia display a remarkably consistent pattern of late Quaternary sedimentation that supports massive shedding of siliciclastic and carbonate components during transgressions. These sedimentation patterns, as well as the processes which influence them, may also be relevant for other passive continental margins. Nonetheless, some uncertainties remain

in the details. Within the inherent limitations of the current age models for available cores, a time lag exists between the onset of shelf flooding ~13 to 11 ka (Larcombe et al., 1995; Lambeck and Chappell, 2001) and increased sediment delivery to slopes ~11 to 8 ka (e.g. Fig. 4.4). This makes sense for shallow marine carbonate (aragonite and HMC), given that reef development along the modern GBR began ~10 to 8 ka (Davies and Hopley, 1983; Johnson et al., 1984; Webster and Davies, 2003; Braithwaite et al., 2004), after initial flooding of the shelf. However, a similar time lag for fluxes of siliciclastic and LMC material is less readily explained.

According to a basic 'physiographic model' (e.g. Dunbar and Dickens, 2003b), siliciclastic and LMC material accumulated on the shelf during glacial lowstands. Theoretically, this sediment could have been remobilised immediately after sea level transgressed the shelf/slope break, currently at 70-80 mbsl. However, significant sediment remobilisation might have lagged sea level rise for two reasons. First, inter-reefal areas on the outer GBR shelf generally lie ~60 m below present sea level (Maxwell, 1968). Thus, sediments deposited in and behind reefs during lowstands may not have been remobilised until well after sea level crossed the shelf/slope break. Second, a critical water depth and energy, such as that to sustain cyclones on the shelf (e.g. Larcombe and Carter, 2004), may have been required to mobilise shelf sediment deposited during lowstands.

4.6. CONCLUSION

The northeast Australian margin, including the GBR, represents the largest modern tropical mixed siliciclastic-carbonate system, where the shelf receives substantial inputs of terrestrial siliciclastic sediment from rivers, and biogenic carbonate from neritic organisms. A current research avenue is how sediment on the

shelf sheds to surrounding slopes and basins in conjunction with late Quaternary changes in sea level. Almost all work addressing this issue, however, has focused on the last glacial-interglacial cycle (MIS 2 and 1) and the central GBR province between 15 and 18°S, a region with a relatively narrow shelf (<100 km) flanked by a wet tropical hinterland, and a deep basin, the Queensland Trough.

Core GC10 comes from the slope offshore the southern GBR province (20.8°S) where a wide shelf (200 km) is flanked by a dry tropical hinterland and a shallow platform, the Marion Plateau. This core provides a record of sediment deposition on Marion Plateau since MIS 6, and our results demonstrate that variations in the accumulation rates of siliciclastic and carbonate sediments were in-phase throughout this time. Over the last 130 ky, fluxes of both components across the southern GBR shelf to Marion Plateau were highest during postglacial transgressions, lowest during sea-level lowstands, and moderate during sea-level highstands. Furthermore, accumulation rates of all carbonate minerals – LMC, aragonite, and HMC – have co-varied with bulk sediment. This record is similar to that found on slopes of Queensland Trough to the north, the only significant differences being that siliciclastic fluxes in GC10 are much less over time.

Clearly, late Quaternary sediment deposition all along slopes offshore northeast Australia does not conform to conventional models for the evolution of passive continental margins. The high siliciclastic fluxes during sea-level transgressions may have resulted from intensified monsoons and higher rainfall. This explanation, however, does not account for the coincident input of LMC. Alternatively, sediment fluxes to the slope were controlled by regional physiography (Fig. 4.8). During lowstands, rivers could not cross the broad, reef-rimmed, and subaerially exposed shelf, and discharged siliciclastic sediment on the middle to outer shelf. Concurrent erosion of

reefs led to an outer shelf with abundant clasts of LMC (e.g. Fig. 3.4). During transgressions, when the shelf was being flooded, both siliciclastic and carbonate sediments were reworked from the middle and outer shelf to the slope. The regeneration of the GBR contributed a coeval flux of aragonite and HMC. During highstands, lower-energy, deeper waters on the outer shelf lessened wave-base reworking and off-shelf sediment transport, while the stabilisation of accommodation space reduced neritic carbonate production.

It is not clear whether the patterns of stratal evolution on the northeast Australian margin through the late Quaternary are similar to that on slopes of other tropical mixed systems, modern or in the ancient geological record. However, similar relationships between physiography, fluvial evolution, and sediment transport and deposition have been identified on shelves of other mixed siliciclastic-carbonate systems (e.g., Ferro et al., 1999; Rankey et al., 1999). Consequently, our results may apply, in whole or in part, to the evolution of other passive continental margins throughout the geological record, especially tropical mixed siliciclastic-carbonate systems with barrier reefs. Furthermore, our work adds to an expanding body of evidence that challenges conventional paradigms concerning continental margin evolution (e.g., Dunbar et al., 2000; Brachert et al., 2003; Dunbar and Dickens, 2003a; Fielding et al., 2003; Page et al., 2003; Walsh and Nittrouer, 2003; Larcombe and Carter, 2004) and highlight the need for caution in interpreting sedimentary successions based on generic models.

ACKNOWLEDGEMENTS

An Australian Postgraduate Award, AAPG Foundation Grant-In-Aid, CRC Reef-Ken Woolfe Scholarship, and ODP (Australia) grant supported this research.

AMS analysis was provided by ANSTO under Australian Institute of Nuclear Science and Engineering grant 01/042P. Thanks are extended to Geoscience Australian and the crew of *RV Franklin*, who facilitated the recovery of core GC-10, to Philipp Reza Heck and Flavio Anselmetti who kindly provided samples from the ETZH core repository, and to Raphael Wust for helpful discussion of the data and manuscript.

Core	Sample code	Depth (mbsl)	Carbonate content (%)
GC10 section 1	10-1-1	0.01	89
	10-1-2	0.07	87
	10-1-3	0.12	85
	10-1-4	0.17	85
	10-1-5	0.22	86
	10-1-6	0.28	83
	10-1-7	0.34	83
	10-1-8	0.38	82
	10-1-9	0.44	83
	10-1-10	0.49	81
	10-1-11	0.54	83
	10-1-12	0.59	83
	10-1-13	0.65	85
	10-1-14	0.70	86
GC10 section 2	10-2-1	0.74	85
	10-2-2	0.79	87
	10-2-3	0.85	87
	10-2-4	0.90	86
	10-2-5	0.95	86
	10-2-6	1.01	87
	10-2-7	1.04	86
	10-2-8	1.09	86
	10-2-9	1.19	86
	10-2-10	1.29	86
	10-2-11	1.39	85
	10-2-12	1.49	83
	10-2-13	1.59	85
	10-2-14	1.69	85
GC10 section 3	10-3-1	1.73	83
	10-3-2	1.83	88
	10-3-3	1.93	86
	10-3-4	2.03	90
	10-3-5	2.13	91
	10-3-6	2.23	87
	10-3-7	2.33	87
	10-3-8	2.43	88
	10-3-9	2.53	87
	10-3-10	2.63	87
GC10 section 4	10-4-1	2.73	86
	10-4-2	2.83	86
	10-4-3	2.93	86
	10-4-4	3.03	86
	10-4-5	3.13	87
	10-4-6	3.23	87
	10-4-7	3.33	90
	10-4-8	3.43	89
	10-4-9	3.53	86
	10-4-10	3.64	84

Table 4.1: Bulk carbonate content of core FR03/99 GC10

Core	Sample code	Depth (mbsf)	JCU-AAC code	LMC (%)	Aragonite (%)	HMC (%)	Sr (ppm)
GC10 section 1	10-1-1	0.01	5675-01	40	33	27	3209
	10-1-2	0.07	5675-02	48	28	24	2885
	10-1-3	0.12	5675-03	40	31	29	2925
	10-1-4	0.17	5675-04	48	26	27	2822
	10-1-5	0.22	5675-05	44	33	24	2804
	10-1-6	0.28	5675-06	41	29	31	2946
	10-1-7	0.34	5675-07	51	23	26	2475
	10-1-8	0.38	5675-08	48	25	27	2417
	10-1-9	0.44	5675-09	52	22	26	2443
	10-1-10	0.49	5675-10	49	23	29	2381
	10-1-11	0.54	5675-11	51	25	24	2294
	10-1-12	0.59	5675-12	54	21	25	2301
	10-1-13	0.65	5675-13	54	21	25	2316
	10-1-14	0.70	5675-14	51	24	26	2437
GC10 section 2	10-2-1	0.74	5860-01	52	24	24	2393
	10-2-2	0.79	5675-15	56	21	23	2391
	10-2-3	0.85	5860-02	55	25	20	2551
	10-2-5	0.95	5860-03	53	24	23	2559
	10-2-6	1.01	5860-04	49	27	24	2621
	10-2-7	1.04	5860-05	46	30	25	2819
	10-2-8	1.09	5860-06	39	36	25	2923
	10-2-9	1.19	5860-07	40	34	26	3135
	10-2-10	1.29	5860-08	39	32	29	3176
	10-2-11	1.39	5860-09	45	34	22	2998
	10-2-12	1.49	5946-01	41	35	24	*
	10-2-13	1.59	5860-10	47	31	22	3061
	10-2-14	1.69	5860-11	46	33	22	3262
	GC10 section 3	10-3-1	1.73	5860-12	48	29	23
10-3-2		1.83	5942-02	44	32	24	*
10-3-3		1.93	5942-03	40	38	23	*
10-3-4		2.03	5860-13	48	33	19	3418
10-3-5		2.13	5942-04	43	35	22	*
10-3-6		2.23	5860-14	39	37	24	3186
10-3-7		2.33	5860-15	46	31	23	3157
10-3-8		2.43	5860-16	39	33	27	3465
10-3-9		2.53	5860-17	41	33	25	3266
10-3-10		2.63	5860-18	44	30	26	3291
GC10 section 4	10-4-1	2.73	5860-19	40	35	25	3052
	10-4-2	2.83	5860-20	45	31	23	3150
	10-4-3	2.93	5860-21	44	32	23	3099
	10-4-4	3.03	5860-22	42	30	28	3044
	10-4-5	3.13	5860-23	49	26	25	2982
	10-4-6	3.23	5860-24	45	32	23	2811
	10-4-8	3.43	5860-25	46	31	24	2847
	10-4-10	3.64	5860-26	51	28	22	2380

* not measured

Table 4.2: Carbonate mineral abundances and Sr concentrations in core FR03/99 GC10

Core	Sample code	Depth (mbsf)	$\delta^{18}\text{O}$ (PDB)	$\delta^{18}\text{O}$ (SMOW)	$\delta^{13}\text{C}$ (PDB)
GC10 section 1	MP 10-1-1	0.01	-1.5	29.3	1.1
	MP 10-1-2	0.07	-1.2	29.7	1.0
	MP 10-1-3	0.12	-1.4	29.5	1.2
	MP 10-1-4*	0.17	-1.7	29.0	0.7
	MP 10-1-5*	0.22	-1.8	29.4	1.1
	MP 10-1-6	0.28	-1.4	29.5	1.0
	MP 10-1-7	0.34	-1.3	29.6	0.8
	MP 10-1-8	0.38	-1.1	29.8	0.6
	MP 10-1-9	0.44	-1.1	29.8	0.4
	MP 10-1-10	0.49	0.1	31.0	1.4
	MP 10-1-11	0.54	0.0	30.9	1.0
	MP 10-1-13	0.65	0.3	31.3	1.4
	MP 10-1-14	0.70	-0.5	30.4	1.3
	GC10 section 2	MP 10-2-1	0.74	-1.1	29.8
MP 10-2-2		0.79	-0.9	30.0	0.6
MP 10-2-3		0.85	-1.0	29.9	1.0
MP 10-2-4*		0.90	-0.9	30.1	0.8
MP 10-2-5		0.95	-1.0	29.9	0.5
MP 10-2-6		1.01	-1.0	29.9	0.9
MP 10-2-7		1.04	-1.0	29.9	0.9
MP 10-2-8		1.09	-1.6	29.3	0.5
MP 10-2-9		1.19	-1.6	29.2	0.8
MP 10-2-10		1.29	-1.3	29.6	1.3
MP 10-2-11		1.39	-1.5	29.3	1.1
MP 10-2-12		1.49	-1.4	29.5	0.8
MP 10-2-13		1.59	-1.4	29.5	1.2
MP 10-2-14		1.69	-1.3	29.6	1.2
GC10 section 3	MP 10-3-1	1.73	-1.6	29.2	1.1
	MP 10-3-2	1.83	-1.9	28.9	1.0
	MP 10-3-3*	1.93	-1.6	29.1	0.7
	MP 10-3-4*	2.03	-1.5	29.3	0.9
	MP 10-3-5	2.13	-1.5	29.4	0.8
	MP 10-3-6*	2.23	-1.4	29.6	0.5
	MP 10-3-7	2.33	-1.6	29.3	0.8
	MP 10-3-8	2.43	-1.5	29.3	0.6
	MP 10-3-9	2.53	-1.4	29.5	0.5
	MP 10-3-10	2.63	-1.6	29.3	0.7
GC10 section 4	MP 10-4-1	2.73	-1.3	29.6	0.7
	MP 10-4-2	2.83	-1.0	29.9	0.8
	MP 10-4-3*	2.93	-1.5	29.2	0.6
	MP 10-4-4	3.03	-1.5	29.3	0.5
	MP 10-4-6	3.13	-1.8	29.1	0.8
	MP 10-4-5	3.23	-1.5	29.4	0.7
	MP 10-4-7	3.33	-1.6	29.3	0.7
	MP 10-4-8	3.43	-1.1	29.8	0.8
	MP 10-4-9	3.53	-1.6	29.2	0.5
	MP 10-4-10	3.64	-0.8	30.1	0.8

* Average isotopic ratio after multiple analyses of same sample

Table 4.3: $\delta^{18}\text{O}$ and $\delta^{13}\text{C}$ in planktonic foraminifers from core FR03/99 GC10

Sample Code	Depth (mbsf)	Lab code	Conventional	Error	Calibrated	1-sigma	Multiple cal BP	Range
			age (¹⁴ C yrs BP)	(yrs +/-)	age (cal BP)	(yrs +/-)	ages (cal BP)	(yrs)
MPRC1	0.01	OZG354	5560	40	5920	40		
MPRC2	0.28	OZG355	8730	60	9210	270	9280, 9260, 9080	200
MPRC3	0.68	OZG356	23080	150	*			
MPRC4	0.99	OZG357	41700	750	*			

* Beyond the range of calibration

Table 4.4: Results of AMS radiocarbon analysis of planktonic foraminifers from core FR03/99 GC10

MIS boundary	Time [‡]	Bulk r_s (cm.ky ⁻¹)	Siliciclastic r_{ma} (g.cm ⁻² ky ⁻¹)	Carbonate r_{ma} (g.cm ⁻² ky ⁻¹)	LMC r_{ma} (g.cm ⁻² ky ⁻¹)	Aragonite r_{ma} (g.cm ⁻² ky ⁻¹)	HMC r_{ma} (g.cm ⁻² ky ⁻¹)
	6270	8.4	1.0	7.4	3.0	2.4	2.0
	6981	8.5	1.1	7.4	3.6	2.1	1.7
	7557	8.9	1.3	7.5	3.0	2.3	2.2
	8105	9.5	1.3	8.2	3.9	2.1	2.2
	8609	10.4	1.4	9.0	3.9	2.9	2.2
	9140	12.4	2.1	10.4	4.2	3.0	3.2
	9644	10.0	1.7	8.3	4.3	1.9	2.2
	10139	6.5	1.2	5.4	2.6	1.3	1.5
1/2	11440	3.4	0.6	2.8	1.5	0.6	0.7
	13233	2.4	0.4	2.0	0.9	0.4	0.6
	15522	2.0	0.3	1.7	0.9	0.4	0.4
	21109	2.1	0.3	1.7	0.9	0.4	0.4
	23360	2.5	0.3	2.1	1.1	0.5	0.5
2/3	24678	2.8	0.4	2.4	1.3	0.6	0.6
	26388	2.9	0.4	2.5	1.4	0.5	0.6
	28674	2.3	0.3	2.0	1.1	0.5	0.4
	31235	1.7	0.3	1.4	*	*	*
	34812	1.2	0.1	1.0	0.6	0.2	0.2
	41000	0.8	0.1	0.7	0.3	0.2	0.2
	44820	0.8	0.1	0.7	0.3	0.2	0.2
	50039	1.1	0.2	1.0	0.4	0.4	0.2
	56081	2.6	0.4	2.2	0.9	0.7	0.6
3/4	58960	4.2	0.6	3.6	1.4	1.2	1.0
	61420	3.9	0.5	3.3	1.5	1.1	0.7
	64220	3.3	0.5	2.8	1.1	1.0	0.7
	67625	2.6	0.4	2.2	1.0	0.7	0.5
	71898	2.1	0.3	1.8	0.8	0.6	0.4
4/5	73910	1.9	0.3	1.6	0.8	0.5	0.4
	79250	2.1	0.3	1.7	0.8	0.5	0.4
	83207	3.1	0.4	2.7	1.1	1.0	0.6
	85846	4.5	0.6	3.9	1.9	1.3	0.8
	87898	5.0	0.5	4.5	1.9	1.6	1.0
	90100	4.0	0.4	3.6	1.4	1.3	0.9
	93000	3.1	0.4	2.7	1.2	0.8	0.6
	96411	2.8	0.4	2.5	1.0	0.8	0.7
	99960	2.9	0.3	2.5	1.0	0.8	0.6
	103377	3.0	0.4	2.6	1.1	0.8	0.7
	107084	2.8	0.4	2.5	1.0	0.9	0.6
	110790	2.6	0.3	2.2	1.0	0.7	0.5
	114882	2.4	0.3	2.0	0.9	0.7	0.5
	118975	2.5	0.4	2.2	0.9	0.7	0.6
	122560	3.2	0.4	2.7	1.3	0.7	0.7
	125244	4.5	0.6	3.9	1.8	1.2	0.9
	127108	6.6	0.9	5.7	*	*	*
	128353	10.0	1.3	8.7	4.0	2.6	2.0
	129178	14.7	1.7	12.9	*	*	*
5/6	129840	17.8	2.9	15.0	7.6	4.1	3.2

[‡] in comparison to the SPECMAP reference curve

* no mineralogical data

Table 4.5: Mass accumulation rates of sedimentary components in core FR03/99 GC10

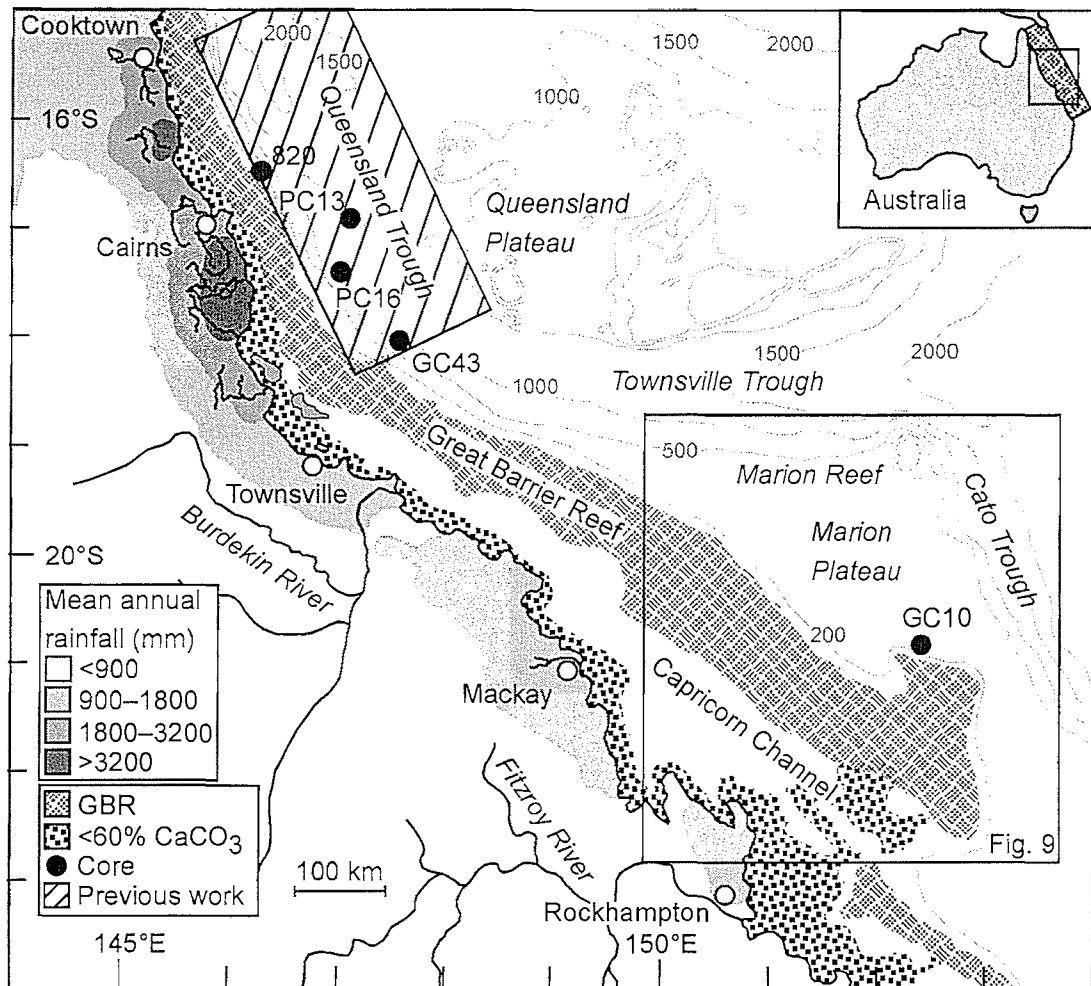


Figure 4.1: The central and southern northeast Australian margin showing major physiographic features, the location of core FR03/99 GC10 on Marion Plateau, previous study areas in Queensland Trough (Harris et al., 1990; Peerdeman and Davies, 1993; Dunbar et al., 2000; Dunbar and Dickens, 2003b; Page et al., 2003), and the locations of four previously studied cores mentioned specifically in the text.

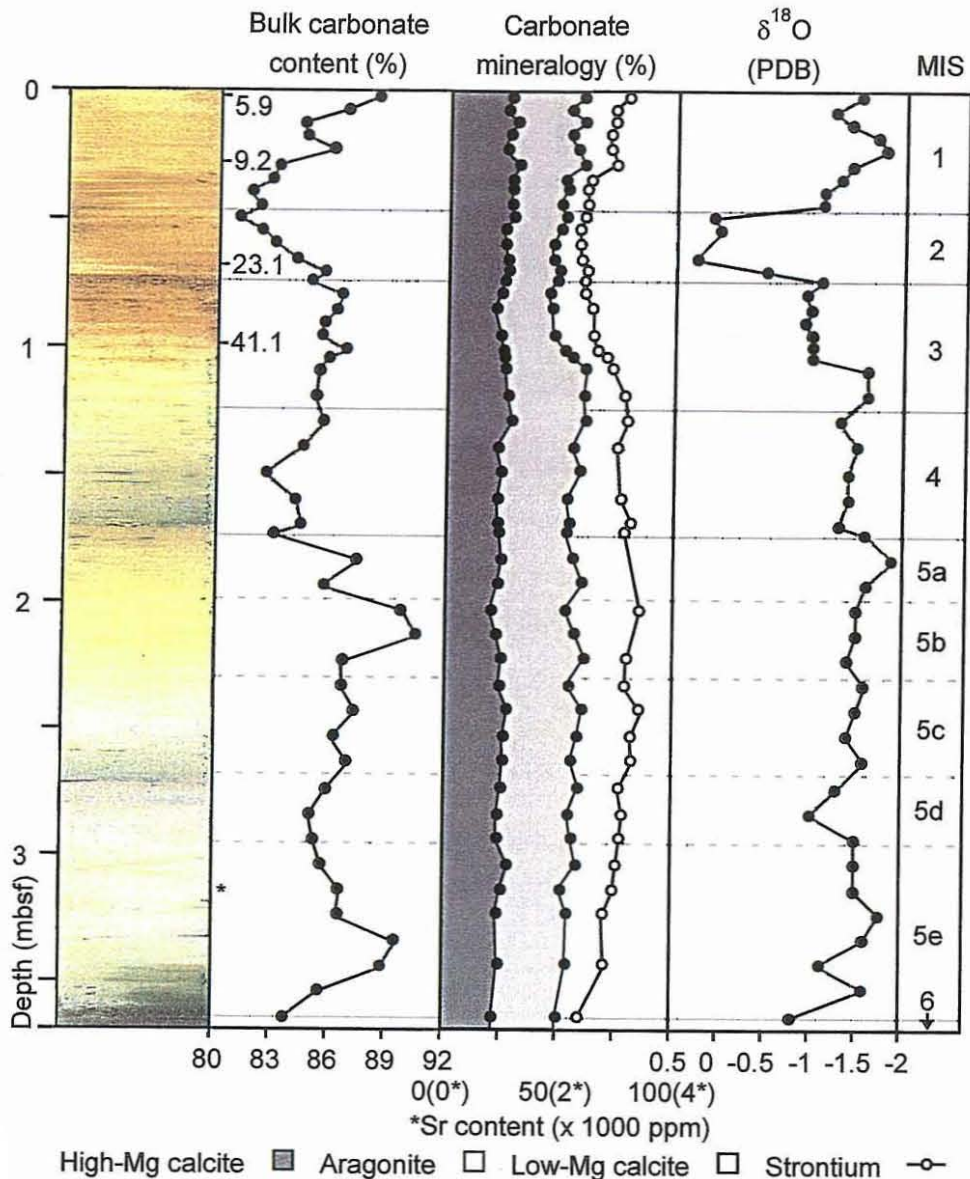


Figure 4.2: Photograph and physical properties of core FR03/99 GC10, including bulk carbonate content, relative abundance of carbonate minerals, Sr concentration in the carbonate fraction, and $\delta^{18}\text{O}$ stratigraphy. Note the position of AMS radiocarbon ages ($\times 1000$ years) and the last occurrence of pink *Globigerinoides ruber* (*) on the right side of the core photograph. Marine isotope stages (MIS) as interpreted from correlation of isotope stratigraphy with the SPECMAP record (Martinson et al., 1987) appear on the far right.

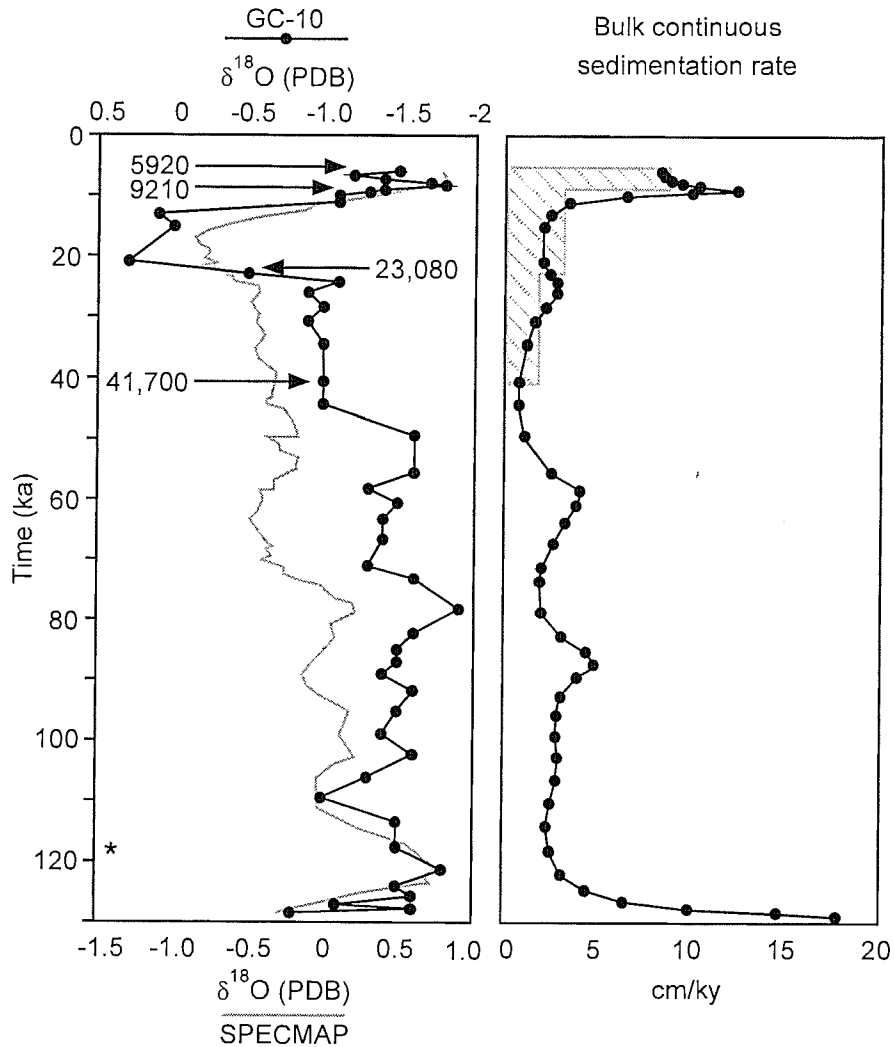


Figure 4.3: Age model for core FR03/99 GC10, produced by correlation of $\delta^{18}\text{O}$ stratigraphy with the SPECMAP record of Martinson et al. (1987). The positions of four AMS radiocarbon ages and the last occurrence of pink *G. ruber* are also noted relative to the isotope data. The bulk continuous sedimentation rate was formulated based on the isotope correlation and calculated by Analyseries v1.1 (Paillard et al., 1996). The bulk linear sedimentation rate was calculated using the AMS radiocarbon ages only. Note that both bulk continuous and bulk linear sedimentation rates increase abruptly during the last postglacial transgression.

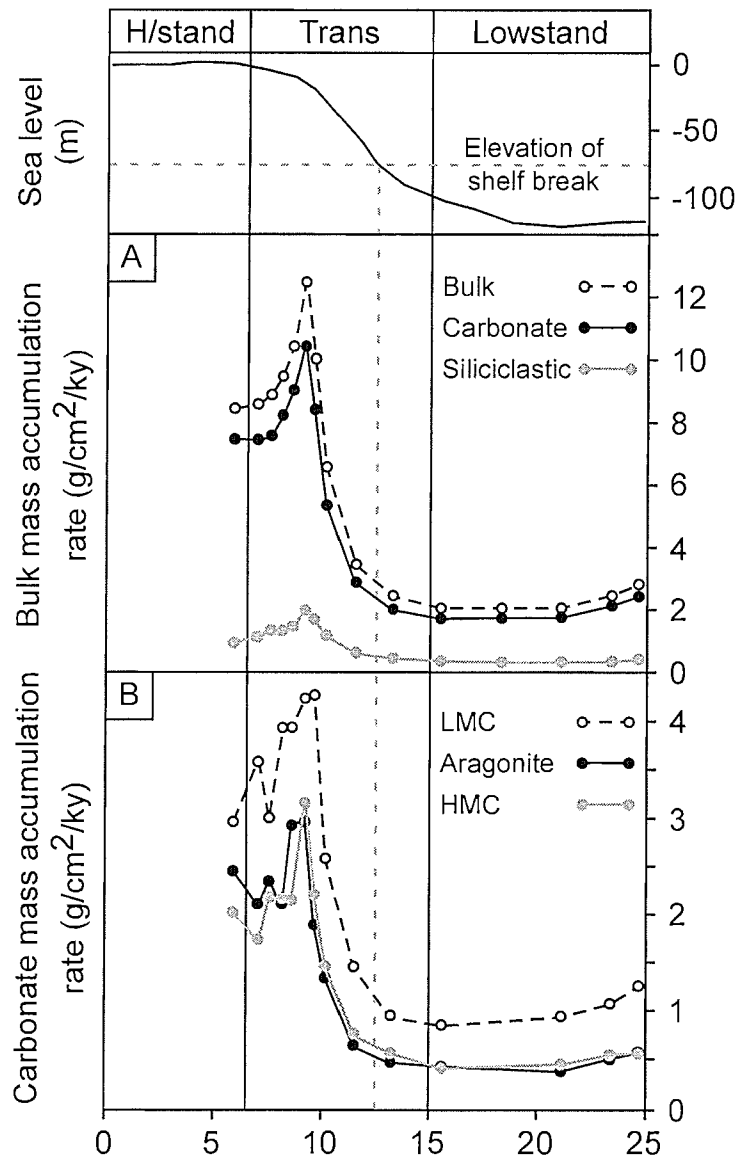


Figure 4.4: Mass accumulation rates of (A) bulk sediment, bulk carbonate, and bulk siliciclastic material, and (B) low-Mg calcite, aragonite, and high-Mg calcite, over the last 25 ky in core FR03/99 GC10, calculated using the continuous sedimentation rate (Fig. 4.3). Mass accumulation rates of all components were lowest during lowstand, highest during transgression, and moderate during highstand.

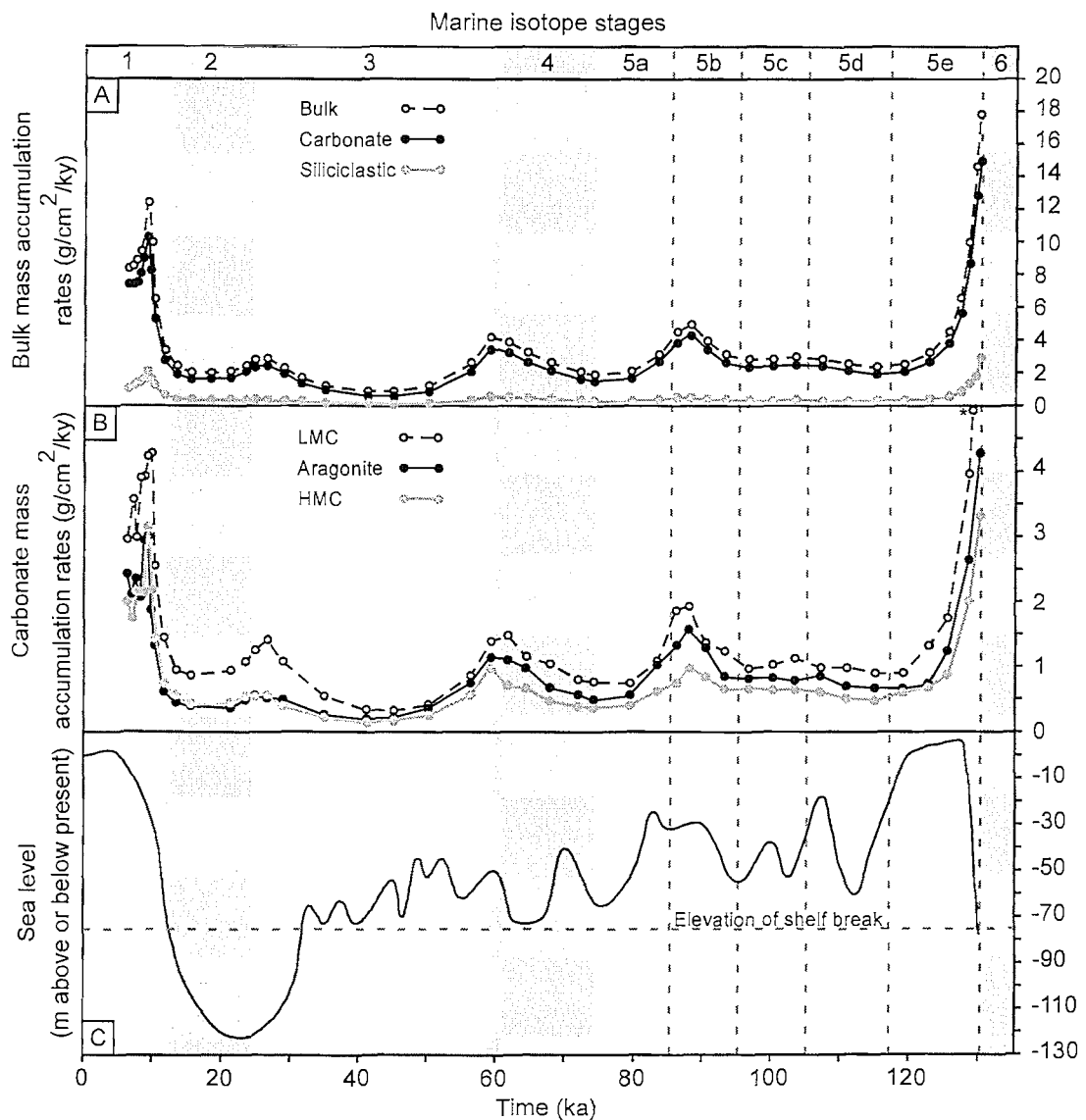


Figure 4.5: Mass accumulation rates of (A) bulk sediment, bulk carbonate, and bulk siliciclastic material, and (B) low-Mg calcite, aragonite, and high-Mg calcite, in core FR03/99 GC10, relative to (C) sea-level changes over the last 130 ky (adapted from Lambeck and Chappell, 2001), calculated using the continuous sedimentation rate (Fig. 4.3). Note the in-phase relationship between all components, and that highest accumulation rates coincide with major sea-level transgressions following MIS 6 and 2.

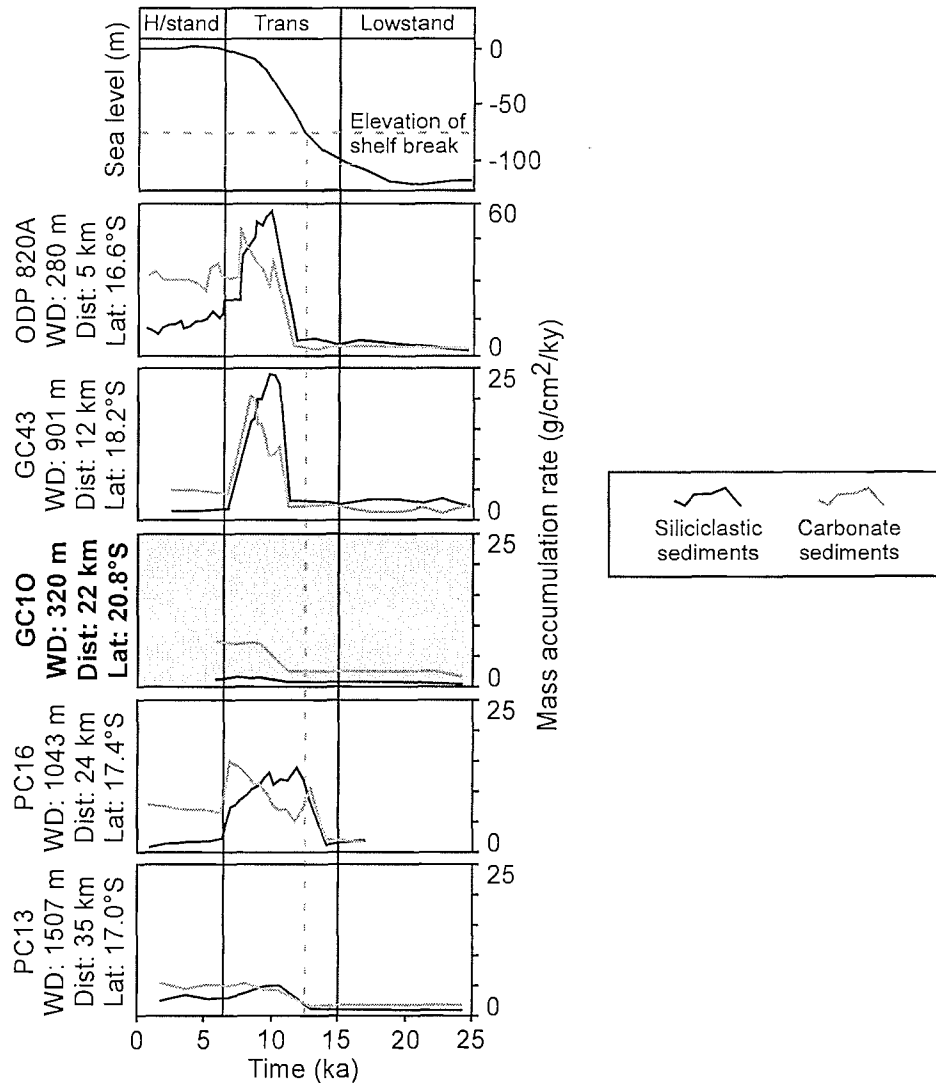


Figure 4.6: Mass accumulation rates of bulk siliciclastic and bulk carbonate components of core FR03/99 GC10 (shaded) and selected cores from Queensland Trough (modified from; Peerdeman and Davies, 1993; Dunbar et al., 2000; Page et al., 2003) since the Last Glacial Maximum, calculated using the bulk linear sedimentation rate (Fig. 4.3) to maintain consistency with data from Queensland Trough. Mass accumulation rates of both components were highest in all cores during transgression, however, the magnitude generally decreases with distance from the shelf. Note that in GC10, carbonate mass accumulation rates were comparable to those in cores at a similar distance from the shelf in Queensland Trough, but mass accumulation rates of siliciclastic material were lower. WD—water depth. Dist—distance from the 120 m isobath. Lat—latitudinal position in degrees south.

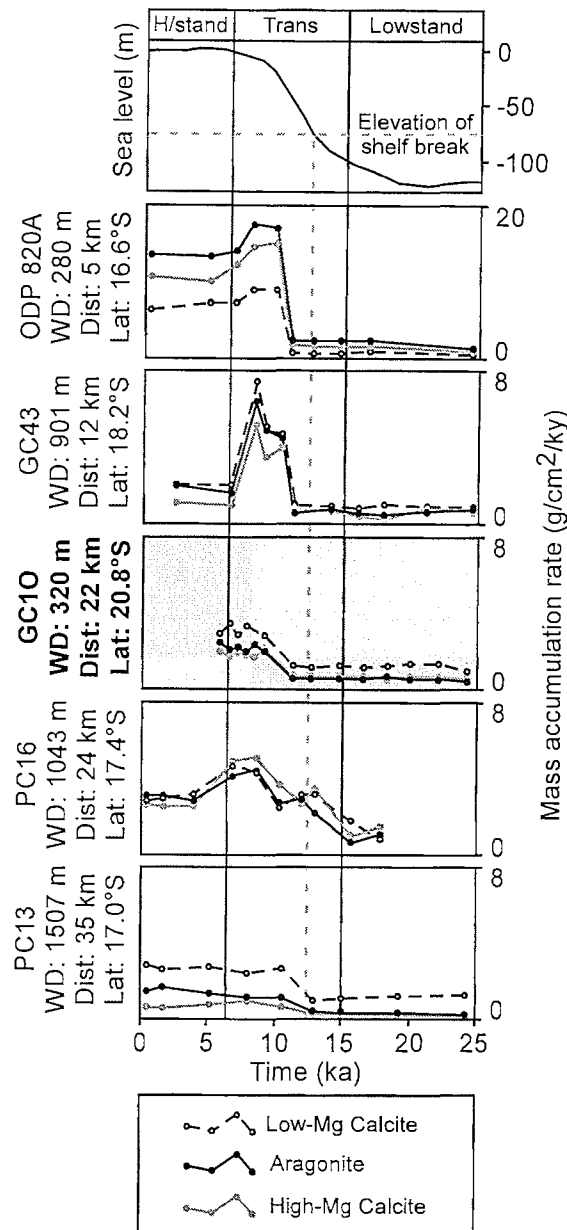


Figure 4.7: Mass accumulation rates of low-Mg calcite, aragonite, and high-Mg calcite in core FR03/99 GC10 (shaded) compared to cores from Queensland Trough (modified from Fig. 3.7) since the Last Glacial Maximum, calculated using the bulk linear sedimentation rate (Fig. 4.3) to maintain consistency with data from Queensland Trough. Note that mass accumulation rates of all components are lowest and highest during lowstand and transgression, respectively, and generally decrease with distance from the shelf. WD—water depth. Dist—distance from the 120 m isobath. Lat—latitudinal position in degrees south.

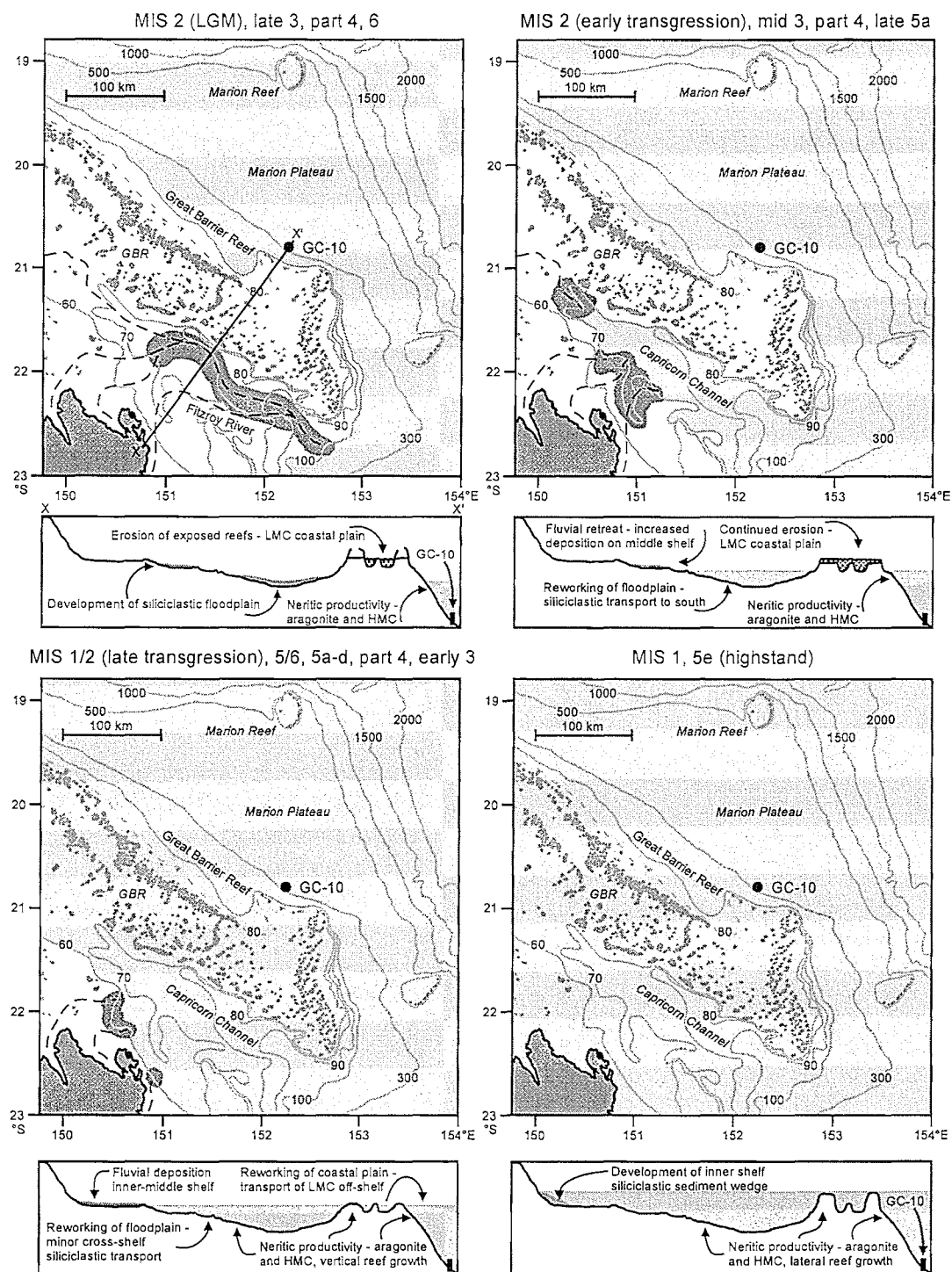


Figure 4.8: Conceptual model for the evolution of the southern GBR province over the last 130 ky. Bathymetric information modified from Shipboard Scientific Party (2002). Sea-level reconstructions based on the eustatic curve of Lambeck and Chappell (2001). Course of the paleo-Fitzroy River and cross-sections of the shelf adapted from Maxwell (1968). Dark shaded areas on the shelf indicate areas of possible siliciclastic deposition.

CHAPTER 5

Conclusion

5.0. CONCLUSION

Generic models of continental margin evolution (e.g., Fig. 1.2B; Vail et al., 1977; van Wagoner et al., 1988; Posamentier and Vail, 1988) predict lowstand shedding of siliciclastics and highstand shedding of carbonates to slopes and basins. These concepts are based on the premise that rivers will incise across exposed shelves during lowstands (e.g. Miall et al., 1991), and that carbonate production will be highest when shelves are completely flooded during highstands (e.g. Schlager et al., 1994). Equally, along mixed siliciclastic-carbonate margins, a condensed section with lows in the accumulation rates of both components should form on the slope during transgressions (e.g. Glenn et al., 1993a). During this time, the locus of siliciclastic deposition from rivers should backstep up the slope and across the shelf with early flooding, but carbonate production should be inhibited by proximal fluvial inputs.

The northeast Australian margin (Fig. 1.3) is the largest and arguably the most spectacular example of an extant tropical mixed siliciclastic-carbonate depositional system. During the Holocene, over 6.0 Mt/yr of terrigenous sediment has been discharged from the Australian continent (Neil et al., 2002) onto a shallow shelf that hosts the GBR and produces in excess of 50 Mt/yr of carbonate sediment (Kinsey and Hopley, 1991). A similar depositional system has existed offshore northeastern Australia for at least the last 500 ky (Davies and McKenzie, 1993; International Consortium for Great Barrier Reef Drilling, 2001), although the sources, production, and shedding of sediment to surrounding slopes and basins undoubtedly has varied in concert with sea-level fluctuations and climatic changes of the late Quaternary.

As expected for mixed siliciclastic-carbonate systems (e.g., Fig. 1.2B; Wilson, 1967; Dolan, 1989; Coniglio and Dix, 1992) late Quaternary sedimentary successions on continental slopes and in basins offshore northeastern Australia are characterised by

alternating dark and light coloured horizons, corresponding to intervals of relatively siliciclastic-rich and relatively carbonate-rich sediment, respectively. However, the timing and magnitude of off-shelf sediment fluxes on the northeast Australian margin during the latest Pleistocene and Holocene are not consistent with generic models for the evolution of mixed siliciclastic-carbonate systems (Fig. 1.2C).

Radiocarbon ages of planktonic foraminifera from sediment cores between ~15 and 21°S (Figs. 2.2, 4.2), offshore the central and southern GBR provinces, consistently reveal that the uppermost siliciclastic-rich horizons are time-correlative along the margin, and unequivocally formed through vastly increased siliciclastic fluxes during the last postglacial transgression ca. 12–7 ka (Figs. 2.3, 4.6). Furthermore, lowest fluxes of siliciclastic sediment to slopes and basins occurred during the last glacial lowstand ca. 25–12 ka. All along the upper to lower slope of Queensland Trough and on Marion Plateau, siliciclastic accumulation rates were lowest when sea level was below the shelf edge, and were by far greatest when sea level first rose above the shelf-slope break, regardless of modern differences in physiography, climate, and fluvial discharge along the northeast Australian margin.

Siliciclastic transport and deposition on the northeast Australian margin during the latest Quaternary could be controlled largely by climatic changes over glacial-interglacial cycles. Increased aridity and reduced fluvial discharge may have lessened siliciclastic delivery to slopes during lowstands (Thomas and Thorp, 1995; Thomas, 2003) and vastly increased rainfall and runoff (Wyrwoll and Miller, 2001) may have supplied enormous quantities of terrigenous sediment to the margin during transgression (Thomas, 2003).

Alternatively, key paradigms regarding the response of rivers to lower depositional base levels may not be applicable to Late Quaternary fluvial evolution

across the GBR shelf (e.g., Woolfe et al, 1998). During lowstand on the northeast Australian margin, reefs of the GBR were subaerially exposed (Johnson et al 1984; Marshall and Davies, 1984) as topographic highpoints across the shelf, which hindered the seaward advance of rivers and prevented fluvial connection with the slope. For example, during the last glacial, the Burdekin River failed to incise the outermost 10 km of the shelf (Fig. 2.1; Fielding et al., 2003) and avulsed and aggraded before reaching the slope, and the Fitzroy River is likely to have flowed parallel to the coast and shelf edge reefs (Fig. 4.8; Maxwell, 1968) before possibly reaching the slope at the southern end of Capricorn Channel. Fluvial bypassing of the upper slope, and sediment deposition only on the middle to lower slope and basin, is also extremely unlikely given that all cores, including those located on the lower slope in over 2000 m of water (PC27a), and those located in over 1300 km of water over 50 km east of the shelf (PC11), all record lows in siliciclastic accumulation rates during the last glacial lowstand. Other rivers on the northeast Australian margin may have experienced a similar fate. The majority of siliciclastic supply to the margin during sea-level lowstands was therefore probably limited to, and deposited on, the shelf, rather than delivered directly to the upper slope. Subsequently, during transgressions this material could be remobilised in shallow, high-energy waters, and consequently be transported to the slope in large quantities.

In further contrast with conventional wisdom regarding the development of mixed siliciclastic-carbonate strata, carbonate fluxes to slopes of Queensland Trough and Marion Plateau have been in-phase with siliciclastic fluxes throughout the latest Pleistocene and Holocene (Figs. 2.3, 3.2, 4.6). This relationship has resulted in a complex pattern of deposition on the slope reflecting variations in siliciclastic and carbonate fluxes that cannot be resolved based purely on sedimentary textures and

composition: (1) during the last glacial lowstand, carbonate accumulation rates on slopes were lowest, but lowstand sedimentary successions are relatively carbonate-rich because siliciclastic fluxes were minimal, (2) during the last postglacial transgression, carbonate accumulation rates on slopes were highest, but transgressive sedimentary successions are relatively siliciclastic-rich because siliciclastic accumulation rates increased more than carbonate accumulation rates, and (3) during the Holocene highstand, carbonate accumulation rates on slopes moderated, but highstand sedimentary successions are relatively carbonate-rich because siliciclastic accumulation rates decreased more than carbonate accumulation rates.

Aside from the unconventional relationship with siliciclastic sediment, patterns of carbonate deposition offshore of the central and southern portions of the northeast Australian margin during the latest Quaternary are generally consistent with existing paradigms for sedimentation on carbonate slopes. Indeed, the progressive addition of accommodation space afforded by rising sea level may facilitate highest rates of carbonate production on the shelf (e.g., Jones and Desrochers, 1992; James and Bourge, 1992), which is evident on the northeast Australian margin by highest fluxes of aragonite and HMC to slopes of Queensland Trough and Marion Plateau during transgression (Figs. 3.7, 4.5). The magnitude of these fluxes decreases with increasing distance from the shelf (Figs. 3.5, 4.7) and co-varies with Sr concentration in the bulk carbonate fraction (Fig. 3.6), clearly indicating neritic organisms on the shelf are the source of this sediment. Thus, rapidly expanding shallow marine accommodation space during early flooding of the shelf (Fig. 3.10) facilitated huge increases in carbonate productivity and shedding associated with the reinitiation of reef systems on the outer shelf. Importantly, carbonate productivity during transgression mostly was unaffected by coincident increases in off-shelf siliciclastic fluxes, which must have been

associated with increased turbidity and suspended sediment concentrations in the water column.

However, carbonate sedimentation on slopes east of the GBR during the latest Quaternary cannot be explained based purely on productivity-driven cycles of periplatform carbonate deposition. Accumulation rates of LMC were also highest during transgression and moderate during highstand (Figs. 3.7, 4.5), and, during these periods, LMC accumulation rates also decrease with increasing distance from the shelf (Figs. 3.5, 4.7). However, increased neritic accommodation space should not increase production and accumulation rates of LMC, because LMC is sourced predominantly from pelagic organisms (Milliman, 1974; Jones and Desrochers, 1992). Notably, sediments deposited on slopes offshore northeastern Australia during both the last postglacial transgression and Holocene highstand contain numerous LMC clasts (Fig. 3.4). This component of the bulk carbonate fraction exhibits recrystallisation and cementation textures consistent with subaerial exposure and meteoric diagenesis, and most likely represent eroded and altered neritic carbonate sourced from Pleistocene reef systems exposed during the last glacial lowstand (Johnson et al., 1984; Marshall and Davies, 1984; International Consortium for Great Barrier Reef Drilling, 2001). In common with siliciclastic sediments, LMC clasts on the shelf were probably remobilised by waves, currents and cyclones and transported to the slope, especially during transgression when shallow, high-energy environments existed on the outer shelf.

Nevertheless, patterns of mixed siliciclastic-carbonate sediment deposition on slopes east of the GBR during the latest Pleistocene and Holocene are not consistent with generic models of continental margin evolution (Fig. 1.2). Variations in the accumulation rates of all sedimentary components have been in-phase since the LGM,

and were lowest during the last glacial lowstand, highest during the postglacial transgression, and moderate to high during the Holocene highstand. Furthermore, in two cores that record slope deposition prior to 130 ka, namely FR03/99 GC10 from offshore of the southern GBR province, and ODP Hole 820A from offshore of the central GBR province, the same pattern of sediment deposition accompanied sea-level changes during the penultimate glacial (MIS 6) to Last Interglacial (MIS 5e).

Generic models for mixed siliciclastic-carbonate systems are inadequate to describe slope sedimentation offshore of the northeast Australian margin during the Late Pleistocene and Holocene, because they can rely on key paradigms that are not always correct, such as notions that (1) rivers will incise across exposed shelves to the continental slope during lowstands, (2) shallow marine carbonate productivity on the outer shelf will be inhibited by proximal riverine inputs when sea level initially floods the shelf during transgression, and (3) carbonate clasts, specifically non-pelagic and non-biogenic LMC, are generally an insignificant component of carbonate sediment budgets.

It is presently unclear if patterns of sediment deposition on slopes east of the GBR have occurred on other passive margins throughout the geological record. However, similar relationships between physiography, fluvial evolution, and sediment transport and deposition have been identified in other mixed siliciclastic-carbonate systems, for example, the deposition of siliciclastic material in front of topographic highs on the shelf during lowstands (Holder Formation, New Mexico; Rankey et al., 1999), and fluvial incision parallel to the shelf edge due to the presence of subaerially exposed reefs (Belize Margin; Ferro et al., 1999). The patterns of sediment deposition evident on the northeast Australian margin during the latest Quaternary may constitute a fundamental sedimentary response of passive continental margins to relative sea-level

changes, especially tropical shallow platforms rimmed by reefs, and may provide a useful analogue for the interpretation of strata throughout the global stratigraphic record.

REFERENCES CITED

- Bathurst, R.G.C., 1993, Microfabrics in carbonate diagenesis: a critical look at forty years in research, *in* Rezak, R., and Lavoie, D.L., eds., *Carbonate Microfabrics*: New York, p. 3-14.
- Belperio, A.P., 1983, Terrigenous sedimentation in the central Great Barrier Reef lagoon: a model from the Burdekin region: *BMR Journal of Australian Geology and Geophysics*, v. 8, p. 179-190.
- Belperio, A.P., and Searle, D.E., 1988, Terrigenous and carbonate sedimentation in the Great Barrier Reef province, *in* Doyle, L.J., and Roberts, H.H., eds., *Carbonate-clastic transitions: Developments in sedimentology*, Volume 42: Amsterdam, Elsevier, p. 143-174.
- Boardman, M.R., and Neumann, A.C., 1984, Sources of periplatform carbonates: Northwest Providence Channel, Bahamas: *Journal of Sedimentary Petrology*, v. 54, p. 1110-1123.
- Boardman, M.R., Neumann, A.C., Baker, P.A., Dulin, L.A., Kenter, R.J., Hunter, G.E., and Kiefer, K.B., 1986, Banktop responses to Quaternary fluctuations in sea level recorded in periplatform sediments: *Geology*, v. 14, p. 28 - 31.
- Borer, J.M., and Harris, P.M., 1991, Depositional facies and model for mixed siliciclastics and carbonates of the Yates Formation, Permian Basin, *in* Lomando, A.J., and Harris, P.M., eds., *Mixed carbonate-siliciclastic sequences*, SEPM Core Workshop No. 15: Tulsa, OK, SEPM, p. 1-133.
- Brachert, T.C., Forst, M.H., Pais, J.J., Legoinha, P., and Reijmer, J.J.G., 2003, Lowstand carbonates, highstand sandstones?: *Sedimentary Geology*, v. 155, p. 1-12.
- Braithwaite, C.J.R., Dalmasso, H., Gilmour, M.A., Harkness, D.D., Henderson, G.M., Kay, R.L.F., Kroon, D., Montaggioni, L.F., and Wilson, P.A., 2004, The Great Barrier Reef; the chronological record from a new borehole: *Journal of Sedimentary Research*, v. 74, p. 298-310.
- Bush, D.M., 1991, Mixed carbonate/siliciclastic sedimentation: northern insular shelf of Puerto Rico, *in* Lomando, A.J., and Harris, P.M., eds., *Mixed carbonate - siliciclastic sequences*, SEPM core workshop No. 15: Tulsa, OK, SEPM, p. 447-484.
- Carter, R.M., Johnson, D.P., and Hooper, K., 1993, Episodic post-glacial sea-level rise and the sedimentary evolution of a tropical continental embayment (Cleveland Bay, Great Barrier Reef shelf, Australia), *Australian Journal of Earth Sciences*, v. 40, p. 229-255.
- Coniglio, M., and Dix, G.R., 1992, Carbonate slopes, *in* Walker, R.G., and James, N.P., eds., *Facies models: response to sea level change*: Geological Association of Canada, p. 349-373.
- Correge, T., 1993, Late Quaternary palaeoceanography of the Queensland Trough (Western Coral Sea) based on Ostracoda and the chemical composition of their shells [PhD thesis]: Canberra, Australian National University.
- Davies, P.J., and Hopley, D., 1983, Growth facies and growth rates of Holocene reefs in the Great Barrier Reef: *BMR Journal of Australian Geology and Geophysics*, v. 8, p. 237-251.
- Davies, P.J., and McKenzie, J.A., 1993, Controls on the Pliocene-Pleistocene evolution of the northeastern Australian continental margin, *in* McKenzie, J.A., Davies, P.J., Palmer-Julson, A., and et al., eds., *Proceedings of the Ocean Drilling*

- Program, Scientific Results, 133: College Station, TX, (Ocean Drilling Program), p. 755-762.
- Davies, P.J., McKenzie, J.A., Palmer-Julson, A., and et al., 1991, Proceedings of the Ocean Drilling Program, Initial Reports, Leg 133: College Station, TX, (Ocean Drilling Program).
- Dolan, J.F., 1989, Eustatic and tectonic controls on the deposition of hybrid siliciclastic/carbonate basinal cycles: discussion with examples: American Association of Petroleum Geologists Bulletin, v. 73, p. 1233-1246.
- Droxler, A.W., Morse, J.W., and Kornicker, W.A., 1988, Controls on carbonate mineral accumulation in Bahamian basins and adjacent Atlantic Ocean sediments: *Journal of Sedimentary Petrology*, v. 58, p. 120 - 130.
- Dunbar, G.B., 2000, Late Quaternary evolution of the northeast Australian continental margin [PhD thesis]: Townsville, James Cook University.
- Dunbar, G.B., and Dickens, G.R., 2003a, Massive siliciclastic discharge to slopes of the Great Barrier Reef Platform during sea-level transgression: constraints from sediment cores between 15°S and 16°S latitude and possible explanations: *Sedimentary Geology*, v. 162, p. 141-158.
- Dunbar, G.B., and Dickens, G.R., 2003b, Late Quaternary shedding of shallow marine carbonate along a tropical mixed siliciclastic-carbonate shelf: Great Barrier Reef, Australia: *Sedimentology*, v. 50, p. 1061-1077.
- Dunbar, G.B., Dickens, G.R., and Carter, R.M., 2000, Sediment flux across the Great Barrier Reef Shelf to the Queensland Trough over the last 300 ky: *Sedimentary Geology*, v. 133, p. 49-92.
- Ewing, M., Hawkins, L.V., and Ludwig, W.J., 1970, Crustal structure of the Coral Sea: *Journal of Geophysical Research*, v. 75, p. 1953-1962.
- Ferro, C.E., Droxler, A.W., Anderson J.B. and Mucciarone, D., 1999, Late Quaternary shift of mixed siliciclastic-carbonate environments induced by glacial eustatic sea-level fluctuations in Belize, *in* Harris, P.M., Saller, A.H., and Simo, J.A.T (eds.), *Advances in carbonate sequence stratigraphy; applications to reservoirs, outcrops and models: SEPM (Society for Sedimentary Geology) Special Publication 63*, p. 385-411.
- Fielding, C.R., Trueman, J.D., Dickens, G.R., and Page, M.C., 2003, Anatomy of the buried Burdekin River channel across the Great Barrier Reef shelf: how does a major river operate on a tropical mixed siliciclastic/carbonate margin during sea level lowstand?: *Sedimentary Geology*, v.157, p. 291-301.
- Flood, P.G., and Orme, G.R., 1988, Mixed siliciclastic/carbonate sediments of the northern Great Barrier Reef province, Australia, *in* Doyle, L.J., and Roberts, H.H., eds., *Carbonate-clastic transitions: developments in sedimentology*, Volume 42: Amsterdam, Elsevier, p. 175-205.
- Foreman, J.L., Walker, K.R., Weber, L.J., Driese, S.G., and Dreier, R.B., 1991, Slope and basinal carbonate deposition in the Nolichucky Shale (Upper Cambrian), east Tennessee: effect of carbonate suppression by siliciclastic deposition on basin-margin morphology, *in* Lomando, A.J., and Harris, P.M., eds., *Mixed carbonate - siliciclastic sequences*, SEPM core workshop No. 15: Tulsa, OK, SEPM, p. 511-540.
- Francis, J.M., Dickens, G.R., and Page, M.C., 2003, Characterization and timing of siliciclastic sediment fluxes to continental slopes of the Coral Sea during the late Quaternary: *Eos Transactions, AGU*, 84 (46), Fall Meeting Supplement, Abstract OS12A-0189, 2003.

- Galloway, W.E., 1998, Siliciclastic slope and base of slope depositional systems: component facies, stratigraphic architecture, and classification: AAPG Bulletin, v. 82, p. 569-595.
- Glenn, C.R., Kronen, J.D., Jr., Symonds, P.A., Wei, W., and Kroon, D., 1993a, High-resolution sequence stratigraphy, condensed sections and flooding events off the Great Barrier Reef: 0-1.5 MA, in McKenzie, J.A., Davies, P.J., Palmer-Julson, A., et al. (Eds), Proceedings of the Ocean Drilling Program, Scientific Results, 133: College Station, TX, (Ocean Drilling Program), p. 353-364.
- Glenn, C.R., Kroon, D., and Wei, W., 1993b, Sedimentary rhythms and climatic forcing of Pleistocene-Holocene mixed carbonate/siliciclastic sediments off the Great Barrier Reef, in McKenzie, J.A., Davies, P.J., Palmer-Julson, A., et al. (Eds), Proceedings of the Ocean Drilling Program, Scientific Results, 133: College Station, TX, (Ocean Drilling Program), p. 189-202.
- Goodbred, S.L., Jr., and Kuehl, S.A., 2000, Enormous Ganges-Brahmaputra sediment discharge during strengthened early Holocene monsoon: *Geology*, v. 28, p. 1083-1086.
- Grant, K.M., and Dickens, G.R., 2002, Coupled productivity and carbon isotope records in the southwest Pacific Ocean during the late Miocene-early Pliocene biogenic bloom: *Palaeogeography, Palaeoclimatology, Palaeoecology*, v. 187, p. 61-82.
- Grindrod, J., Moss, P., and Van der Kaars, S., 1999, Late Quaternary cycles of mangrove development and decline on the north Australian continental shelf: *Journal of Quaternary Science*, v. 14, p. 465-470.
- Hallock, P., 2001, Coral reefs, carbonate sediments, nutrients, and global change, in Stanley, G., D. Jr, ed., *The history and sedimentology of ancient reef systems*: New York, Kluwer Academic/Plenum Publishers, p. 387-427.
- Handford, C.R., and Loucks, R.G., 1993, Carbonate depositional sequences and systems tracts - responses of carbonate platforms to relative sea level changes, in Loucks, R.G., and Sarg, J.F., eds., *Carbonate sequence stratigraphy: recent developments and applications*. AAPG Memoir, Volume 57: Tulsa, OK, AAPG, p. 3-41.
- Harris, P.T., Davies, P.J., and Marshall, J.F., 1990, Late Quaternary sedimentation on the Great Barrier Reef continental shelf and slope east of Townsville, Australia: *Marine Geology*, v. 94, p. 55-77.
- Heap, A.D., Dickens, G.R., and Stewart, L.K., 2001, Late Holocene sediment in Nara Inlet, central Great Barrier Reef platform: sediment accumulation on the middle shelf of a tropical mixed clastic/carbonate system: *Marine Geology*, v. 176, p. 39-54.
- Heath, K.C., and Mullins, H.T., 1984, Open-ocean, off bank transport of fine-grained carbonate sediments in the Northern Bahamas, in Stow, D.A.V., and Piper, D.J.W., eds., *Fine-grained sediments: Deep-water processes and facies*: Oxford, Blackwell Science, p. 199-208.
- Heck, P.R., Anselmetti, F.S., and Isern, A.R., 2004. Data report: Late Pleistocene and Holocene sedimentation on the Marion Plateau: data from precruise ODP Leg 194 site survey gravity cores. In Anselmetti, F.S., Isern, A.R., Blum, P., and Betzler, C. (Eds.), Proceedings of the Ocean Drilling Program, Scientific Results, 194 [Online]. Available from World Wide Web: <http://www-odp.tamu.edu/publications/194_SR/006/006.htm>.

- International Consortium for Great Barrier Reef Drilling, 2001, New constraints on the origin of the Australian Great Barrier Reef: Results from an international project of deep coring: *Geology*, v. 29, p. 483-486.
- Jackson, J.A. (ed.), 1997, *Glossary of Geology*: Alexandria, Virginia, American Geological Institute, 769 p.
- James, N.P., and Bourge, P.-A., 1992, Reefs and mounds, *in* Walker, R.G., and James, N.P., eds., *Facies models: Response to sea-level change: Ontario*, Geological Association of Canada, p. 323-347.
- James, N.P., and Choquette, P.W., 1990, Diagenesis-9: Limestones: the meteoric diagenetic environment, *in* McIlreath, I.A., and Morrow, D.W., eds., *Diagenesis: Geoscience Canada Reprint Series 4*: Ottawa, Canada, p. 35-73.
- James, N.P., and Kendall, A.C., 1992, Introduction to carbonate and evaporite facies models, *in* Walker, R.G., and James, N.P., eds., *Facies Models: response to sea level change: Ontario*, Geological Association of Canada, p. 265-276.
- Johnson, D.P., Cuff, C., and Rhodes, E., 1984, Holocene reef sequences and geochemistry, Britomart Reef, central Great Barrier Reef, Australia: *Sedimentology*, v. 31, p. 515-529.
- Johnson, D.P., and Searle, D.E., 1984, Postglacial seismic stratigraphy, central Great Barrier Reef, Australia: *Sedimentology*, v. 31, p. 335-352.
- Jones, B., and Desrochers, A., 1992, Shallow Platform Carbonates, *in* Walker, R.G., and James, N.P., eds., *Facies Models: response to sea-level change: Ontario*, Geological Association of Canada, p. 277-302.
- Kershaw, A.P., 1985, An extended late Quaternary vegetation record from north-eastern Queensland and its implications for the seasonal tropics of Australia: *Proceedings of the Ecological Society of Australia*, v. 13, p. 179-189.
- Kershaw, A.P., 1994, Pleistocene vegetation of the humid tropics of northeastern Queensland, Australia: *Palaeogeography, Palaeoclimatology, Palaeoecology*, v. 109, p. 399-412.
- Kier, J.S., and Pilkey, O.H., 1971, The influence of sea-level changes on sediment carbonate mineralogy, Tongue of the Ocean, Bahamas: *Marine Geology*, v. 11.
- Kinsey, D.W., and Hopley, D., 1991, The significance of coral reefs as global carbon sinks - response to Greenhouse: *Global and Planetary Change*, v. 3, p. 363-377.
- Kronen, J.D., Jr., and Glenn, C.R., 2000, Pristine to reworked verdine: keys to sequence stratigraphy in mixed carbonate-siliciclastic forereef sediments (Great Barrier Reef), *Marine Authigenesis: From Global to Microbial*, SEPM Special Publication No. 66, SEPM, p. 387-403.
- Lambeck, A., and Woolfe, K.J., 2000, Composition and textural variability along the 10 m isobath, Great Barrier Reef: evidence for pervasive northward sediment transport: *Australian Journal of Earth Sciences*, v. 47, p. 327-335.
- Lambeck, K., and Chappell, J., 2001, Sea-level change through the Last Glacial cycle: *Science*, v. 292, p. 679-686.
- Larcombe, P., and Carter, R.M., 1998, Sequence architecture during the Holocene transgression: an example from the Great Barrier Reef shelf, Australia: *Sedimentary Geology*, v. 117, p. 97-121.
- Larcombe, P., and Carter, R.M., 2004, Cyclone pumping, sediment partitioning and the development of the Great Barrier Reef shelf system: a review: *Quaternary Science Reviews*, v. 23, p. 107-135.
- Larcombe, P., Carter, R.M., Dye, J., Gagan, M.K., and Johnson, D.P., 1995, New evidence for episodic post-glacial sea-level rise, central Great Barrier Reef, Australia: *Marine Geology*, v. 127, p. 1-44.

- Larcombe, P., and Woolfe, K.J., 1999, Terrigenous sediments as influences upon Holocene nearshore coral reefs, central Great Barrier Reef, Australia: *Australian Journal of Earth Sciences*, v. 46. p. 141-154.
- Loutit, T.S., Hardenbol, J., Vail, P.R., and Baum, G.R., 1988, Condensed sections: the key to age determination and correlation of continental marginal sequences, *in* Wilgus, C.K., et al., (eds.) *Sea-level changes: An integrated approach*, Society of Economic Paleontologists and Mineralogists Special Publication 42, p. 183-213.
- Marshall, J.F., and Davies, P.J., 1984, Last Interglacial reef growth beneath modern reefs in the southern Great Barrier Reef: *Nature*, v. 307, p. 44-46.
- Martinson, D.G., Pisias, N.G., Hays, J.D., Imbrie, J., Moore, T.C.J., and Shackleton, N.J., 1987, Age dating and the orbital theory of the ice ages: Development of a high-resolution 0 to 300,000-year chronostratigraphy: *Quaternary Research*, v. 27, p. 1-29.
- Maxwell, W.G.H., 1968, *Atlas of the Great Barrier Reef*: Amsterdam, Elsevier, 258 p.
- Maxwell, W.G.H., and Swinchatt, J.P., 1970, Great Barrier Reef: Regional variation in a terrigenous-carbonate province: *Geological Society of America Bulletin*, v. 81.
- Miall, A.D., 1991, Stratigraphic sequences and their chronostratigraphic correlation: *Journal of Sedimentary Petrology*, v. 61, p. 497-505.
- Miall, A.D., 1997, *The Geology of Stratigraphic Sequences*: Berlin, Springer, 433 p.
- Milliman, J.D., 1974, *Recent Sedimentary Carbonates Part I: Marine Carbonates*: Berlin, Springer-Verlag, 375 p.
- Milliman, J.D., Freile, D., Steinen, R.P., and Wilber, R.J., 1993, Great Bahama Bank aragonitic muds: mostly inorganically precipitated, mostly exported: *Journal of Sedimentary Petrology*, v. 63, p. 589-595.
- Mount, J.F., 1984, Mixing of siliciclastic and carbonate sediments in shallow shelf environments: *Geology*, v. 12, p. 432-435.
- Mueller, G., and Gastner, M., 1971, The "Karbonat-Bombe", a simple device for the determination of the carbonate content in sediments, soils and other materials: *Neues Jahrbuch Fuer Mineralogie*, v. 10, p. 466-469.
- Neil, D., and Yu, B., 1995, Fluvial sediment yield to the Great Barrier Reef lagoon: spatial patterns and the effect of land use, *in* Hunter, H.M., Eyles, A.G., and Rayment, G.E., eds., *Proceedings of the conference on downstream effects of land use*: Rockhampton. April, 1995, Department of Natural Resources, Queensland.
- Neil, D.T., Orpin, A.R., Ridd, P.V., and Yu, B., 2002, Sediment yield and impacts from river catchments to the Great Barrier Reef lagoon: *Marine and Freshwater Research*, v. 53, p. 733-752.
- Odin, G.S., and Sen Gupta, B.K., 1988, Geological significance of the verdine facies, *in* Odin, G.S., ed., *Green marine clays: Oolitic ironstone facies, verdine facies, glaucony facies and celadonite-bearing facies: A comparative study*: Amsterdam, Elsevier, p. 205-219.
- Orme, G.R., Flood, P.G., and Sargent, G.E.G., 1978, Sedimentation trends in the lee of outer (ribbon) reefs, Northern Region of the Great Barrier Reef Province: *Philosophical Transactions of the Royal Society of London, Series A*, v. 291, p. 85-99.
- Page, M.C., Dickens, G.R., and Dunbar, G.B., 2003, Tropical view of Quaternary sequence stratigraphy: siliciclastic accumulation on slopes east of the Great Barrier Reef since the Last Glacial Maximum: *Geology*, v. 31, p. 1013-1016.

- Pak, H., Zaneveld, R.V., and Kitchen, J., 1980, Intermediate nepheloid layers observed off Oregon and Washington: *Journal of Geophysical Research*, v. 85, p. 6697-6708.
- Paillard, D., Labeyrie, L., and Yiou, P., 1996, Macintosh program performs time-series analysis: *Eos transactions, AGU*, v. 77, p. 379.
- Peerdeman, F.M., and Davies, P.J., 1993, Sedimentological response of an outer-shelf, upper-slope sequence to rapid changes in Pleistocene eustatic sea-level: Hole 820A, Northeastern Australian Margin, *in* McKenzie, J.A., Davies, P.J., Palmer-Julson, A., and et al., eds., *Proceedings of the Ocean Drilling Program, Scientific Results, 133*: College Station, TX, (Ocean Drilling Program), p. 303-313.
- Pigram, C.J., 1993, Carbonate platform growth, demise and sea level record: Marion Plateau, Northeast Australia [PhD thesis]: Canberra, Australian National University.
- Posamentier, H.W., and Vail, P.R., 1988, Eustatic controls on clastic deposition, II-Sequence and systems tract models, *in* Wilgus, C.K., et al. (Eds) *Sea-level changes: An integrated approach*, Society of Economic Paleontologists and Mineralogists Special Publication 42, p. 125-154.
- Rankey, E.C., 1997, Relations between relative changes in sea level and climate shifts: Pennsylvanian-Permian mixed carbonate-siliciclastic strata, western United States: *Geological Society of America Bulletin*, v. 109, p. 1089-1100.
- Rankey, E.C., Bachtel, S.L., and Kaufman, J., 1999, Controls on stratigraphic architecture of mixed carbonate/siliciclastic systems: A case study from the Holder Formation (Pennsylvanian, Virgilian), Sacramento Mountains, New Mexico, *in* Harris, P.M., Saller, A.H., and Simo, J.A.T (Eds), *Advances in carbonate sequence stratigraphy; applications to reservoirs, outcrops and models: SEPM (Society for Sedimentary Geology) Special Publication 63*, p. 127-150.
- Ryan, D.A., Opdyke, B.N., and Jell, J.S., 2001, Holocene sediments of Wistari Reef: towards a global quantification of coral reef related neritic sedimentation in the Holocene: *Palaeogeography, Palaeoclimatology, Palaeoecology*, v. 175, p. 173-184.
- Sarg, J.F., 1988, Carbonate sequence stratigraphy, *in* Wilgus, C.K., et al. (Eds), *Sea-level changes: an integrated approach*, SEPM Special Publication 42, p. 155-181.
- Schlager, W., Reijmer, J.J.G., and Droxler, A.W., 1994, Highstand shedding of carbonate platforms: *Journal of Sedimentary Research*, v. B64, p. 270 - 281.
- Scott, D.L., 1993, Architecture of the Queensland Trough: implications for the structure and tectonics of the Northeastern Australian Margin: *AGSO Journal of Australian Geology and Geophysics*, v. 14, p. 21-34.
- Shanmugan, G., and Moiola, R.J., 1988, Submarine fans: characteristics, models, classification, and reservoir potential: *Earth Science Reviews*, v. 24, p. 383-428.
- Shipboard Scientific Party, 2002, Leg 194 Summary, *in* Isern, A., Anselmetti, F., Blum, P., et al. (Eds), *Proc. ODP, Init. Repts., 194*: College Station TX, (Ocean Drilling Program), p. 1-88.
- Smithers, S., and Larcombe, P., 2003, Late Holocene initiation and growth of a nearshore turbid-zone coral reef: Paluma Shoals, central Great Barrier Reef, Australia: *Coral Reefs*, v. 22, p. 499-505.
- Steckler, M.S., Mountain, G.S., Miller, K.G., and Christie-Blick, N., 1999, Reconstruction of Tertiary progradation and clinoform development on the

- New Jersey passive margin by 2-D backstripping: *Marine Geology*, v. 154, p. 399-420.
- Stuiver, M., Reimer, P.J., Bard, E., Beck, J.W., Burr, G.S., Hughen, K.A., Kromer, B., McCormac, G., van der Plicht, J., and Spurk, M., 1998, INTCAL 98 radiocarbon age calibration, 24,000-0 cal BP: *Radiocarbon*, v. 40, p. 1041-1083.
- Suppiah, R., 1992, The Australian summer monsoon: a review: *Progress in Physical Geography*, v. 16, p. 283-318.
- Sutherland, I.A., 2000, A GIS approach to modelling Holocene carbonate sediments on the north Queensland margin, Australia [Honours thesis]: Townsville, James Cook University.
- Symonds, P.A., Davies, P.J., and Parisi, A., 1983, Structure and stratigraphy of the Great Barrier Reef: *BMR Journal of Australian Geology and Geophysics*, v. 8, p. 277-291.
- Taylor, J.C., 1991, Computer programs for standardless quantitative analysis of minerals using the full powder diffraction profile: *Powder Diffraction*, v. 6, p. 2-9.
- Thomas, M.F., 2003, Late Quaternary sediment fluxes from tropical watersheds: *Sedimentary Geology*, v. 162, p. 63-81.
- Thomas, M.F., Nott, J., and Price, D.M., 2001, Late Quaternary stream sedimentation in the humid tropics: a review with new data from NE Queensland, Australia: *Geomorphology*, v. 39, p. 53-68.
- Thomas, M.F., and Thorp, M.B., 1995, Geomorphic response to rapid climatic and hydrologic change during the late Pleistocene and early Holocene in the humid and subhumid tropics: *Quaternary Science Reviews*, v. 14, p. 193-207.
- Thompson, P.R., Be, A.W.H., Duplessy, J.C., and Shackleton, N.J., 1979, Disappearance of pink-pigmented *Globigerinoides ruber* at 120,000 yr BP in the Indian and Pacific Oceans: *Nature*, v. 280, p. 554-557.
- Tirsgaard, H., 1996, Cyclic sedimentation of carbonate and siliciclastic deposits on a late Precambrian ramp; the Elisabeth Bjerg Formation (Eleonore Bay Supergroup), East Greenland: *Journal of Sedimentary Research*, v. 66, p. 699-712.
- Tucker, K.E., and Chalcraft, R.G., 1991, Cyclicity in the Permian Queen Formation, U.S.M. Queen Field, Pecos County, Texas, in Lomando, A.J., and Harris, P.M., eds., Mixed carbonate - siliciclastic sequences, SEPM core workshop No. 15, p. 385-428.
- Vail, P.R., Mitchum, R.M., and Thompson, S., 1977, Seismic stratigraphy and global changes of sea level, part 4: global cycles of relative changes of sea level, in Payton, C. R. (Ed): AAPG Memoir 26, p. 83-97.
- van Heijst, M.W.I.M., and Postma, G., 2001, Fluvial response to sea-level changes: a quantitative analogue, experimental approach: *Basin Research*, v. 13, p. 269-292.
- Van Wagoner, J.C., Posamentier, H.W., Mitchum, R.M., Vail, P.R., Sarg, J.F., Loutit, T.S., and Hardenbol, J., 1988, An overview of the fundamentals of sequence stratigraphy and key definitions, in Wilgus, C.K., et al. (Eds), Sea-level changes: an integrated approach, SEPM Special Publication 42, p. 39-45.
- Walker, R.G., 1992, Facies, facies models and modern stratigraphic concepts, in Walker, R.G., and James, N.P., eds., Facies Models: response to sea level change: Ontario, Geological Association of Canada, p. 1-14.
- Walsh, J.P., and Nittrouer, C.A., 1999, Observations of sediment flux on the Eel continental slope, northern California: *Marine Geology*, v. 154, p. 55-68.

- Walsh, J.P., and Nittrouer, C.A., 2003, Contrasting styles of off-shelf sediment accumulation in New Guinea: *Marine Geology*, v. 196, p. 105-125.
- Webster, J.M., and Davies, P.J., 2003, Coral variation in two deep drill cores: significance for the Pleistocene development of the Great Barrier Reef: *Sedimentary Geology*, v. 159, p. 61-80.
- Whitmarsh, R.B., et al., 1974, DSDP Site 219 site report, *in* Whitmarsh, R.B., and Weser, O.E., eds., Initial reports of the deep sea drilling project, Volume 23, p. 35-115.
- Wilson, J.L., 1967, Cyclic and reciprocal sedimentation in Virgilian strata of southern New Mexico: *Geological Society of America Bulletin*, v. 78, p. 805-818.
- Woolfe, K.J., Larcombe, P., Naish, T., and Purdon, R.G., 1998, Lowstand rivers need not incise the shelf: An example from the Great Barrier Reef, Australia, with implications for sequence stratigraphic models: *Geology*, v. 26, p. 75-78.
- Wyrwoll, K.-H., and Miller, G.H., 2001, Initiation of the Australian summer monsoon 14,000 years ago: *Quaternary International*, v. 83-85, p. 119-128.
- Yang, W., and Kominz, M.A., 2003, Characteristics, stratigraphic architecture, and time framework of multi-order mixed siliciclastic and carbonate depositional systems, outcropping Cisco Group (Late Pennsylvanian and Early Permian), Eastern Shelf, north-central Texas, USA: *Sedimentary Geology*, v. 154, p. 53-87.

APPENDIX A

High-resolution amino-stratigraphy of cores from
Queensland Trough and Marion Plateau: insights into
AAR kinetics in the western Coral Sea since the Last
Glacial Maximum

Michael C. Page, Michael J. O’Leary, Paul J. Hearty

School of Earth Sciences, James Cook University, Townsville QLD 4811 Australia

Darrell S. Kaufman

Departments of Geology and Environmental Sciences, Northern Arizona University,

Flagstaff AZ 86011-4099 U.S.A.

A paper prepared for submission to *Quaternary Research*

ABSTRACT

Recent studies on sediment cores from Queensland Trough (QT) in the western Coral Sea investigated amino-acid racemization (AAR) in single tests of the pelagic, planktonic foraminifera, *Pulleniatina obliquiloculata* (*Po*), and found that racemization occurred systematically with time over several hundred thousand years. Here we investigate the high-resolution amino-stratigraphy of five of these cores from QT over the last 25 ky, and introduce new results from a core from Marion Plateau (MP), a shallow setting south of QT. Multiple amino-acids were separated from 268 individual *Po* from 49 horizons using reverse-phase high-performance liquid chromatography. Age control was provided by 29 accelerator mass spectrometry radiocarbon ages. D-alloisoleucine/L-isoleucine (D/L) ratios increase progressively down each core and with increasing age of the sediments. D/L ratios also increase faster in cores that are shallower, reflecting apparent sensitivity to modern bottom-water temperatures in the Coral Sea. The kinetic pathway of racemization for aspartic acid in each core is best modelled using power functions because the resulting models satisfy several basic criteria that other models do not: (1) modelled initial D/L ratios in each core are very similar, (2) AAR is faster in cores bathed by warmer water, and (3) kinetic pathways of different cores rarely intersect. The power function models also imply that AAR in all cores has progressively slowed over the last 25 ky, which is to be expected considering the racemization reaction of amino acids inevitably reaches equilibrium. However, AAR may have also been slower during the Last Glacial Maximum (LGM) because of cooler bottom water temperatures in the western Coral Sea. This possibility is consistent with records deduced from independent paleotemperature proxies, but remains equivocal pending the results of laboratory heating experiments on modern tests of *Po*. Nevertheless, our results demonstrate the integrity of high-resolution

amino-stratigraphy in sediment cores from QT and MP, and suggest AAR in *Po* tests may be a useful paleo-temperature and geochronological tool for future studies of Quaternary marine sediments.

A.1. INTRODUCTION

The process of amino-acid racemization (AAR) from L-isoleucine to D-alloisoleucine over time has been firmly established (Hare and Mitterer, 1967) and has been used as the basis for establishing an effective stratigraphic tool for sedimentary correlations (e.g., Hearty and Aharon, 1988; Hearty et al., 1992; Rutter and Blackwell, 1995; Hearty et al., 2000). AAR in fossil foraminifera has also been widely investigated: being used to estimate the ages of Quaternary marine sediment (e.g., Muller, 1984; Macko and Aksu, 1986; Knudsen and Sejrup, 1993; Harada and Handa, 1995; Harada et al., 1996) and to reconstruct paleo-temperature histories (e.g., Bada and Man, 1980; Lehman et al., 1988; Johnson et al., 1990). The degree to which L-isoleucine has racemized to D-alloisoleucine in biogenic matter is commonly expressed as a D/L ratio. The specific rates at which this reaction proceeds in the natural environment, however, is dependant on several factors, including time, temperature, and the taxon of the organisms containing the amino acids.

Recently, Hearty et al. (submitted) demonstrated the utility of the AAR method for establishing amino-stratigraphy (cf. Miller and Hare, 1980) in deep marine sediments offshore northeastern Australia. D/L ratios of multiple amino-acids including Aspartic (Asp), Glutamic (Glu), and Serine (Ser), were separated from individual fossil foraminifera, *Pulleniatina obliquiloculata* (*Po*), in cores from Queensland Trough (QT; Fig. A.1), whose chronologies had been independently determined by radiocarbon dating and oxygen isotope stratigraphy. A systematic increase in D/L ratios over time was demonstrated in all cores and modelling of the racemization kinetics enabled age estimation for sediments in QT to at least 500 ka.

Here we focus on the kinetics of the AAR reaction over the last 25 ky in five cores from QT, first presented by Hearty et al. (submitted), and in a new core from

Marion Plateau (MP; Fig. A.1). We model the kinetics of Asp racemization since the Last Glacial Maximum (LGM) using power functions, and demonstrate the sensitivity of racemization rates to temperature differences between sites in the western Coral Sea. The kinetic models also effectively model the slowing of racemization over time, which is inherent to biogeochemical reactions that inevitably reach equilibrium. However, the extent to which the modelled kinetic pathway of racemization reflects (1) the natural decay of amino acids over time, and (2) changes in the rates of racemization due to bottom-water temperature variations, remains equivocal. This is because the modelled kinetic pathway is consistent with independent paleotemperature proxies, including Mg/Ca ratios in deep sea ostracodes (Correge, 1993b), and the stable isotope record from benthic foraminifera presented herein, that suggest bottom waters in the western Coral Sea were cooler during the last glacial than at present.

A.2. APPROACH AND METHODS

A.2.1. Core selection

Five of the cores used in this study have been discussed previously in a more general sense (Hearty et al. submitted). These cores were collected during cruises 5/90 (core PC27a) and 4/97 (cores PC11, PC13, and PC16) of the *RV Franklin*, and cruise 051 (core GC43) of the *RV Rig Seismic*. The cores are located between 15 and 19°S in QT (Fig. A.1), a north-south trending rift basin offshore northeastern Australia in the western Coral Sea (Scott, 1993), and come from between 901 and 2163 m below sea level (mbsl). Antarctic Intermediate Water (AAIW) has influenced the temperature histories for all these cores (Fig. A.2), except PC27a, which is located in a deeper, undefined water mass (Pickard et al., 1977; Correge, 1993a). Further documentation of the cores is available elsewhere (Table A.1; Hearty et al., submitted).

The sixth core in our study (GC10) was taken ~20.8°S on MP, a shallow block of subsided continental crust (Ewing et al., 1970) immediately south of QT and adjacent to the modern continental shelf (Fig. A.1). GC10 was collected during cruise 03/99 of the *RV Franklin* and is located 320 mbsl. The uppermost thermocline (regionally known as South Pacific Central Water; Corregge, 1993a) has influenced the temperature history of sediments in GC10 (Fig. A.2).

The cores used in this study were chosen because they all have well-developed, previously determined chrono-stratigraphies (PC16, Dunbar et al., 2000; PC27a, PC11, PC13, GC43, Page et al., 2003; GC10, Page and Dickens, submitted) based on between 3 and 7 accelerator mass spectrometry (AMS) radiocarbon ages of pelagic planktonic foraminifera, which when calibrated (CALIB v4.3: Stuiver et al., 1998) fall within the range 0 to 25,000 cal BP. This period of time was considered appropriate to test both the integrity of the single foraminifera method at high-resolution, and the kinetics of the AAR reaction, for two main reasons, (1) this timeframe is well within the limit of detectability for radiocarbon dating (<40 ky BP), thus providing robust chronostratigraphic datums with which to correlate D/L data, and (2) this period encompasses significant environmental changes, including >100 m of relative sea level change (Fig. 1.2A) on the northeast Australian margin (Larcombe et al., 1995; Lambeck and Chappell, 2001), which may have resulted in temperature variations at the cored sites (Corregge, 1993b). In addition to these reasons, GC10 was specifically chosen to complement the existing dataset from QT because this core has been subject to vastly different environmental parameters. In particular, GC10 is significantly shallower than the cores from QT, lies in a different water mass, and has been subject to a warmer temperature history. GC10 thus provides the opportunity to assess the utility of the AAR method in these disparate conditions.

A.2.2. The AAR method

Samples from GC10 were subject to the same methods of collection, pre-treatment, and AAR analysis as the samples from QT cores. A detailed description of the methods specific to this study is available in Hearty et al. (submitted), with further detail on the techniques of AAR analysis available in Kaufman and Manley (1998) and Kaufman (2000). Briefly, samples for AAR analysis were collected at the James Cook University Sedimentology Laboratory by extracting nominally 4 cm³ of bulk sediment from horizons adjacent to those previously analysed for AMS radiocarbon ages, as well as at intermittent levels to increase sample resolution with respect to time. Bulk sediment samples were wet-sieved at 125 µm, rinsed with deionised water, and dried at low temperature. The coarse fraction was inspected under binocular microscope and between 6 and 12 pristine tests of the pelagic, planktonic foraminifera, *Po*, were picked from each sample. All samples were restricted to a single taxon to negate taxon-specific effects on racemization rates. *Po* was chosen because its physical and chemical properties are apparently well suited to AAR studies (for discussion see Hearty et al., submitted and refs therein).

Pre-treatment and AAR analysis were performed at Northern Arizona University. Pre-treatment involved cleaning of the tests in an ultrasonic bath for 2 min and soaking in 3% H₂O₂ for 2 hr. AAR analysis was performed via reverse-phase high-performance liquid chromatography (RP-HPLC) using a Hewlett-Packard HP1100 liquid chromatograph and HP Chemstation software. This technique allows D/L ratios to be measured in sub-milligram quantities of shell (and thus in individual *Po* tests) with an internal reproducibility of 2 to 5%, depending on the specific amino acid measured (Kaufman and Manley, 1998; Hearty et al., submitted).

A.2.3. Age models

Independent age control was available for each core in the form of between 3 and 7 AMS radiocarbon ages, calibrated to account for both variable atmospheric ^{14}C levels and marine reservoir effects. One AMS radiocarbon age from PC27a (22,100 ^{14}C yrs BP) could not be calibrated because it was beyond the range of the calibration program (20,750 ^{14}C yrs BP; Stuiver et al., 1998). Age models were based on least squares polynomial fits to the age data (Fig. A.3). For QT cores, third-order polynomial trends best fit the age data (Hearty et al., submitted) and correctly model that maximum sedimentation rates occurred during late transgression along slopes of QT (Dunbar et al., 2000; Dunbar and Dickens, 2003; Page et al., 2003). Here we make a slight modification to the original age model for PC13 (Hearty et al., submitted), which predicted the age for the top of this core as -1327 yrs BP, even though a calibrated radiocarbon age of 1250 cal BP occurs within 5 cm of the core top. Given further consideration, and the fact that the age models for all other cores return positive ages for the core tops, this result (although obviously impossible) seemed beyond the scope of error within the data. Thus, similar to the approach taken for PC11 because of a comparable issue (Hearty et al., submitted), we assumed that the top of PC13 was equivalent to 0 yrs BP for the purpose of developing a more appropriate age model. The resulting model yields a core top age for PC13 of -384 yrs BP, which while still naturally impossible is probably within the combined error of the dating techniques and modelling approach.

A least-squares polynomial equation was also used to construct an age model for GC10. However, a second-order polynomial trend fits the age data from this core better, mostly because the latest Holocene sedimentation was apparently unrecovered in

this core (Page and Dickens, submitted). Nonetheless, the second-order polynomial trend provides an excellent fit to the age data for GC10 and correctly models highest sedimentation rates on MP during late transgression (Page and Dickens, submitted). Derived age models for each core were subsequently used to estimate the age of each of the 49 intervals in which D/L ratios were determined.

A.2.4. Stable Isotopes

Foraminifera from the northeast Australian margin display variations in oxygen isotope composition that primarily reflect changes in seawater chemistry associated with changes in global ice volume (Peerdeman and Davies, 1993; Dunbar et al., 2000). Deviations from the global ice volume record are mostly attributable to temperature variations over time, but because pelagic species of benthic foraminifera live at considerable depth they are generally isolated from surface heating effects over glacial-interglacial cycles. Oxygen isotopes were thus analysed on 19 multi-specimen samples from GC43 of the pelagic benthic foraminifera *Cibicidoides mundulus*, to identify anomalies in oxygen isotope composition that may reflect changes in bottom-water temperature since the LGM.

Core GC43 was chosen for investigations of stable isotopes because it contains one of the most expanded records of Late Pleistocene-Holocene sedimentation recovered from QT (Page et al., 2003) and has been located both (1) well below the influence of surface heating effects, and (2) well within the influence of AAIW, for the duration of the last 25 ky. Nominally 5 cm³ samples were taken from GC43 every 7 to 20 cm (average 10 cm) between 3 and 210 cm below sea floor. Bulk sediment samples were wet sieved at 250 µm and dried at 50°C for 2–3 hours. Three to seven tests of *C. mundulus* were picked from the sieved fraction of each sample after examination under

binocular microscope and rejection of specimens with secondary cements or chamber infilling. This species was chosen because (1) it is bathyal, epifaunal, and common in sediments from GC43, and (2) the *Cibicidoides* genus has been demonstrated as a reliable species for use in stable isotope studies and precipitates its test in near isotopic equilibrium with seawater (Sen Gupta, 1999 and refs therein). Isotopic ratios were determined at the University of Wollongong using a Micromass multi-preparation unit attached to a Prism III mass spectrometer calibrated against NBS 18 and NBS 19 standards. All isotopic ratios are reported in standard delta notation with respect to Pee Dee Belemnite (PDB). Repeated analysis of standards indicated internal reproducibility of <0.1‰.

A.3. RESULTS

A.3.1. D/L ratios

Between 4 and 9 *Po* tests were analysed from each of the 49 levels across the 6 cores in this study for a total of 268 analyses. On average, 5 to 6 tests were analysed from each horizon, and each core had an average of 8 sampled horizons over the period 0 to 25 ka (Table A.2). Of the 268 individual *Po* tests analysed the results from 51 (19%) were rejected as being unreliable for determination of amino-stratigraphy because they returned anomalous D/L ratios. Notably, however, 22 of these were from GC10 alone, while the other 29 rejected results were spread fairly evenly amongst the other 5 cores. In effect, 36% of the tests measured from GC10 were rejected, while only 14% were rejected from QT cores.

The first criterion for rejecting individual results was D/L ratios that were significantly higher, or significantly lower, than the rest of the group within an individual horizon. For QT cores, results from individual tests were considered aberrant

if they were greater than twice the standard deviation ($\pm 2\sigma$) from the mean of the group (Hearty et al., submitted). For GC10 from MP, this was reduced to $\pm 1\sigma$, because when compared to QT cores the faster rates of racemization and greater range in measured D/L ratios resulted in a disproportionately larger standard deviation within individual horizons.

A second criterion for screening aberrant results was the covariance relationship between the D/L ratios of Asp and Glu (Fig. A.4). In GC10, the results from 2 tests (3.3%) were rejected because the D/L ratios of Asp and Glu were considered to be well outside the covariance trend exhibited by the rest of the samples. This result is almost identical to the number rejected from QT cores (3.4%; Hearty et al., submitted) because of spurious covariance data.

It is unclear why the covariance between D/L ratios of Asp and Glu in a small number of tests are clearly different than the rest of a measured population. This could perhaps indicate small errors in the measurement of D/L ratios, or minor contamination of individual *Po* tests, however, this seems unlikely given the reproducibility of analytical standards and the not unexpected results associated with the secondary amino acid Ser. It is more likely that these results reflect poorly understood processes associated with complex bio-geochemical reactions in the natural environment, the significance of which is probably limited. Conversely, tests with typical covariance but which were excluded because of values that were significantly different than the mean of the group most likely represent tests that were introduced from adjacent stratigraphic levels by bioturbation or slumping. These results are probably very important for understanding the magnitude and extent of biological mixing in sediments from the shelf and slope, and perhaps the identification of regional slumping events, although we do not pursue this line of investigation in this paper.

Excluding the rejected tests, overall mean D/L ratios for Asp range from 0.054 ± 0.011 (PC16) to 0.434 ± 0.025 (GC10). Asp D/L ratios and inter-shell variability in QT cores are lower than those from the MP core GC10. In QT, Asp D/L ratios reach a maximum of 0.222 ± 0.030 : a total range of 0.168. Total range in Asp D/L ratios on MP is 0.291.

Importantly, apart from a few exceptions, mean Asp D/L ratios increase progressively with depth in all cores (Fig. A.5). Of the 49 intervals analysed in this study, Asp D/L ratios in 45 abide by the principles of superposition (i.e. the ratios are greater than the ratios in sedimentary horizons above them). However, all of the stratigraphically reversed D/L ratios are statistically insignificant because they overlap within a $\pm 1\sigma$ error with the D/L ratios immediately above them. In fact, 3 of the 4 reversed Asp D/L ratios are especially insignificant because the means themselves are within a $\pm 1\sigma$ error of the mean D/L ratios above them. Thus the overlap in only 1 reversed ratio is constrained purely by overlapping error bars.

A.3.2. $\delta^{18}\text{O}$

Measured $\delta^{18}\text{O}$ in *C. mundulus* tests from GC43 (Fig. A.6; Table A.3) varies from 3.3 to 1.8‰ in samples deposited between ~21 and 2 ka, a total decrease of least 1.5‰. During this time, $\delta^{18}\text{O}$ decreased relatively steadily between ~21 and 8 ka, and generally stabilised after ~8 ka. These results are generally in-phase with glacio-eustatic sea level variations relative to the northeast Australian margin over the last 20 to 25 ky (Fig. A.6; Larcombe et al., 1995; Lambeck and Chappell 2001): sea level rose steadily and fairly rapidly between ~20 and 8 ka, with transgression slowing and sea level stabilising between ~8 ka and present. However, these results also represent a positive 0.2‰ deviation from the global ice volume record over the last glacial-

interglacial cycle, and suggest AAIW at a depth of approximately 800 to 900 mbsl in QT may have been $\sim 1.0^{\circ}\text{C}$ cooler during the last glacial compared to the Holocene.

A.4. Modelling racemization rates

The D/L ratios of Asp in all cores increase progressively with increasing age. The specific rates at which racemization proceeds in each core over time, however, is not exactly clear, and in some cases the time–D/L relationships in different cores appear quite dissimilar (e.g. PC27a and PC13; Fig. 5.5). Previous studies (O’Leary, 2001; Hearty et al., submitted) have concluded that the long-term racemization rates (up to >500 ka) of *Po* tests in QT cores may conform to models derived from power functions, but these provide few constraints on the kinetics of racemization over the last 25 ky, save for the fact that the reaction was much faster in the initial stages. Hence, in order to evaluate the dominant trends in downcore Asp D/L progressions among the suite of cores, and to better define the kinetic pathway of racemization over the last 25 ky in the western Coral Sea, we evaluated the fit of several different mathematical models. For GC10 we also re-evaluated the fit with one ratio removed from the dataset (the $\sim 19,000$ cal BP Asp D/L ratio). Although this reversal of the mean Asp D/L ratio in GC10 is statistically insignificant, it is the only reversed ratio in the dataset in which the mean itself does not overlap within a $\pm 1\sigma$ error with the overlying ratio, and therefore genuinely appears to be a possible outlier.

Similar to modelling of AAR over longer time frames (O’Leary, 2001; Hearty et al., submitted), power functions appear to model the downcore D/L progressions of Asp the most effectively over short periods of time (Fig. A.7), especially when all the resulting kinetic models are considered together (Fig A.8). Power functions provide varying levels of fit with the Asp D/L data in each core, ranging from very good for

PC27a, PC16, PC11 and GC43 (average $r^2 = 0.94$), to average for PC13 ($r^2 = 0.74$). The level of fit to the Asp D/L data in GC10 is poor when all data are considered ($r^2 = 0.59$) but improves considerably when the 'outlier' is removed ($r^2 = 0.76$).

Notwithstanding these levels of correlation, it is noteworthy that power functions do not always provide the best fit to the Asp D/L ratios in each core. In some cases linear models or polynomial models provide better fits to the downcore progressions in Asp D/L ratios. However, the kinetic models resulting from the use of power functions (Fig. A.8) are the only models that satisfy several fundamental criteria for AAR in fossil shells (e.g., Kaufman and Manley, 1998; Kaufman, 2000; Hearty et al., submitted): (1) projected initial D/L ratios should be very similar in each core regardless of modern environmental differences between cored sites (e.g. temperature), (2) racemization should proceed faster in cores bathed by warmer water, and (3) assuming modern differences in water temperature between sites was maintained over time (i.e. shallower cores were always bathed by warmer water), kinetic pathways of different cores should not intersect.

A.5. SUMMARY, CONCLUSIONS AND FUTURE WORK

Pulleniatina obliquiloculata tests in sediment cores from the western Coral Sea display a systematic increase in the D/L ratios of Asp and Glu over the last 25 ky (Table A.2). D/L ratios in all cores increase progressively with depth, and of the 49 intervals analysed from the six cores in this study the mean Asp D/L ratios in 92% comply with the laws of superposition. Nevertheless, none of the stratigraphically reversed mean Asp D/L ratios are statistically significant because each has a $\pm 1\sigma$ overlap with the D/L ratios from overlying horizons. One anomalous ratio from GC10,

however, might be considered a genuine outlier, although presently there is no physical evidence to support this conclusion.

Specific rates of racemization over the last glacial-interglacial cycle differ among the cores. In QT racemization rates of Asp over the last 20–25 ky range from 0.0047 to 0.0089 ky^{-1} . On MP racemization rates of Asp in GC10 were 0.0180 ky^{-1} over the last 20–25 ky. Thus, Asp racemization over the last glacial-interglacial cycle on MP proceeded approximately 2 to 4 times faster in comparison to cores from greater than 900 m depth in QT. This result is to be expected given that modern bottom water temperatures on MP are 10 to 15°C higher than temperatures within or below AAIW in QT (Fig. A.2). Notably, however, our results also demonstrate the sensitivity of Asp racemization rates to relatively minor temperature differences, such as those between cored sites in QT, where modern bottom water temperatures are different by only a few degrees or less (Fig. A.8).

Power functions model the downcore progressions in Asp D/L ratios the most successfully, providing good to reasonable correlations with the data in each core and satisfying four basic principles of AAR for which other modelling approaches fail in one or more respects: (1) predicted initial Asp D/L ratios are very similar in each core (2) D/L ratios increase progressively over time, (3) racemization rates are faster in cores bathed by warmer water, and (4) kinetic pathways do not intersect and describe a similar history of racemization at all cored sites.

The kinetic pathway of racemization as modelled by the power functions describes a history of racemization in QT and on MP that is faster in progressively younger sediments. These models are consistent with the natural slowing of racemization over time as the reaction approaches equilibrium. However, slower racemization rates during the last glacial may also indicate that bottom waters in QT

and on MP were cooler during the last glacial than at present. This possibility is consistent with the benthic isotope record from GC43, which displays a positive 0.2‰ deviation from the global ice volume record since the LGM (equivalent to a ~1.0°C increase in bottom water temperature), as well as Mg/Ca ratios measured in deep sea ostracodes at Ocean Drilling Program Site 822 in QT (Correge, 1993b). Our results remain equivocal, but experimental work in progress at Northern Arizona University addressing the kinetics of racemization at various temperatures and under different chemical conditions should help resolve some of these key issues.

Nonetheless, our results strengthen the integrity of the single foraminifera RPC method (Hearty et al., submitted), and demonstrate the utility of high-resolution amino-stratigraphy for geochronology and paleotemperature reconstructions over relatively short intervals of time. Furthermore, our results demonstrate that the technique is not only useful in deep marine settings such as QT, where bottom water temperatures are less than ~5°C and racemization rates are relatively slow, but is also robust in shallow settings such as MP, where bottom waters are substantially warmer (up to ~20°C) and the rate of racemization is relatively fast. AAR in single *Po* tests appears to be an effective geoscientific tool for investigations of Quaternary marine sediments.

ACKNOWLEDGEMENTS

An Australian Postgraduate Award and an AAPG Foundation Grant-In-Aid to MCP, and James Cook University Doctoral Research Scheme awards to MCP and MJO supported this research. Thanks are extended to Flavio Anselmetti and Phillip Reza Heck (ETZH) who kindly provided samples from core FR03/99 GC10, and to Raphael Wust (JCU) for insightful discussion of the data and manuscript.

Core	Latitude (°S)	Longitude (°E)	Water Depth (m)	Bottom water temperature (°C)	Water mass
FR03/99-GC10	20.8	152.3	320	16.5*	SPCW
51GC43	18.1	147.5	901	5.4	AAIW
FR4/92-PC16	17.4	146.9	1043	4.3	AAIW
FR4/92-PC11	17.6	147.4	1320	3.5	AAIW
FR4/92-PC13	17.0	146.9	1507	3.0	AAIW
FR5/90-PC27a	15.3	146.0	2163	2.4	Undefined

Table A.1: Location and other information for sediment cores FR03/99 GC10, 51GC43, FR4/92 PC16, FR4/92 PC11, FR4/92 PC12, and FR5/90 PC27a. Bottom water temperatures in Queensland Trough were measured on CSIRO cruises 1985/05, 1990/06, 1991/07, 1992/09 and 1997/01 and are available at www.marine.csiro.au/datacentre. *Temperature estimated from same depth in Queensland Trough. SPCW – South Pacific Central Water; AAIW – Antarctic Intermediate Water.

Lab ID (UAL)	Sample #	Age (cal yr BP)	Depth (cm bsl)	n	ex	D/L Asp	stdev	D/L Glu	stdev	D/L Ser	stdev
4090	MPRC-1 001	5920	1	4	4	0.143	0.022	0.052	0.009	0.264	0.037
4091	MPRC-2 012	6670	12	3	4	0.261	0.057	0.096	0.016	0.215	0.101
4092	MPRC-3 022	8056	22	7	2	0.210	0.067	0.075	0.027	0.269	0.033
4093	MPRC-4 028	9210	28	5	2	0.347	0.019	0.140	0.008	0.371	0.050
4094	MPRC-5 038	11670	38	6	1	0.371	0.02	0.154	0.010	0.373	0.036
4095	MPRC-6 049	15152	49	5	3	0.405	0.077	0.169	0.052	0.326	0.082
4096	MPRC-7 059	19023	59	3	5	0.301	0.033	0.112	0.023	0.316	0.106
4097	MPRC-8 066	22131	66	5	2	0.434	0.025	0.190	0.023	0.402	0.065
3936	GC43-005	2460	5	3	2	0.115	0.010	0.044	0.000	0.186	0.020
3935	GC43-031	5930	31	5	0	0.139	0.010	0.048	0.007	0.220	0.019
3949	GC43-051	8290	51	5	0	0.149	0.010	0.053	0.007	0.255	0.018
3934	GC43-071	9010	77	3	1	0.171	0.010	0.062	0.010	0.288	0.030
3933	GC43-153	11120	153	5	0	0.178	0.014	0.059	0.010	0.235	0.074
3937	GC43-171	14130	171	4	1	0.181	0.003	0.068	0.000	2.660	0.040
3950	GC43-189	16250	189	5	0	0.191	0.010	0.066	0.008	0.298	0.041
3932	GC43-209	21080	209	4	1	0.222	0.030	0.085	0.010	0.300	0.030
3733	PC16-015	258	2	4	1	0.054	0.011	0.027	0.007	0.052	0.021
3627	PC16-034	1740	21	6	0	0.076	0.006	0.028	0.003	0.136	0.008
3979	PC16-056	4361	43	4	1	0.097	0.003	0.038	0.003	0.166	0.003
3977	PC16-078	5392	58	3	2	0.129	0.008	0.058	0.010	0.199	0.017
3621	PC16-100	6720	80	5	1	0.134	0.010	0.046	0.013	0.206	0.046
3978	PC16-118	7331	98	3	2	0.153	0.004	0.062	0.009	0.257	0.026
3625	PC16-185	10060	165	5	1	0.162	0.022	0.061	0.013	0.245	0.043
3628	PC16-253	13020	230	4	1	0.172	0.009	0.053	0.005	0.271	0.016
3975	PC16-263	14767	240	4	1	0.174	0.014	0.064	0.004	0.271	0.045
3976	PC16-272	15781	249	5	0	0.200	0.013	0.075	0.009	0.317	0.032
3624	PC16-282	17420	259	3	3	0.207	0.010	0.072	0.100	0.251	0.040
3987	PC11-023	4816	13	3	2	0.101	0.005	0.043	0.007	0.172	0.028
3990	PC11-036	6980	26	5	0	0.125	0.009	0.041	0.004	0.249	0.031
3988	PC11-048	8232	38	5	0	0.141	0.020	0.049	0.005	0.261	0.039
3986	PC11-060	10280	50	3	2	0.160	0.010	0.058	0.004	0.243	0.012
3991	PC11-070	13639	60	4	0	0.173	0.009	0.064	0.005	0.278	0.007
3983	PC11-079	18720	69	5	0	0.190	0.008	0.069	0.008	0.322	0.024
3989	PC11-090	28459	80	5	0	0.197	0.019	0.067	0.009	0.322	0.031
3971	PC13-005	1250	5	3	2	0.101	0.006	0.047	0.004	0.139	0.028
3967	PC13-020	5668	20	4	1	0.103	0.002	0.043	0.007	0.176	0.025
3974	PC13-040	7379	40	4	1	0.115	0.005	0.042	0.004	0.207	0.024
3969	PC13-055	8150	55	4	1	0.131	0.011	0.044	0.005	0.230	0.017
3968	PC13-079	10990	79	5	0	0.150	0.012	0.054	0.005	0.275	0.022
3970	PC13-086	13512	86	5	0	0.149	0.007	0.051	0.007	0.256	0.049
3966	PC13-095	17725	95	5	0	0.189	0.007	0.068	0.006	0.304	0.015
3972	PC13-104	23750	104	4	1	0.206	0.013	0.074	0.008	0.327	0.046
3973	PC13-121	40703	121	5	0	0.204	0.008	0.071	0.005	0.307	0.047

3942	PC27a-007	1520	7	5	0	0.079	0.008	0.035	0.006	0.143	0.028
3943	PC27a-052	4990	52	5	0	0.112	0.009	0.045	0.008	0.212	0.019
3944	PC27a-084	7620	84	5	0	0.132	0.004	0.047	0.006	0.240	0.018
3945	PC27a-151	9910	151	4	1	0.131	0.006	0.045	0.004	0.222	0.025
3946	PC27a-193	12870	193	5	0	0.140	0.006	0.049	0.003	0.243	0.033
3947	PC27a-218	14340	218	5	0	0.148	0.013	0.056	0.008	0.262	0.045
3948	PC27a-318	22100	318	5	0	0.184	0.009	0.063	0.006	0.293	0.031

Table A.2: Sample information, extrapolated ages, and results of RP-HPLC analysis (D/L ratios) for cores FR03/99 GC10, 51GC43, FR4/92 PC16, FR4/92 PC11, FR4/92 PC12, and FR5/90 PC27a. n – number of tests included in average. ex – number of tests excluded from average.

Sample	Depth (cm)	Age (ka)	$\delta^{18}\text{O}$ (PDB)	$\delta^{13}\text{C}$ (PDB)	$\delta^{18}\text{O}$ (SMOW)
MP GC43-3*	3	1996	1.9	1.4	32.9
MP GC43-10	10	3314	1.8	1.3	32.8
MP GC43-20	20	4893	2.0	1.3	32.9
MP GC43-30*	30	6152	1.9	1.3	32.9
MP GC43-40	40	7130	1.9	1.3	32.9
MP GC43-50	50	7871	1.9	1.2	32.9
MP GC43-60	60	8416	2.0	1.2	33
MP GC43-76	76	8981	2.1	1.1	33.1
MP GC43-90	90	9283	2.2	1.0	33.2
MP GC43-110	110	9638	2.3	0.8	33.3
MP GC43-120	120	9873	2.2	0.8	33.2
MP GC43-130	130	10200	2.0	0.7	33
MP GC43-150	150	11301	2.3	1.0	33.2
MP GC43-160	160	12157	2.3	1.1	33.3
MP GC43-170	170	13271	2.3	1.0	33.3
MP GC43-180	180	14686	2.7	0.9	33.7
MP GC43-190	190	16442	2.8	1.0	33.8
MP GC43-200	200	18582	3.1	1.1	34.1
MP GC43-210	210	21146	3.3	1.2	34.4

* Average result after multiple analyses of tests from same sample

Table A.3: Results of stable isotope analysis of benthic foraminifera from core 51GC43.

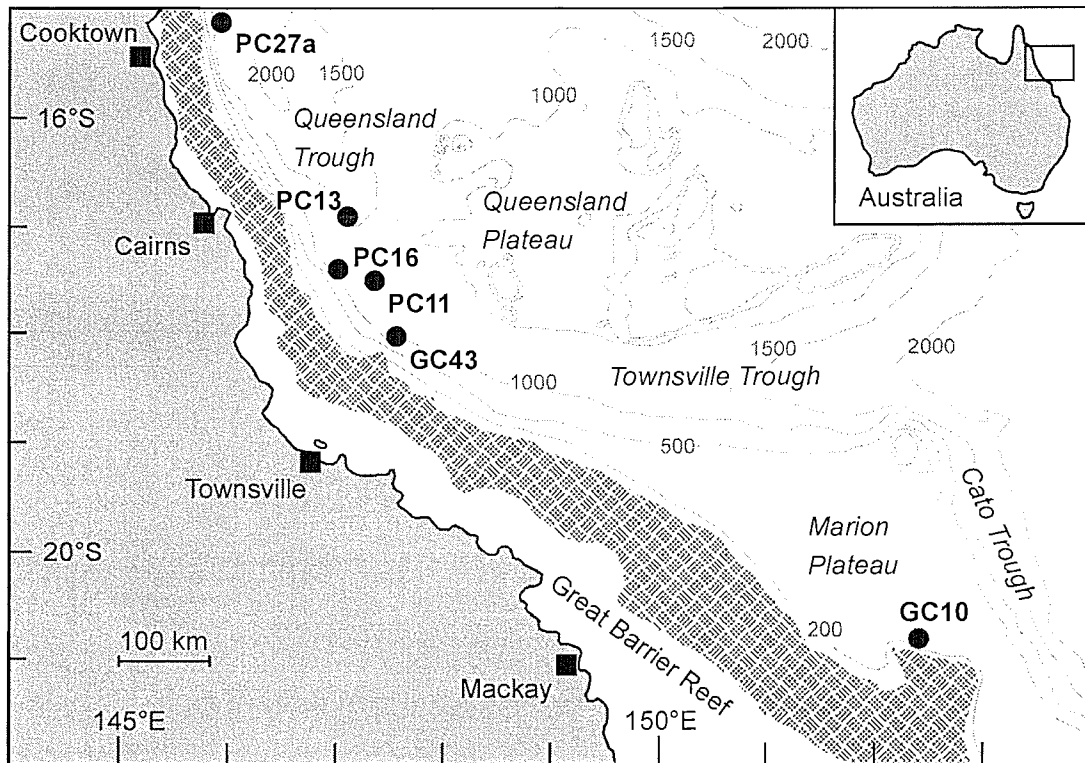


Figure A.1: The continental margin of northeastern Australia. Circles indicate the position of cores FR03/99 GC10, 51GC43, FR4/92 PC16, FR4/92 PC11, FR4/92 PC12, and FR5/90 PC27a. Bathymetry of the western Coral Sea is indicated in metres.

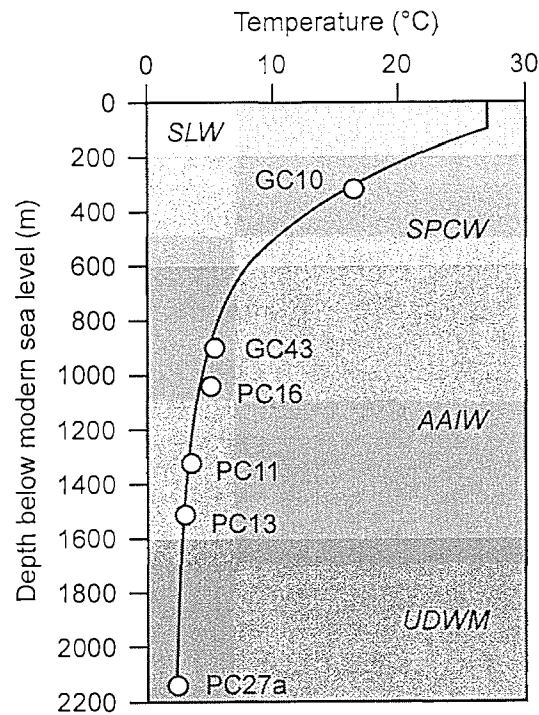


Figure A.2: Generalised temperature profile and water mass boundaries in the western Coral Sea (modified after: Corregge, 1993a; Hearty et al., submitted). Circles indicate the modern depth below sea level of cores FR03/99 GC10, 51GC43, FR4/92 PC16, FR4/92 PC11, FR4/92 PC12, and FR5/90 PC27a. SLW – Subtropical Lower Water; SPCW – South Pacific Central Water; AAIW – Antarctic Intermediate Water; UDWM – Undefined deep water mass.

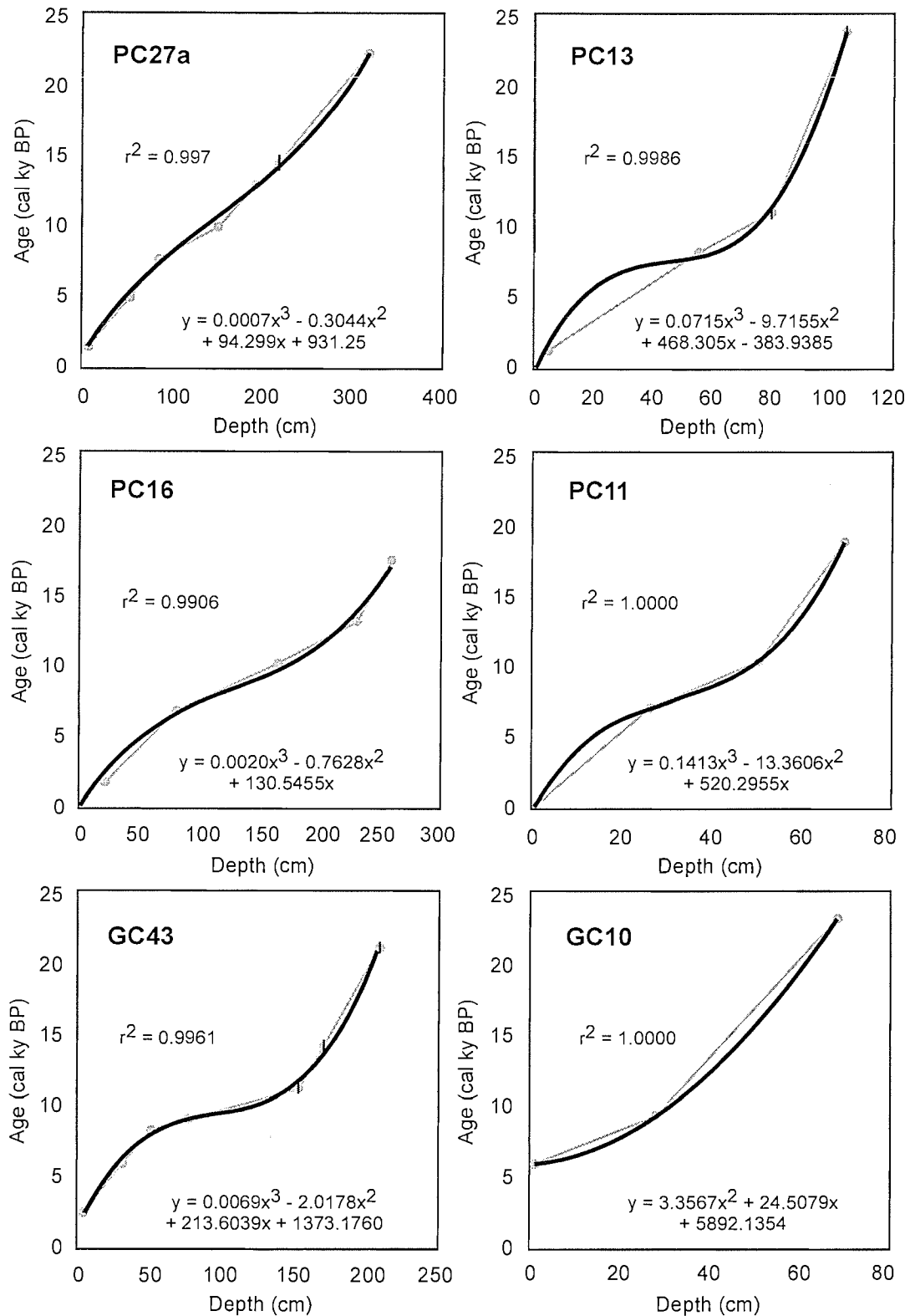


Figure A.3: Age/depth relationships in cores FR03/99 GC10, 51GC43, FR4/92 PC16, FR4/92 PC11, FR4/92 PC12, and FR5/90 PC27a, based on calibrated radiocarbon dates, and derived age models using least squares polynomial functions.

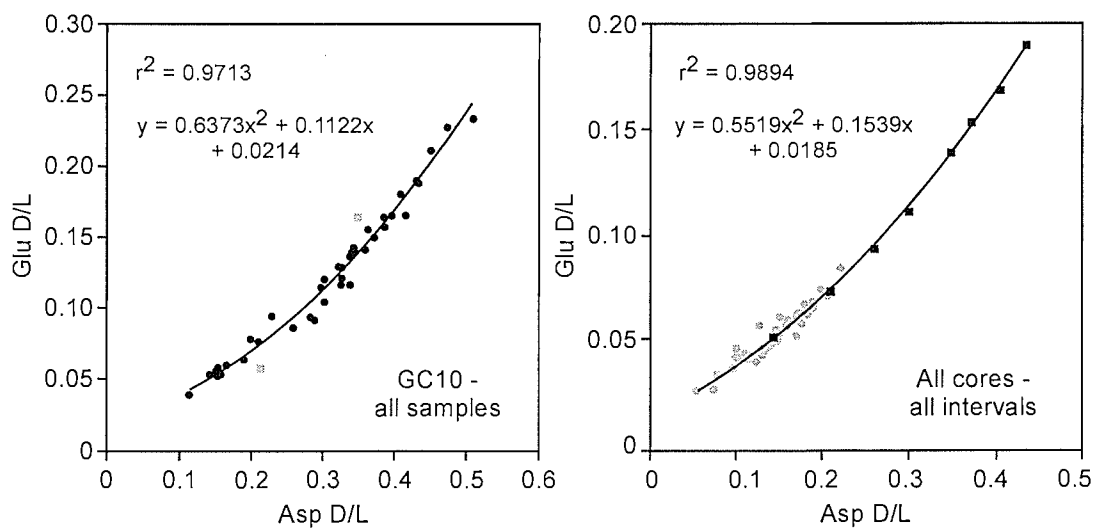


Figure A.4: Covariance relationships between the D/L ratios of Asp and Glu for all samples from core FR03/99 GC10 (left) and for the mean D/L ratios of all intervals from cores FR03/99 GC10, 51GC43, FR4/92 PC16, FR4/92 PC11, FR4/92 PC12, and FR5/90 PC27a (right). Black circles – GC10 samples. Grey circles – samples from Queensland Trough cores. Grey squares – rejected ratios.

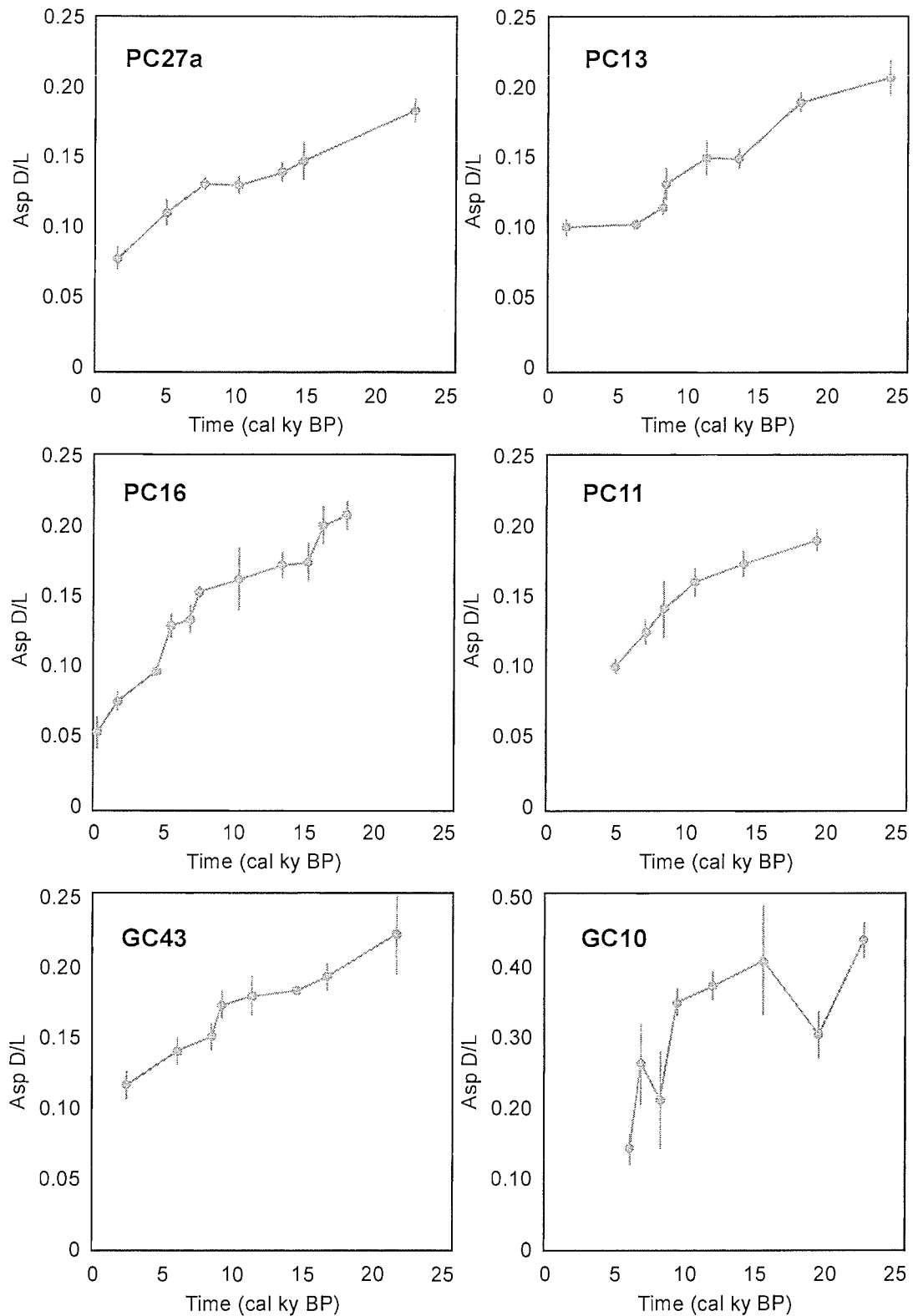


Figure A.5: The relationship between time and the D/L ratios of Aspartic acid in foraminifera from cores FR03/99 GC10, 51GC43, FR4/92 PC16, FR4/92 PC11, FR4/92 PC12, and FR5/90 PC27a.

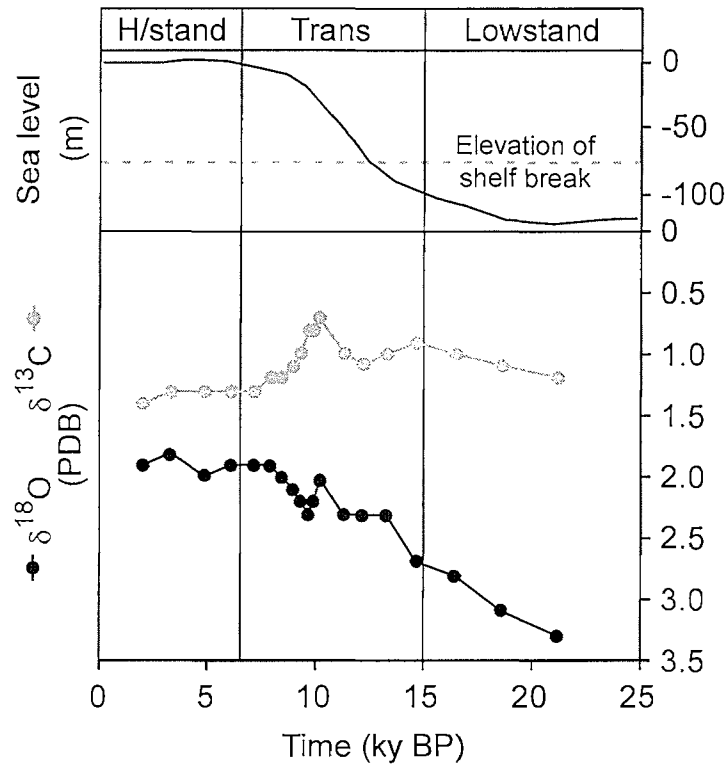


Figure A.6: Variations in $\delta^{18}\text{O}$ and $\delta^{13}\text{C}$ in benthic foraminifera from core 51GC43, relative to sea level changes on the northeast Australian margin over the last glacial-interglacial cycle. H/Stand – sea level highstand. Trans – sea level transgression.

Lowstand – sea level lowstand

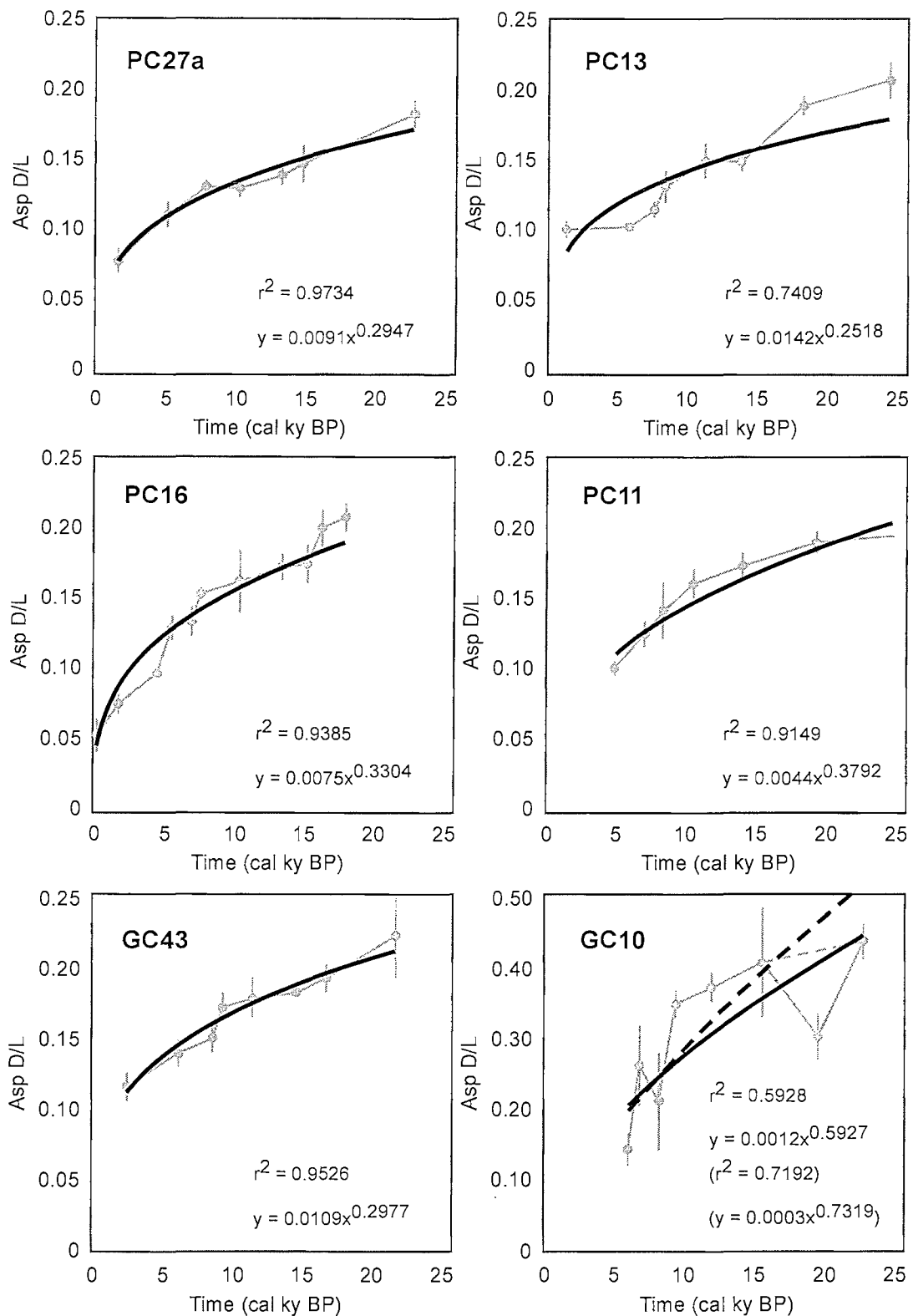


Figure A.7: The relationship between time and the D/L ratios of Aspartic acid in foraminifera from cores FR03/99 GC10, 51GC43, FR4/92 PC16, FR4/92 PC11, FR4/92 PC12, and FR5/90 PC27a, modelled using power functions. Correlation coefficient and equation shown in brackets indicate modelling results for FR03/99 GC10 with one outlier removed.

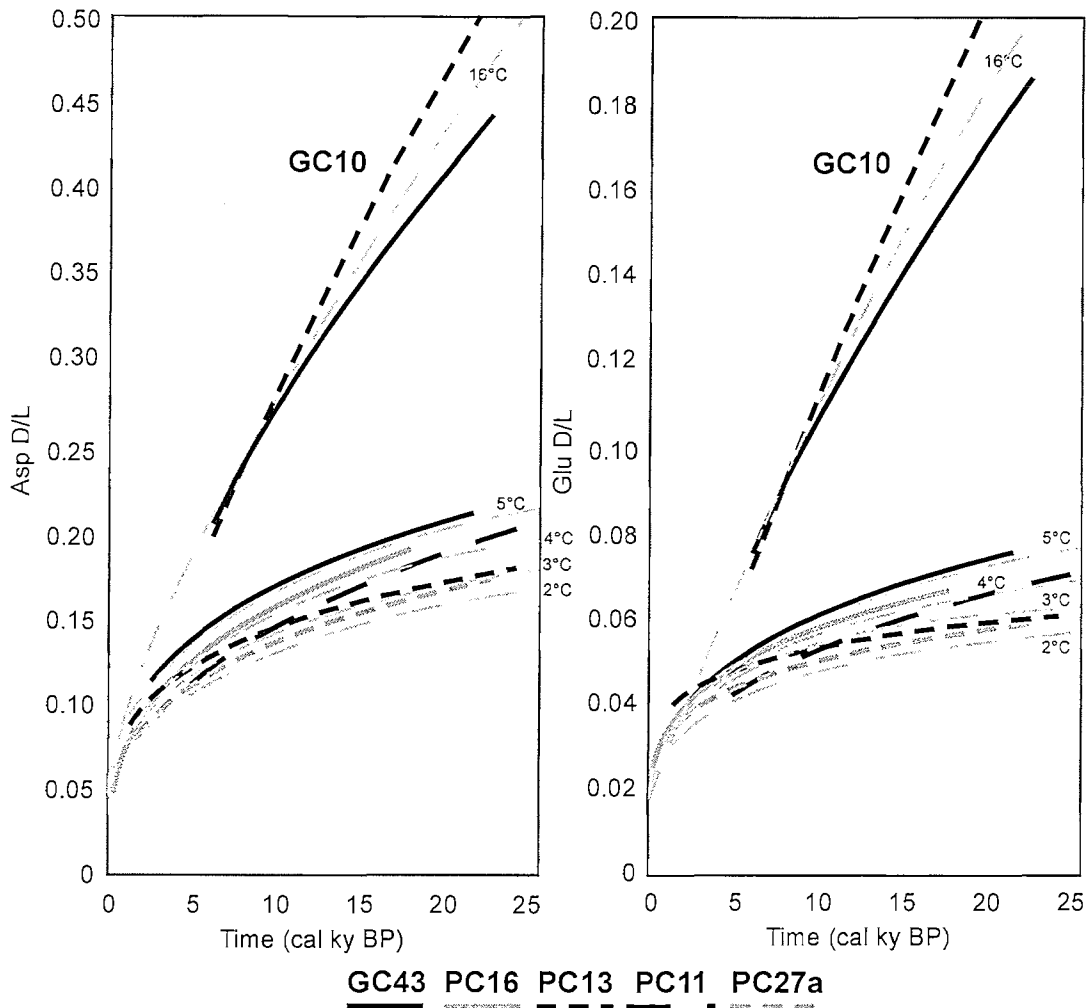


Figure A.8: Comparison of the modelled kinetic pathways for Aspartic acid in cores FR03/99 GC10, 51GC43, FR4/92 PC16, FR4/92 PC11, FR4/92 PC12, and FR5/90 PC27a, over the last 20 to 25 ky. GC10: solid line – all data, dashed line – outlier removed. Grey dashed lines indicate the estimated position of temperature gradients for racemization rates of Aspartic acid in the western Coral Sea.

REFERENCES

- Bada, J.L., and Man, E.H., 1980, Amino acid diagenesis in Deep Sea Drilling Project cores: kinetics and mechanisms of some reactions and their applications in geochronology and in paleotemperature and heat flow determinations: *Earth Science Reviews*, v. 16, p. 21-55.
- Correge, T., 1993a, Late Quaternary palaeoceanography of the Queensland Trough (Western Coral Sea) based on Ostracoda and the chemical composition of their shells [PhD thesis]: Canberra, Australian National University.
- Correge, T., 1993b, Preliminary results of paleotemperature reconstructions using the magnesium to calcium ratio of deep-sea ostracode shells from the late Quaternary of Site 822, Leg 133 (western Coral Sea), *in* McKenzie, J.A., Davies, P.J., Palmer-Julson, A., et al. (Eds), *Proceedings of the Ocean Drilling Program, Scientific Results, 133*: College Station, TX, (Ocean Drilling Program), p. 175-180.
- Dunbar, G.B., and Dickens, G.R., 2003, Massive siliciclastic discharge to slopes of the Great Barrier Reef Platform during sea-level transgression: constraints from sediment cores between 15°S and 16°S latitude and possible explanations: *Sedimentary Geology*, v. 162, p. 141-158.
- Dunbar, G.B., Dickens, G.R., and Carter, R.M., 2000, Sediment flux across the Great Barrier Reef Shelf to the Queensland Trough over the last 300 ky: *Sedimentary Geology*, v. 133, p. 49-92.
- Ewing, M., Hawkins, L.V., and Ludwig, W.J., 1970, Crustal structure of the Coral Sea: *Journal of Geophysical Research*, v. 75, p. 1953-1962.
- Harada, N., and Handa, N., 1995, Amino acid chronology in the fossil planktonic foraminifera, *Pulleniatina obliquiloculata* from the Pacific Ocean: *Geophysical Research Letters*, v. 20, p. 2353-2356.
- Harada, N., Handa, N., Ito, M., Oba, T., and Matsumoto, E., 1996, Chronology of marine sediments by the racemization reaction of aspartic acid in planktonic foraminifera: *Organic Chemistry*, v. 24, p. 921-930.
- Hare, P.E., and Mitterer, R.M., 1967, Non-protein amino acids in fossil shells: *Carnegie Institute of Washington Yearbook*, v. 65, p. 362-364.
- Hearty, P., and Aharon, P., 1988, Amino acid chronostratigraphy of late Pleistocene coral reef sites: Huon Peninsula, New Guinea and the Great Barrier Reef, *Australia: Geology*, v. 16, p. 579-583.
- Hearty, P., Kaufman, D.S., Olson, S.L., and James, H.F., 2000, Stratigraphy and whole-rock amino acid geochronology of key Holocene and Last Interglacial carbonate deposits in the Hawaiian Islands: *Pacific Science*, v. 54, p. 423-442.
- Hearty, P., Vacher, H.L., and Mitterer, R.M., 1992, Aminostratigraphy and ages of Pleistocene limestones of Bermuda: *Geological Society of America Bulletin*, v. 104, p. 471-480.
- Johnson, B.J., Lehman, S.J., and Miller, G.H., 1990, Arrhenius parameters for the foram species, *Globorotalia menardii*, and the deduction of bottom water temperature changes during the Pleistocene-Holocene transition: *Abstracts with Programs, Geological Society of America*, v. 22(7), p. 146.
- Kaufman, D.S., 2000, Amino acid racemization in ostracodes, *in* Goodfriend, G., Collins, M., Fogel, M., Macko, S., and Wehmiller, J. (Eds), *Perspectives in amino acid and protein geochemistry*: New York, Oxford University Press, p. 145-160.

- Kaufman, D.S., and Manley, W.F., 1998, A new procedure for determining enantiomeric (D/L) amino acid ratios in fossil using reverse phase liquid chromatography: *Quaternary Science Reviews*, v. 17, p. 987-1000.
- Knudsen, K.L., and Sejrup, H.P., 1993, Pleistocene stratigraphy in the Devil's Hole area, central North Sea: foraminiferal and amino-acid evidence: *Journal of Quaternary Science*, v. 8, p. 1-14.
- Lambeck, K., and Chappell, J., 2001, Sea level change through the Last Glacial cycle: *Science*, v. 292, p. 679-686.
- Larcombe, P., Carter, R.M., Dye, J., Gagan, M.K., and Johnson, D.P., 1995, New evidence for episodic post-glacial sea-level rise, central Great Barrier Reef, Australia: *Marine Geology*, v. 127, p. 1-44.
- Lehman, S.J., Miller, G.H., and Jones, G.A., 1988, Glacial-Holocene bottom water temperature changes deduced from epimerization rate changes in foraminifers: *Eos transactions, AGU*, v. 69(44).
- Macko, S.A., and Aksu, A.E., 1986, Amino acid epimerization in planktonic foraminifera suggests low sedimentation rates for Alpha Ridge, Arctic Ocean: *Nature*, v. 322, p. 730-732.
- Miller, G.H., and Hare, P.E., 1980, Amino acid geochronology: Integrity of the carbonate matrix and potential of molluscan fossils, *in* Hare, P.E., Hoering, T.C., and King, K.J. (Eds), *Recent advances in biogeochemistry of amino acids*: New York, Wiley, p. 415-444.
- Muller, P.J., 1984, Isoleucine epimerization in Quaternary planktonic foraminifera; effects of diagenetic hydrolysis and leaching, and Atlantic-Pacific intercore correlations: *Meteor-Forschungsergebnisse. Reihe C.: Geologie und Geophysik*, v. 38, p. 25-47.
- O'Leary, M.J., 2001, Amino acid racemization of the planktonic foraminifera, *Pulleniatina obliquiloculata*, from Queensland Trough piston cores [Hons thesis]: Townsville, James Cook University.
- Page, M.C., Dickens, G.R., and Dunbar, G.B., 2003, Tropical view of Quaternary sequence stratigraphy: siliciclastic accumulation on slopes east of the Great Barrier Reef since the Last Glacial Maximum: *Geology*, v. 31, p. 1013-1016.
- Peerdeman, F.M., and Davies, P.J., 1993, Sedimentological response of an outer-shelf, upper-slope sequence to rapid changes in Pleistocene eustatic sea-level: Hole 820A, Northeastern Australian Margin, *in* McKenzie, J.A., Davies, P.J., Palmer-Julson, A., et al. (Eds), *Proceedings of the Ocean Drilling Program, Scientific Results, 133*: College Station, TX, (Ocean Drilling Program), p. 303-313.
- Pickard, G.L., Donguy, J.R., Henin, C., and Rougerie, F., 1977, A review of the physical oceanography of the Great Barrier Reef and western Coral Sea. AIMS Monograph Series, 133 p.
- Rutter, N.W., and Blackwell, B., 1995, Amino acid racemization dating, *in* Rutter, N.W., and Catto, N.R., eds., *Dating methods for Quaternary deposits*: Newfoundland, Geological Association of Canada, p. 125-167.
- Scott, D.L., 1993, Architecture of the Queensland Trough: implications for the structure and tectonics of the Northeastern Australian Margin: *AGSO Journal of Australian Geology and Geophysics*, v. 14, p. 21-34.
- Sen Gupta, B.K., 1999, *Modern Foraminifera*: Dordrecht, Kluwer Academic Publishers, 371 p.
- Stuiver, M., Reimer, P.J., Bard, E., Beck, J.W., Burr, G.S., Hughen, K.A., Kromer, B., McCormac, G., van der Plicht, J., and Spurk, M., 1998, INTCAL 98 radiocarbon age calibration, 24,000-0 cal BP: *Radiocarbon*, v. 40, p. 1041-1083.

APPENDIX B

DATA REPORT: VARIATIONS IN BULK CARBONATE CONTENT IN ODP HOLE 1198A, 0 – 23.69 MBSF

Michael C. Page

School of Earth Sciences, James Cook University, Townsville, QLD 4811 Australia

Adapted from a data report published online at:

http://www-odp.tamu.edu/publications/194_SR/004/004.htm

Proceedings of the Ocean Drilling Program, Scientific Results Leg 194

ABSTRACT

Upper Quaternary sediment sequences east of the Great Barrier Reef are characterised by alternating siliciclastic-rich and carbonate-rich horizons caused by changes in the input of various sedimentary components and reflected in cores by variations in bulk carbonate content. A total of 153 measurements of bulk carbonate content were determined using the carbonate-bomb technique for late Pleistocene sediments between 0 and 23.69 mbsf (metres below sea floor) in Ocean Drilling Program Hole 1198A. Average sample resolution was 15 cm and multiple analyses were performed on each sample. Bulk carbonate content ranges from a maximum of 94 wt% at 13.63 mbsf to a minimum of 73 wt% at 14.54 mbsf. Five cyclic trends are observed that may relate to five major glacial events during the last 500 ky of the Quaternary.

B.1. INTRODUCTION

The northeast Australian margin is the largest extant tropical mixed siliciclastic-carbonate depositional system. For more than 500 ky (Davies and McKenzie, 1993; International Consortium for Great Barrier Reef Drilling, 2001), rivers have discharged large masses of clay, quartz, and other weathered residue from the Australian continent into a region with an extensive network of carbonate reefs on the outer shelf, the Great Barrier Reef (GBR). The Marion Plateau (Fig. B.1) lies eastward of the main GBR system, acting as a repository for carbonate material shed from the GBR platform as well as siliciclastic sediments sourced from the Australian landmass (Shipboard Scientific Party, 2002a). The plateau also accumulates carbonate sediments sourced from pelagic rain and local reef systems detached from the high-density reef network on the adjoining GBR shelf.

Eustatic fluctuations are widely believed to be the primary control on off-shelf fluxes of siliciclastic and carbonate sediments along passive continental margins (e.g., Vail et al., 1977; Walker, 1992). The northeast Australian margin is no exception, although considerable conjecture surrounds the specific processes affecting sediment transport and the timing of off-shelf sediment fluxes in relation to specific eustatic phases (e.g., Harris et al., 1990; Peerdeman and Davies, 1993; Dunbar et al., 2000; Kronen and Glenn, 2000; Page et al., 2003). Ocean Drilling Program Hole 1198A (Fig. B.1) provides an expanded record of mixed siliciclastic-carbonate deposition on the Marion Plateau from the late Pliocene to Pleistocene (Shipboard Scientific Party, 2002b). The site contrasts with the more heavily investigated Queensland and Townsville troughs north of the plateau because a significantly wider shelf separates it further from fluvial sources of siliciclastic sediment.

This data report does not attempt to quantify the rates of sediment accumulation at Site 1198A, or to resolve the question of off-shelf sediment fluxes and their relation to eustatic variations (cf. Page et al., 2003). The high-resolution record of variations in bulk carbonate content, however, should prove useful for future studies that may address these questions, as well as other problems relating to the evolution of the mixed siliciclastic-carbonate margin of northeastern Australia.

B.2. METHODS

A total of 153 samples from the upper part of Subunit 1A of Megasequence D were taken at an average 15 cm resolution between 0 and 23.69 mbsf (metres below sea floor) in Hole 1198A (Table B.1). Based on shipboard biostratigraphic datums (Shipboard Scientific Party, 2002b), this interval approximately represents the last 500 ky of deposition on the Marion Plateau. This period is also thought to be roughly congruous with the presence of large barrier reef systems, analogous to the present GBR, on the adjacent continental shelf during sea level highstands (International Consortium for Great Barrier Reef Drilling, 2001).

Approximately 3 cm³ of sediment was subsampled from nominally 10 cm³ of bulk sample and freeze-dried to remove pore fluids. Subsamples were crushed using a ceramic hand mortar and pestle and ground into a fine powder. From each sample, 150 to 250 mg of powder was weighed and utilised for the determination of bulk carbonate content following the principles of the carbonate-bomb technique (Mueller and Gastner, 1971). Duplicate sample analyses and comparisons with laboratory standards place the accuracy and precision of reported carbonate contents within a maximum of \pm 2.6%, with an average reproducibility of \pm 0.9% (Table B.1).

Sediment on the northeast Australian margin comprises two basic components, terrigenous siliciclastic sediment and biogenic carbonate, with only trace amounts of other material (Harris et al., 1990; Dunbar et al., 2000; Heap et al., 2001). Consequently, within the precision of the technique, quantification of bulk carbonate content also renders accurate values for siliciclastic abundance.

B.3. RESULTS

Bulk carbonate contents in the upper part of Subunit 1A of Megasequence D in Hole 1198A are generally very high (Table B.1, Figure B.2). More than 95% of the 153 intervals sampled between 0 and 23.69 mbsf had bulk carbonate concentrations greater than 80 wt%, with over 76% of these samples being greater than 85 wt% carbonate. Maximum bulk carbonate content of 94.1 wt% occurs at 13.63 mbsf and minimum bulk carbonate content of 72.7 wt% occurs at 14.54 mbsf. The interval between 14.54 and 14.35 mbsf shows the highest short-term range in bulk carbonate content with a variation of approximately 20 wt% occurring in adjacent samples separated by less than 20 cm.

Variations in bulk carbonate content occur with a general cyclicity that has a period of between 3 and 7 m and amplitude of between 10 and 20 wt%. Overall, five cyclic trends are observed. Peaks occur at 3.35, 6.85, 13.63, 17.00, and 22.04 mbsf, and troughs occur at 0.35, 5.04, 7.50, 14.54, and 20.69 mbsf. The five cyclic variations in bulk carbonate content in Hole 1198A are potentially related to the five major glacial events that have occurred in the last 500 ky of the Quaternary. Based on shipboard biostratigraphic datums, including the fact that it is likely that the Holocene sediment section is missing from Hole 1198A (Shipboard Scientific Party, 2002b), peaks in the

bulk carbonate content may loosely correlate with highs in fifth-order sea level and marine isotope stages 3, 5, 7, 9, and 11.

ACKNOWLEDGEMENTS

This research used samples and/or data provided by the Ocean Drilling Program (ODP). ODP is sponsored by the U.S. National Science Foundation (NSF) and participating countries under management of Joint Oceanographic Institutions (JOI), Inc.

I would sincerely like to thank co-chief scientists Flavio Anselmetti and Alexandra Isern, staff scientist Peter Blum, and the entire shipboard scientific party for the opportunity to be a part of ODP Leg 194, and to participate in shipboard and postcruise scientific meetings. The knowledge, experience, and enjoyment gained from these endeavours are currently unparalleled and have been instrumental in my enthusiasm for science since.

ODP Hole 1198A

Core	Section	Interval (cm)		Depth (mbsf)	Carbonate (wt%)			Average	Std. Dev.
		Top	Bottom		Analysis 1	Analysis 2	Analysis 3		
1H	1	3	5	0.04	86.0	85.9		86.0	0.1
1H	1	18	20	0.19	89.5	89.4	90.2	89.7	0.4
1H	1	34	36	0.35	84.9	84.6		84.8	0.2
1H	1	51	53	0.52	88.5	86.1		87.3	1.7
1H	1	66	68	0.67	87.2	88.5	87.7	87.8	0.7
1H	1	83	85	0.84	87.9	87.9	86.8	87.5	0.6
1H	1	99	101	1.00	89.2	90.4	89.0	89.5	0.8
1H	1	112	114	1.13	90.7	87.6		89.2	2.2
1H	1	130	132	1.31	90.5	90.1	91.7	90.8	0.8
1H	1	144	146	1.45	90.8	92.4	91.8	91.7	0.8
1H	2	153	155	1.54	85.7	89.6	90.2	88.5	2.4
1H	2	168	170	1.69	85.3	88.9	88.0	87.4	1.9
1H	2	184	186	1.85	90.3	89.7		90.0	0.4
1H	2	201	203	2.02	90.5	90.5	87.9	89.6	1.5
1H	2	216	218	2.17	89.1	88.1		88.6	0.7
1H	2	233	235	2.34	88.8	89.5	91.1	89.8	1.2
1H	2	249	251	2.50	89.8	89.3		89.6	0.4
1H	2	262	264	2.63	89.8	91.3	92.8	91.3	1.5
1H	2	280	282	2.81	91.0	91.3		91.2	0.2
1H	3	303	305	3.04	91.1	91.6		91.4	0.4
1H	3	318	320	3.19	90.5	90.2		90.4	0.2
1H	3	334	336	3.35	91.5	94.7	92.3	92.8	1.7
1H	3	351	353	3.52	90.6	91.5		91.1	0.6
1H	3	366	368	3.67	90.0	90.0	88.3	89.4	1.0
1H	3	383	385	3.84	87.8	90.1	90.2	89.4	1.4
1H	3	399	401	4.00	87.2	87.2		87.2	0.0
1H	3	412	414	4.13	83.2	85.1		84.2	1.3
1H	3	430	432	4.31	81.6	82.7		82.2	0.8
1H	3	444	446	4.45	82.9	85.1	85.8	84.6	1.5
1H	4	453	455	4.54	87.2	87.2	88.4	87.6	0.7
1H	4	468	470	4.69	84.0	83.4	84.9	84.1	0.8
1H	4	484	486	4.85	85.2	83.6	86.7	85.2	1.6
2H	1	503	505	5.04	81.7	80.5		81.1	0.8
2H	1	518	520	5.19	85.7	83.7		84.7	1.4
2H	1	534	536	5.35	81.2	81.5	83.8	82.2	1.4
2H	1	551	553	5.52	83.5	84.3	86.2	84.7	1.4
2H	1	566	568	5.67	83.8	84.1	85.4	84.4	0.9
2H	1	583	585	5.84	85.8	83.6	85.6	85.0	1.2
2H	1	599	601	6.00	85.7	86.1	85.1	85.6	0.5
2H	1	612	614	6.13	86.5	88.9		87.7	1.7
2H	1	630	632	6.31	89.4	88.6	93.4	90.5	2.6
2H	1	644	646	6.45	89.1	92.4	90.7	90.7	1.7
2H	2	653	655	6.54	91.1	91.1	87.9	90.0	1.8
2H	2	668	670	6.69	89.3	88.9		89.1	0.3
2H	2	684	686	6.85	90.7	91.7	90.0	90.8	0.9

2H	2	701	703	7.02	88.2	89.5	88.8	88.8	0.7
2H	2	716	718	7.17	83.8	85.5	85.8	85.0	1.1
2H	2	733	735	7.34	79.6	79.9		79.8	0.2
2H	2	749	751	7.50	78.4	78.6		78.5	0.1
2H	2	762	764	7.63	80.0	80.9		80.5	0.6
2H	2	780	782	7.81	82.5	84.0	84.0	83.5	0.9
2H	2	794	796	7.95	81.8	82.4		82.1	0.4
2H	3	803	805	8.04	83.0	83.0	79.3	81.8	2.1
2H	3	818	820	8.19	87.4	89.2	86.2	87.6	1.5
2H	3	834	836	8.35	88.1	88.6		88.4	0.4
2H	3	851	853	8.52	88.3	90.2	87.2	88.6	1.5
2H	3	866	868	8.67	87.3	87.4		87.4	0.1
2H	3	883	885	8.84	85.5	84.4		85.0	0.8
2H	3	899	901	9.00	85.5	83.2		84.4	1.6
2H	3	912	914	9.13	84.9	84.9	81.3	83.7	2.1
2H	3	930	932	9.31	87.0	87.6	87.4	87.3	0.3
2H	3	944	946	9.45	83.6	82.4		83.0	0.8
2H	4	953	955	9.54	83.9	85.8		84.9	1.3
2H	4	968	970	9.69	85.7	86.5		86.1	0.6
2H	4	984	986	9.85	86.1	86.6		86.4	0.4
2H	4	1001	1003	10.02	89.2	89.2	88.3	88.9	0.5
2H	4	1016	1018	10.17	89.3	86.0		87.7	2.3
2H	4	1033	1035	10.34	88.4	85.5		87.0	2.1
2H	4	1049	1051	10.50	88.5	88.8	89.9	89.1	0.7
2H	4	1062	1064	10.63	85.7	86.3		86.0	0.4
2H	4	1080	1082	10.81	88.1	86.9		87.5	0.8
2H	5	1103	1105	11.04	89.9	91.4	89.8	90.4	0.9
2H	5	1118	1120	11.19	86.5	87.4	85.8	86.6	0.8
2H	5	1134	1136	11.35	91.1	91.1	87.4	89.9	2.1
2H	5	1151	1153	11.52	90.7	92.2	93.4	92.1	1.4
2H	5	1166	1168	11.67	90.3	91.3	91.6	91.1	0.7
2H	5	1183	1185	11.84	89.3	91.0		90.2	1.2
2H	5	1199	1201	12.00	90.0	88.5	92.8	90.4	2.2
2H	5	1212	1214	12.13	89.7	89.0	92.1	90.3	1.6
2H	5	1230	1232	12.31	89.7	88.4	91.6	89.9	1.6
2H	5	1244	1246	12.45	89.3	88.7	91.7	89.9	1.6
2H	6	1253	1255	12.54	89.7	90.8	90.8	90.4	0.6
2H	6	1268	1270	12.69	89.4	89.0		89.2	0.3
2H	6	1284	1286	12.85	90.0	90.0	87.9	89.3	1.2
2H	6	1301	1303	13.02	88.7	89.3	88.8	88.9	0.3
2H	6	1316	1318	13.17	90.6	89.0		89.8	1.1
2H	6	1333	1335	13.34	90.8	88.6		89.7	1.6
2H	6	1349	1351	13.50	92.2	90.5		91.4	1.2
2H	6	1362	1364	13.63	93.3	93.6	95.5	94.1	1.2
2H	6	1380	1382	13.81	92.1	90.8		91.5	0.9
2H	6	1394	1396	13.95	92.1	90.2		91.2	1.3
2H	7	1403	1405	14.04	91.7	91.1		91.4	0.4
2H	7	1418	1420	14.19	91.3	91.3	87.3	90.0	2.3
2H	7	1434	1436	14.35	91.4	91.0		91.2	0.3
3H	1	1453	1455	14.54	72.6	72.6	72.9	72.7	0.2
3H	1	1468	1470	14.69	78.4	76.2		77.3	1.6

3H	1	1484	1486	14.85	80.1	78.1		79.1	1.4
3H	1	1501	1503	15.02	79.1	79.2		79.2	0.1
3H	1	1516	1518	15.17	81.1	79.6		80.4	1.1
3H	1	1533	1535	15.34	82.7	80.0	80.2	81.0	1.5
3H	1	1549	1551	15.50	83.0	81.3		82.2	1.2
3H	1	1562	1564	15.63	87.5	85.8		86.7	1.2
3H	1	1580	1582	15.81	85.8	84.7		85.3	0.8
3H	1	1594	1596	15.95	88.6	87.0		87.8	1.1
3H	2	1603	1605	16.04	88.9	89.2		89.1	0.2
3H	2	1618	1620	16.19	88.0	88.1		88.1	0.1
3H	2	1634	1636	16.35	90.3	90.3	87.3	89.3	1.7
3H	2	1651	1653	16.52	88.9	89.4		89.2	0.4
3H	2	1666	1668	16.67	89.7	90.6		90.2	0.6
3H	2	1683	1685	16.84	92.0	90.2		91.1	1.3
3H	2	1699	1701	17.00	91.6	90.6		91.1	0.7
3H	2	1712	1714	17.13	89.2	88.5		88.9	0.5
3H	2	1730	1732	17.31	89.8	91.2		90.5	1.0
3H	2	1744	1746	17.45	90.2	90.4		90.3	0.1
3H	3	1753	1755	17.54	89.4	87.5		88.5	1.3
3H	3	1768	1770	17.69	88.7	88.7	87.7	88.4	0.6
3H	3	1784	1786	17.85	88.5	87.8		88.2	0.5
3H	3	1801	1803	18.02	90.9	89.2		90.1	1.2
3H	3	1816	1818	18.17	90.9	89.6		90.3	0.9
3H	3	1833	1835	18.34	91.4	90.0		90.7	1.0
3H	3	1849	1851	18.50	90.0	90.9		90.5	0.6
3H	3	1862	1864	18.63	90.3	90.8		90.6	0.4
3H	3	1880	1882	18.81	88.2	89.1		88.7	0.6
3H	3	1894	1896	18.95	87.6	87.3		87.5	0.2
3H	4	1903	1905	19.04	89.6	90.2		89.9	0.4
3H	4	1918	1920	19.19	89.0	89.0		89.0	0.0
3H	4	1934	1936	19.35	88.0	89.1		88.6	0.8
3H	4	1951	1953	19.52	87.3	89.0		88.2	1.2
3H	4	1966	1968	19.67	86.7	87.6		87.2	0.6
3H	4	1983	1985	19.84	88.0	88.1		88.1	0.1
3H	4	1999	2001	20.00	87.3	87.7		87.5	0.3
3H	4	2012	2014	20.13	87.5	87.7		87.6	0.1
3H	4	2030	2032	20.31	84.1	84.6		84.4	0.4
3H	5	2053	2055	20.54	82.3	85.2		83.8	2.1
3H	5	2068	2070	20.69	75.4	79.0	77.0	77.1	1.8
3H	5	2084	2086	20.85	89.4	90.4		89.9	0.7
3H	5	2101	2103	21.02	88.6	91.0		89.8	1.7
3H	5	2116	2118	21.17	89.5	90.5		90.0	0.7
3H	5	2133	2135	21.34	89.5	89.5	89.0	89.3	0.3
3H	5	2149	2151	21.50	88.7	92.2		90.5	2.5
3H	5	2162	2164	21.63	89.8	92.9		91.4	2.2
3H	5	2180	2182	21.81	89.8	93.1		91.5	2.3
3H	5	2194	2196	21.95	92.4	92.7		92.6	0.2
3H	6	2203	2205	22.04	92.4	93.1		92.8	0.5
3H	6	2218	2220	22.19	92.1	91.7		91.9	0.3
3H	6	2234	2236	22.35	91.7	92.0		91.9	0.2
3H	6	2251	2253	22.52	90.8	90.6		90.7	0.1

3H	6	2266	2268	22.67	90.3	90.3	90.1	90.2	0.1
3H	6	2283	2285	22.84	87.4	87.0		87.2	0.3
3H	6	2299	2301	23.00	90.7	90.7		90.7	0.0
3H	6	2312	2314	23.13	87.4	88.7		88.1	0.9
3H	6	2330	2332	23.31	86.2	86.5		86.4	0.2
3H	7	2353	2355	23.54	85.8	85.8	87.1	86.2	0.8
3H	7	2368	2370	23.69	83.9	83.7		83.8	0.1
									0.9
									Average
									Std. Dev.

Table B.1: Bulk carbonate content, ODP Hole 1198A, 0 – 23.69 mbsf

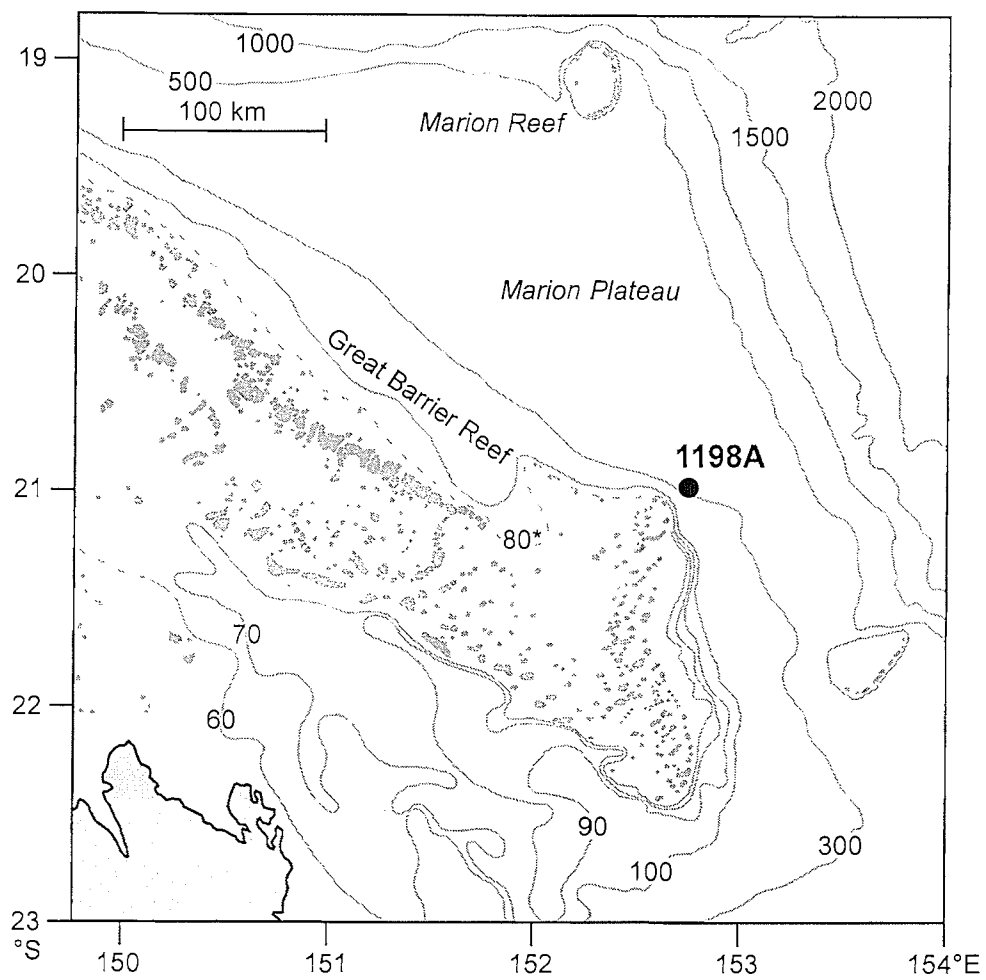


Figure B.1: Major physiographic and bathymetric features of Marion Plateau and the location of ODP Site 1198A

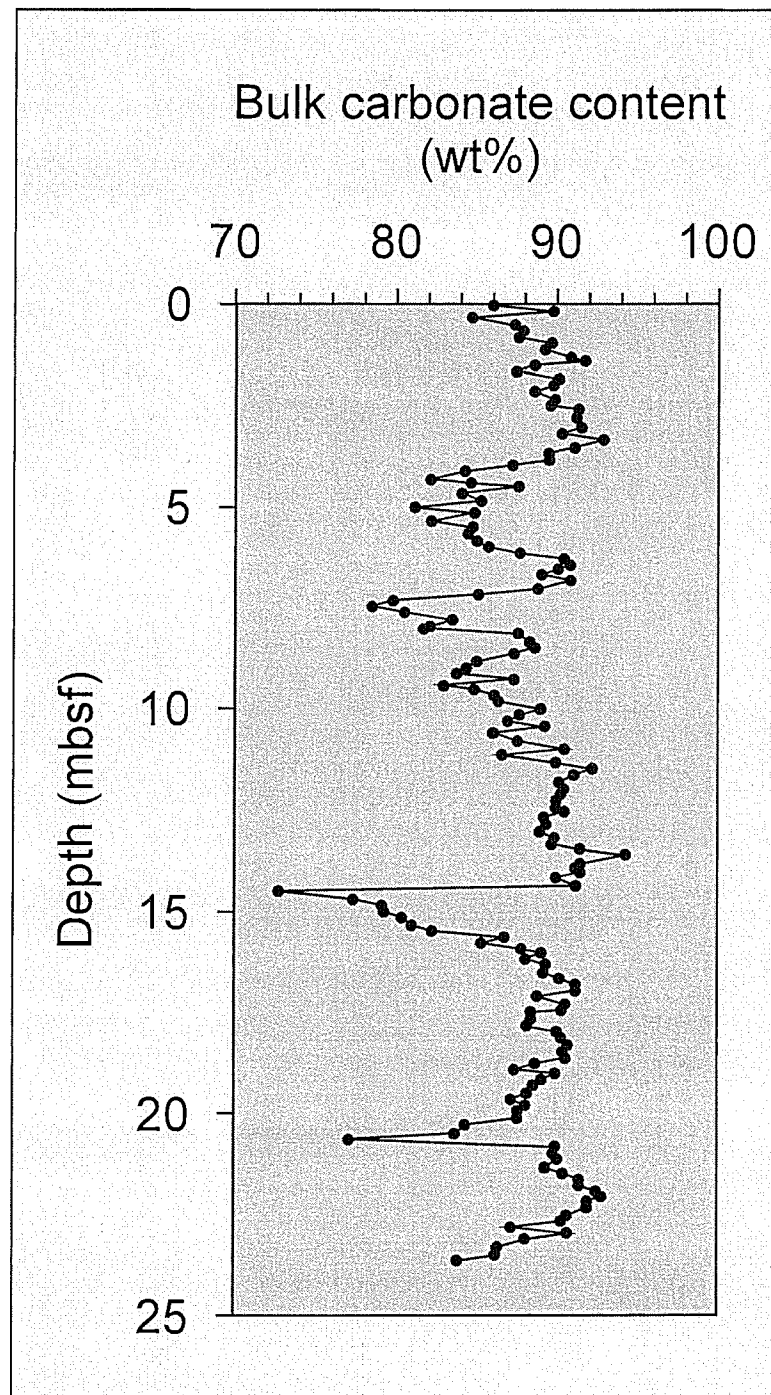


Figure B.2: Variations in bulk carbonate content from 0 to 23.69 mbsf in ODP Hole

1198A

REFERENCES

- Davies, P.J., and McKenzie, J.A., 1993, Controls on the Pliocene-Pleistocene evolution of the northeastern Australian continental margin, *in* McKenzie, J.A., Davies, P.J., Palmer-Julson, A., and et al., eds., Proceedings of the Ocean Drilling Program, Scientific Results, 133: College Station, TX, (Ocean Drilling Program), p. 755-762.
- Dunbar, G.B., Dickens, G.R., and Carter, R.M., 2000, Sediment flux across the Great Barrier Reef Shelf to the Queensland Trough over the last 300 ky: *Sedimentary Geology*, v. 133, p. 49-92.
- Harris, P.T., Davies, P.J., and Marshall, J.F., 1990, Late Quaternary sedimentation on the Great Barrier Reef continental shelf and slope east of Townsville, Australia: *Marine Geology*, v. 94, p. 55-77.
- Heap, A.D., Dickens, G.R., and Stewart, L.K., 2001, Late Holocene sediment in Nara Inlet, central Great Barrier Reef platform: sediment accumulation on the middle shelf of a tropical mixed clastic/carbonate system: *Marine Geology*, v. 176, p. 39-54.
- International Consortium for Great Barrier Reef Drilling, 2001, New constraints on the origin of the Australian Great Barrier Reef: Results from an international project of deep coring: *Geology*, v. 29, p. 483-486.
- Kronen, J.D., Jr., and Glenn, C.R., 2000, Pristine to reworked verdine: keys to sequence stratigraphy in mixed carbonate-siliciclastic forereef sediments (Great Barrier Reef), *Marine Authigenesis: From Global to Microbial*, SEPM Special Publication No. 66, SEPM, p. 387-403.
- Mueller, G., and Gastner, M., 1971, The "Karbonat-Bombe", a simple device for the determination of the carbonate content in sediments, soils and other materials: *Neues Jahrbuch Fuer Mineralogie*, v. 10, p. 466-469.
- Page, M.C., Dickens, G.R., and Dunbar, G.B., 2003, Tropical view of Quaternary sequence stratigraphy: siliciclastic accumulation on slopes east of the Great Barrier Reef since the Last Glacial Maximum: *Geology*, v. 31, p. 1013-1016.
- Peerdeman, F.M., and Davies, P.J., 1993, Sedimentological response of an outer-shelf, upper-slope sequence to rapid changes in Pleistocene eustatic sea-level: Hole 820A, Northeastern Australian Margin, *in* McKenzie, J.A., Davies, P.J., Palmer-Julson, A., et al. (Eds), Proceedings of the Ocean Drilling Program, Scientific Results, 133: College Station, TX, (Ocean Drilling Program), p. 303-313.
- Shipboard Scientific Party, 2002a, Leg 194 Summary, *in* Isern, A., Anselmetti, F., Blum, P., et al. (Eds), Proc. ODP, Init. Repts., 194: College Station TX, (Ocean Drilling Program), p. 1-88.
- Shipboard Scientific Party, 2002b, Site 1198, *in* Isern, A., Anselmetti, F., Blum, P., et al. (Eds), Proc. ODP, Init. Repts., 194: College Station TX, (Ocean Drilling Program), p. 1-75.
- Vail, P.R., Mitchum, R.M., and Thompson, S., 1977, Seismic stratigraphy and global changes of sea level, part 4: global cycles of relative changes of sea level: American Association of Petroleum Geologists, Memoir 26, p. 83-97.
- Walker, R.G., 1992, Facies, facies models and modern stratigraphic concepts, *in* Walker, R.G., and James, N.P., eds., *Facies Models: response to sea level change*: Ontario, Geological Association of Canada, p. 1-14.